



**Luís Pedro  
Gomes Monteiro**

**Development of new anticancer metallodrugs**

**Desenvolvimento de novos metalofármacos  
anticancerígenos**



**Luís Pedro  
Gomes Monteiro**

## **Development of new anticancer metallodrugs**

### **Desenvolvimento de novos metalofármacos anticancerígenos**

Dissertação apresentada à Universidade de Aveiro para cumprimento dos requisitos necessários à obtenção do grau de Mestre em Mestrado de Biomedicina Molecular, realizada sob a orientação científica da Doutora Bárbara Joana Martins Leite Ferreira, Investigadora da Universidade de Aveiro na Unidade Orgânica CICECO/Departamento de Química e da Professora Doutora Teresa Margarida dos Santos, professora Auxiliar do Departamento de Química da Universidade de Aveiro.

This work was developed within the scope of the project CICECO-Aveiro Institute of Materials, FCT Ref. UID/CTM/50011/2019, financed by national funds through the FCT/MCTES.

Dedico este trabalho aos meus pais pelo apoio incondicional e por terem sempre acreditado em mim.

**o júri**  
presidente

Prof. Doutora Luisa Alejandra Helguero Shepherd  
Professora Auxiliar do Departamento de Ciências Médicas da Universidade de Aveiro

Doutora Bárbara Joana Martins Leite Ferreira (Orientadora)  
Investigadora do Departamento de Química da Universidade de Aveiro

Prof. Doutora Alberta Paula Lobo Machado Gameiro dos Santos  
Professora Auxiliar com agregação do Departamento de Química e Bioquímica da Faculdade de Ciências da Universidade do Porto

## **agradecimentos**

Quero agradecer em primeiro lugar à Dr.<sup>a</sup> Bárbara Ferreira e à Dr.<sup>a</sup> Teresa Santos pela orientação fantástica que me deram, pela paciência, frontalidade, por acreditarem em mim e pelas oportunidades que me proporcionaram neste ano transato.

Quero dar também um agradecimento especial a todos os que contribuíram para o sucesso desta dissertação, mas em especial ao Ricardo Mendes pela determinação das estruturas, à Eng. Celeste Azevedo por todas as análises que realizou com os meus complexos, à Cláudia Silva e à Dr.<sup>a</sup> Fátima Martel da Faculdade de Medicina da Universidade do Porto pela realização dos ensaios biológicos *in vitro*.

Quero deixar também uma palavra de agradecimento a todos os colegas com quem partilhei o laboratório, pois acredito que só num bom ambiente laboratorial se consegue chegar ao sucesso.

Gostaria de agradecer aos meus pais que sempre me incentivaram a perseguir aquilo em que acredito e por todo o apoio durante estes cinco anos. Por me dizerem constantemente “se fosse fácil não para era para ti”.

Um muito obrigado muito grande a todos os amigos que Aveiro me deu e a todos os que já trazia comigo, por todo o apoio e por estarem lá nos bons e maus momentos.

Um agradecimento muito especial à Vera, por todo o amor, amizade, carinho, paciência e incentivo durante a realização deste trabalho.

## palavras-chave

Cancro; Complexos metálicos; Metalofármacos; FAINes; Anti-tumorais; ADN; BSA; Intercalação; Peroxidação lipídica; MTT; Seletividade

## resumo

O sucesso da quimioterapia tem sido conseguido à base de fármacos de baixo peso molecular que têm demonstrado capacidade para destruir as células cancerígenas ou para controlar a sua proliferação. No entanto, existem vários efeitos secundários associados ao uso de muitos destes fármacos, maioritariamente devido ao facto de não apresentarem seletividade, isto é, tanto atuarem nas células tumorais como nas não tumorais. O uso de compostos de coordenação (metalofármacos) para terapia anticancerígena começou com o uso de compostos de platina, os quais, apesar das suas bem conhecidas severas limitações, continuam ainda a ser muito utilizados. Estas desvantagens levaram à necessidade de explorar novos metalofármacos com diferentes metais de transição. Iões metálicos diversificados podem levar à obtenção de complexos com características diferentes, como por exemplo, no que diz respeito a geometrias ou potenciais de redução. Esta flexibilidade torna-os atraentes para o desenvolvimento de novos agentes terapêuticos. O uso de fármacos pré-ativos como ligandos é um bom exemplo de como os compostos metálicos podem alterar/melhorar a atividade dos fármacos parentais. O presente trabalho mostra os resultados da síntese e caracterização de novos metalofármacos de diferentes metais de transição, do estudo da sua capacidade de interação com o ácido desoxirribonucleico (ADN) e com a albumina de origem bovina (BSA), bem como do seu comportamento anticancerígeno. Este desempenho foi avaliado através de ensaios biológicos *in vitro*, em linhas celulares cancerígenas e normais da mama que permitiram aferir da sua capacidade anti-tumoral e seletividade.

**Keywords**

Cancer; Metal complexes; Metallopharmaceuticals, NSAIDs; Anti-tumour; DNA; BSA; Intercalation, Lipid Peroxidation, MTT; Selectivity

**Abstract**

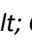
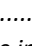
The success of chemotherapy has been achieved with low molecular weight drugs that have been shown to destroy cancer cells or to control their proliferation. However, there are several side effects associated with the use of many of these drugs, mainly due to the fact that they do not have selectivity, acting on both tumor and non-tumor cells. The use of coordinating compounds (metallo-pharmaceuticals) for anticancer therapy began with the use of platinum compounds, which, despite their well-known severe limitations, are still widely used. These disadvantages led to the need to explore new metallo-pharmaceuticals with different transition metals. Diversified metal ions can lead to complexes with different characteristics, such as geometries or reduction potentials. This flexibility makes them attractive for the development of new therapeutic agents. The use of pre-active drugs as ligands is a good example of how metal compounds can alter/enhance the activity of parent drugs. The present work shows the results of the synthesis and characterization of new metallo-pharmaceuticals of different transition metals, the study of their ability to interact with deoxyribonucleic acid (DNA) and bovine albumin (BSA), as well as their anticancer behaviour. This performance was evaluated by *in vitro* biological assays, in tumoral and normal breast cell lines, which allowed to measure their anti-tumor capacity and selectivity.





## Figure List

Figure 1: Structure of carboplatin (A) and oxaliplatin (B).....	2
Figure 2: Strategies to control A $\beta$ aggregation by transition metal complexes. Adapted <sup>18</sup> .....	4
Figure 3: Crystal field d orbital splitting diagram in the formation of an octahedral complex. Adapted <sup>26,79</sup> .....	10
Figure 4: Pyridine ring and its nitrogen lone electron pair. Adapted <sup>82</sup> .....	10
Figure 5: Types of coordination modes between a metal ion and the deprotonated carboxylic group. Adapted <sup>19</sup> .....	11
Figure 6: Structure of (S)-Ibuprofen and diclofenac.....	11
Figure 7: Paddle-wheel structural types involving Cu <sup>2+</sup> . (a) Paddle-wheel dimer and (b) polymeric dimer. Adapted <sup>90</sup> .....	12
Figure 8: B-DNA form and its major and minor grooves. Adapted <sup>91</sup> .....	13
Figure 9: Adduct between cisplatin and DNA. Adapted <sup>93</sup> .....	14
Figure 10: Cisplatin hydrolysis and formation of aqua-complexes. Adapted <sup>104</sup> .....	15
Figure 11: Phenanthridine DNA- binding mechanism. Adapted <sup>108</sup> .....	16
Figure 12: Two modes of DNA-intercalation. Left: classical intercalation; right: threading intercalation. Adapted <sup>101</sup> .....	17
Figure 13: Two types of intercalation. Full and partial intercalation by the ligands dppz (dipyridophenazine) and phen (phenanthroline). Adapted <sup>113</sup> .....	18
Figure 14: Structure of pentacationic manganese (III) porphyrin. Adapted <sup>115</sup> .....	19
Figure 15: Experimental and by crystal X-ray data XRD graph for complex (1). Black line = single crystal X-ray data; Grey line = Complex (1).....	30
Figure 16: Representation of the complex [Cu(Ibu)(2,2'-dipy)Cl] (1) showing all atoms represented as small spheres with arbitrary radius. The asymmetric unit is composed of two [Cu(Ibu)(2,2'-dipy)Cl] units.....	31
Figure 17: IR spectra of complex (1) with all the relevant peak highlighted. ....	31
Figure 18: TGA/DSC results for complex 1.....	33
Figure 19: The fluorescence quenching spectra of BSA in the presence of various concentrations of complex (1) at $\lambda_{ex}$ = 295 nm and [BSA] = 5 $\mu$ M. Arrow indicates the change upon increasing the complex concentration (R=0.2; R=1; R=2; R=3; R=4; R=5; R=6; R=7). The plot $F_0/F$ versus [Q] according with the Stern-Volmer equation is depicted in the inset. ....	36
Figure 20: CD spectra of BSA in the presence of various concentrations of complex 1. Arrow indicates the change upon increasing the complex concentration. ([BSA]= 0.25 $\mu$ M; R=0.5; R=1). ....	37
Figure 21: UV-visible absorption spectra of BSA in the presence and absence of complex (1). Arrow indicates the change upon increasing the complex concentration ([BSA]= 0.47 $\mu$ M; R=0.2; R=2.1; R=10.6; R=21.3; R=53.1). ....	38
Figure 22: Structure of ethidium bromide [(3,8-diamino-5-ethyl-6-phenyl phenanthridinium bromide)].....	39
Figure 23: Effect of addition [complex (1)]=1-30 $\mu$ M on the fluorescence intensity of the CT-DNA bound ethidium bromide (EB). Arrow show the effect of complex (1) on the EB-DNA adduct fluorescence.....	40
Figure 24: UV spectra of CT-DNA in the absence (a) and absence of different concentrations of complex (1). ([CT-DNA] = 0.5 $\mu$ M; [Complex (1)]= b-5 $\mu$ M; c-15 $\mu$ M; d-30 $\mu$ M). ....	41
Figure 25: Cytotoxicity assessment by MTT assay induced by complex (1). The cells were exposed to different concentrations of each complex for 24h. *p<0,05 vs control. ....	42
Figure 26: Principal steps in the formation of MDA. PLA <sub>2</sub> – Phospholipase A2. Adapted from <sup>162</sup> .....	43
Figure 27: Lipid peroxidation levels of the cell lines after 24h treatment with complex (1). *p<0,05 vs control (t-test).....	44
Figure 28: Experimental and by crystal X-ray data XRD graph for complex (2). Black line = single crystal X-ray data; Grey line = Complex (2).....	46
Figure 29: Asymmetric unit of [Ni(terpy) <sub>2</sub> ](diclof) <sub>2</sub> ·8H <sub>2</sub> O (2) showing all atoms represented as small spheres with arbitrary radius.....	46
Figure 30: IR spectra of complex (2) with all the relevant peak highlighted. ....	47
Figure 31: TGA/DSC results for complex (2).....	48

Figure 32: The fluorescence quenching spectra of BSA in the presence of various concentrations of complex (2) at $\lambda_{ex} = 295$ nm and $[BSA] = 6.5$ $\mu$ M. Arrow indicates the change upon increasing the complex concentration ( $R=0.02$ ; $R=0.04$ ; $R=0.06$ ).....	50
Figure 33: CD spectra of BSA in the presence of various concentrations of complex (2). Arrow indicates the change upon increasing the complex concentration. ( $[BSA] = 0.25$ $\mu$ M; $R=1$ ; $R=2$ ). .....	51
Figure 34: UV-visible absorption spectra of $[BSA]=0.16$ $\mu$ M in the absence (black line) and presence of complex (2). ( $R=0.1$ ; $R=0.9$ ; $R=25$ ) .....	52
Figure 35: Effect of addition $[complex (2)]=0.5-35$ $\mu$ M on the fluorescence intensity of the CT-DNA bound ethidium bromide (EB).....	52
Figure 36: UV spectra of CT-DNA in the absence (a) and presence of different concentrations of complex (2). ( $\alpha$ -[CT-DNA] = 0,5 $\mu$ M; b- 2 $\mu$ M; c- 4 $\mu$ M; d- 7 $\mu$ M, e- 35 $\mu$ M). The arrow shows the absorbance changes upon increasing concentrations of the complex. ....	53
Figure 37: Cytotoxicity assessment by MTT assay induced by complex (2). The cells were exposed to different concentrations of each complex for 24h. * $p<0,05$ vs control. ....	54
Figure 38: Lipid peroxidation levels of the cell lines after 24h treatment with complex (2). * $p<0,05$ vs control (t-test).....	55
Figure 39: Crystal Structure of $[M(diclo)_2(2,2'-bipy)]$ (where $M^{2+} = Co^{2+}$ (3) or $Ni^{2+}$ (4)) showing all non-hydrogen atoms represented as thermal ellipsoids drawn at the 50% probability level and hydrogen atoms as small spheres with arbitrary radius. The asymmetric unit is composed of only half of the represented complex, with the remaining atoms being generated by symmetry. ....	56
Figure 40: Packaging diagram of complex (3) and (4) showing the interactions (dashed line in the figure; $\pi$ - $\pi$ interaction) between various structural units of the complexes. ....	57
Figure 41: Crystal Structure of $[M(diclo)_2(1,10-phen)]$ (where $M^{2+} = Co^{2+}$ (5) or $Ni^{2+}$ (6)) showing all non-hydrogen atoms represented as thermal ellipsoids drawn at the 50% probability level and hydrogen atoms as small spheres with arbitrary radius. The asymmetric unit is composed of only half of the represented complex, with the remaining atoms being generated by symmetry. Complex (5)  = Cobalt; Complex (6)  = Nickel.....	58
Figure 42: Packaging diagram of complex (5) and (6) showing the interactions (dashed line in the figure; $\pi$ - $\pi$ interaction) between various structural units of the complexes. ....	59
Figure 43: Experimental and by crystal X-ray data XRD graph for complex (3). Black line = single crystal X-ray data; Grey line = Complex (3). ....	59
Figure 44: Experimental and by crystal X-ray data XRD graph for complex (4). Black line = single crystal X-ray data; Grey line = Complex (4). ....	60
Figure 45: Experimental and by crystal X-ray data XRD graph for complex (5). Black line = single crystal X-ray data; Grey line = Complex (5) .....	60
Figure 46: Experimental and by crystal X-ray data XRD graph for complex (6). Black line = single crystal X-ray data; Grey line = Complex (6) .....	60
Figure 47: IR spectra of complex (3) with all the relevant peak highlighted. ....	63
Figure 48: IR spectra of complex (4) with all the relevant peak highlighted. ....	63
Figure 49: IR spectra of complex (5) with all the relevant peak highlighted. ....	64
Figure 50: IR spectra of complex (6) with all the relevant peak highlighted. ....	64
Figure 51: TGA/DSC results for complex (3) to (6). ....	67
Figure 52: The fluorescence quenching spectra of BSA in the presence of various concentrations of complexes at $\lambda_{ex} = 295$ nm and $[BSA] = 3$ $\mu$ M. Arrow indicates the change upon increasing the complex concentration. Complex (3) - ( $R=0.02$ ; $R=0.07$ ; $R=0.3$ ; $R=3.3$ ; $R=6.7$ ; $R=10$ ); Complex (4) - ( $R=0.02$ ; $R=0.07$ ); Complex (5) - ( $R=0.07$ ; $R=1.7$ ; $R=3.3$ ); Complex (6) - ( $R=0.07$ ; $R=0.33$ ; $R=1.67$ ; $R=1.33$ ). The plots $F_0/F$ versus $[Q]$ according with the Stern-Volmer equation are depicted in the insets. ....	70
Figure 53: CD spectra of BSA in the presence of various concentrations of complex (3), (4), (5) and (6). Arrows indicates the change upon increasing the complex concentration. ( $[BSA] = 0.25$ $\mu$ M; $R=0.5$ ; $R=1$ ). ....	71
Figure 54: UV-visible absorption spectra of $[BSA]$ in the absence (orange line) and presence of the four complexes. (Complex (3) - $[BSA] = 0.5$ $\mu$ M; $R=20$ ; $R=40$ ; $R=100$ ); (Complex (4) - $[BSA] = 0.47$ $\mu$ M; $R=0.02$ ;	

<i>R=0.05; R=21; (Complex (5) – [BSA] = 0.46 <math>\mu</math>M; R=0.11; R=1.1); (Complex (6) – [BSA] = 0.4 <math>\mu</math>M; R=12; R=50; R=74); .....</i>	<i>73</i>
<i>Figure 55: Circular dichroism spectra of [CT-DNA]=100 <math>\mu</math>M in the absence and presence the complexes. [Complex (3)] - 0.05 <math>\mu</math>M; [Complex (4)] - 0.1 <math>\mu</math>M; [Complex (5)] - 0.05 <math>\mu</math>M; [Complex (6)] - 0.2 <math>\mu</math>M;.....</i>	<i>74</i>
<i>Figure 56: Effect of addition of complex (3), (4), (5) and (6) on the fluorescence intensity of the CT-DNA bound ethidium bromide (EB). The arrows show the tendency upon the addition of increasing concentrations of the complexes. [Complex (3)] – 0.05 <math>\mu</math>M; 0.2 <math>\mu</math>M; 1 <math>\mu</math>M; 10 <math>\mu</math>M; 20 <math>\mu</math>M; 30 <math>\mu</math>M; [Complex (4)] - 0.1 <math>\mu</math>M; 0.25 <math>\mu</math>M; 1 <math>\mu</math>M; 2 <math>\mu</math>M; 7.4 <math>\mu</math>M; 14.8 <math>\mu</math>M; [Complex (5)] - 0.05 <math>\mu</math>M; 1 <math>\mu</math>M; 5 <math>\mu</math>M; 10 <math>\mu</math>M; 29.6 <math>\mu</math>M; [Complex (6)] - 0.05 <math>\mu</math>M; 0.2 <math>\mu</math>M; 1 <math>\mu</math>M; 20 <math>\mu</math>M; 30 <math>\mu</math>M; Zoom of the quenching zone are displayed in insets. ....</i>	<i>75</i>
<i>Figure 57: UV spectra of complex (3) and (6) (black line) with increasing concentrations of CT-DNA. The arrows show the effect upon the addition of CT-DNA. [Complex (3)]=20 <math>\mu</math>M; [CT-DNA]=10 <math>\mu</math>M; 20 <math>\mu</math>M; [Complex (6)]= 20 <math>\mu</math>M; [CT-DNA]=10 <math>\mu</math>M; 15 <math>\mu</math>M; 25 <math>\mu</math>M;.....</i>	<i>76</i>
<i>Figure 58: Cytotoxicity assessment by MTT assay induced by complex (3), (4), (5) and (6). The cells were exposed to different concentrations of each complex for 24h. *<math>p&lt;0,05</math> vs control. ....</i>	<i>78</i>
<i>Figure 59: Lipid peroxidation levels of the cell lines after 24h treatment with the metal complexes. *<math>p&lt;0,05</math> vs control (t-test). ....</i>	<i>80</i>



## Table list

Table 1: The characteristic IR absorption frequencies ( $\text{cm}^{-1}$ ) of the free ligands and complex (1).....	32
Table 2: Elementary analysis data for complex (1). "AE" = obtained values; "Cal" = calculated values base on the chemical formula from single crystal X-ray. ....	33
Table 3: TG analysis data for complex (1). "AE" = obtained values; "Cal" = calculated values base on the chemical formula from single crystal X-ray. ....	34
Table 4: $\alpha$ -helix content in free [BSA]=0.25 $\mu\text{M}$ (Ratio=0) and in the presence of different ratios of complex (1). ....	37
Table 5: The characteristic IR absorption frequencies ( $\text{cm}^{-1}$ ) of the free ligands and complex (2). ....	47
Table 6: Results of the elementary analysis. "AE" are the values obtain from the analysis and "Cal" are the calculated values based on the chemical structure given by the x-ray.....	48
Table 7: Results of the TGA analysis. Comparison between the "TG" values, obtain by the analysis and the "Cal" that were calculated based on their chemical structure. ....	49
Table 8: $\alpha$ -helix content in free BSA at 0.25 $\mu\text{M}$ (Ratio=0) and in the presence of different ratios of complex (2) .....	51
Table 9: Crystal data collection and structure refinement details.....	61
Table 10: The characteristic IR absorption frequencies ( $\text{cm}^{-1}$ ) of the free ligands and complex (3) to (6). ....	62
Table 11: Elementary analysis data for complex (1). "AE" = obtained values; "Cal" = calculated values base on the chemical formula from single crystal X-ray. ....	65
Table 12: Results of the elementary analysis. "AE" are the values obtain from the analysis and "Cal" are the calculated values based on the chemical structure given by the x-ray.....	67
Table 13: Quenching constant ( $K_{\text{sv}}$ ) for the interactions of complex (3), (5) and (6) with BSA.....	70
Table 14: $\alpha$ -helix content in free BSA at 0,25 $\mu\text{M}$ (R=0) and in the presence of different ratios of complex (3) to (6). ....	71



## Abbreviations

**BSA** – Bovine serum albumin

**COX** – Cyclooxygenase

**COX-1** – Cyclooxygenase 1

**COX-2** – Cyclooxygenase 2

**DNA** – Deoxyribonucleic acid

**HSA** – Human serum albumin

**NSAIDs** – Nonsteroidal anti-inflammatory drugs

**PG** – Prostaglandin

**RNA** – Ribonucleic acid

**SOD** – Superoxide dismutase

**NSAIDs** – Non-steroidal anti-inflammatory drugs

**LPO** – Lipid Peroxidation

**1,10-Phen** – 1,10-phenantroline

**2,2'-bipy** – 2,2'-bipyridine

**2,2'-dipy** – 2,2'-dipyridylamine

**DMF** – Dimethylformamide

**Ct-DNA** – Calf thymus deoxyribonucleic acid

**Terpy** – 2,2':6',2''-terpyridine

**Diclof** – Diclofenac

**Ibu** – Ibuprofen

**KBr** – Potassium bromide

**EB** – Ethidium bromide

**ROS** – Reactive oxygen species





## Table of Contents

<b>CHAPTER 1 – INTRODUCTION.....</b>	<b>1</b>
1.1 A BRIEF HISTORY OF METALLODRUGS.....	2
1.1.1 <i>The d-block metals – Biological Roles</i> .....	4
1.2 METAL IONS AND LIGANDS: COORDINATION CHEMISTRY.....	9
1.2.1 <i>N-donor ligands</i> .....	10
1.2.2 <i>NSAID's as O-donors</i> .....	11
1.2.3 <i>Complexes structure determination analytical techniques and spectroscopic studies</i> .....	12
1.2 MOLECULAR TARGETS OF THE METAL COMPLEXES .....	13
1.3.1 <i>Binding modes of metal complexes to DNA</i> .....	15
1.3.2 <i>Target proteins</i> .....	19
1.3.3 <i>Spectroscopic studies for biological measurements</i> .....	20
1.4 OBJECTIVES .....	21
<b>CHAPTER 2 – EXPERIMENTAL PROCEDURE.....</b>	<b>21</b>
2.1 REAGENTS AND MATERIALS .....	22
2.2 METHODS AND INSTRUMENTATION .....	22
2.3 X-RAY CRYSTALLOGRAPHY (SINGLE-CRYSTAL X-RAY) .....	22
2.4. SYNTHESIS OF THE COMPLEXES .....	23
2.4.1 <i>Synthesis of complex [Cu(ibu)(2,2'-dipy)Cl] (1)</i> .....	23
2.4.2 <i>Synthesis of complex [Ni(terpy)<sub>2</sub>](dicl)<sub>2</sub>·8H<sub>2</sub>O (2)</i> .....	23
2.4.3 <i>Synthesis of complexes [M(dicl)<sub>2</sub>(2,2'-bipy)]; M = Co(II) and Ni(II), for (3) and (4)</i> .....	23
2.4.4 <i>Synthesis of complexes [M(dicl)<sub>2</sub>(1,10-phen)]; M = Co(II) and Ni(II) for (5) and (6)</i> .....	23
2.5 ALBUMIN BINDING STUDIES .....	24
2.5.1 <i>Experimental details</i> .....	24
2.5.2 <i>BSA interaction studies by UV-vis spectroscopy</i> .....	24
2.5.3 <i>BSA interaction studies by circular dichroism spectroscopy</i> .....	24
2.5.4 <i>BSA interaction studies by fluorescence spectroscopy</i> .....	25
2.6 INTERACTION WITH CT-DNA.....	25
2.6.1 <i>Experimental details</i> .....	25
2.6.2 <i>EB competitive studies by fluorescence spectroscopy</i> .....	25
2.6.3 <i>CT-DNA interaction studies by circular dichroism spectroscopy</i> .....	26
2.6.4 <i>CT-DNA interaction studies by UV-vis spectroscopy</i> .....	26
2.7 IN VITRO BIOLOGICAL ASSAYS .....	26
2.7.1 <i>Materials</i> .....	26
2.7.2 <i>MTT assay</i> .....	27
2.7.3 <i>TBARS assays</i> .....	27
2.8 STATISTICAL ANALYSIS .....	28
<b>CHAPTER 3 – RESULTS AND DISCUSSION .....</b>	<b>29</b>
3.1. COMPLEX [Cu(ibu)(2,2'-dipy)Cl] (1).....	30
3.1.1 <i>Synthesis</i> .....	30
3.1.2 <i>Single crystal structure</i> .....	30
3.1.3 <i>Infrared spectra</i> .....	31
3.1.4 <i>Elemental and thermogravimetric analysis</i> .....	32
3.2 BSA INTERACTION STUDIES .....	34
3.2.1 <i>Fluorescence quenching and binding constant</i> .....	34
3.2.2 <i>Circular Dichroism spectroscopic studies</i> .....	36
3.2.3 <i>UV absorption spectra</i> .....	38

3.3 CT-DNA INTERACTION STUDIES .....	39
3.3.1 <i>Competitive DNA-Binding studies</i> .....	39
3.3.2 <i>UV-Vis absorption spectroscopic studies</i> .....	40
3.4 <i>IN VITRO</i> BIOLOGICAL ASSAYS .....	41
3.4.1 <i>MTT assay</i> .....	41
3.4.2 <i>TBARS assay</i> .....	42
3.5. COMPLEX [Ni(TERPY) <sub>2</sub> ](DICLOF) <sub>2</sub> ·8H <sub>2</sub> O (2) .....	45
3.5.1 <i>Synthesis</i> .....	45
3.5.2 <i>Single crystal structure</i> .....	45
3.5.3 <i>Infrared spectra</i> .....	46
3.5.4 <i>Elemental and thermogravimetric analysis</i> .....	47
3.6 BSA INTERACTION STUDIES .....	49
3.6.1 <i>Fluorescence quenching studies</i> .....	49
3.6.2 <i>Circular Dichroism spectroscopic studies</i> .....	50
3.6.3 <i>UV-Vis absorption spectroscopic studies</i> .....	51
3.7 CT-DNA INTERACTION STUDIES .....	52
3.7.1 <i>Competitive DNA-Binding studies</i> .....	52
3.7.2 <i>UV-Vis absorption spectroscopic studies</i> .....	53
3.8 <i>IN VITRO</i> BIOLOGICAL ASSAYS .....	54
3.8.1 <i>MTT assay</i> .....	54
3.8.2 <i>TBARS assays</i> .....	54
3.9 COMPLEXES [M(DICLO) <sub>2</sub> (2,2'-BIPY)] (M <sup>2+</sup> = Co <sup>2+</sup> (3) OR Ni <sup>2+</sup> (4)) .....	56
3.9.1 <i>Synthesis</i> .....	56
3.9.2 <i>Single crystal structures</i> .....	56
3.10 COMPLEXES [M(DICLO) <sub>2</sub> (1,10-PHEN)] (M <sup>2+</sup> = Co <sup>2+</sup> (5) OR Ni <sup>2+</sup> (6)).....	57
3.10.1 <i>Synthesis</i> .....	57
3.10.2 <i>Single crystal structures</i> .....	57
3.11 INFRARED SPECTRA .....	62
3.12 ELEMENTAL AND THERMOGRAVIMETRIC ANALYSIS .....	65
3.13 BSA INTERACTION STUDIES .....	68
3.13.1 <i>Fluorescence quenching studies</i> .....	68
3.13.2 <i>Circular Dichroism spectroscopic studies</i> .....	70
3.13.3 <i>UV-Vis absorption spectroscopic studies</i> .....	72
3.14 CT-DNA INTERACTION STUDIES .....	73
3.14.1 <i>Circular Dichroism spectroscopic studies</i> .....	73
3.14.2 <i>Competitive DNA-binding studies</i> .....	74
3.14.3 <i>UV-Vis absorption spectroscopy studies</i> .....	75
3.15 <i>IN VITRO</i> BIOLOGICAL ASSAYS .....	76
3.15.1. <i>MTT assay</i> .....	76
3.15.2. <i>TBARS assay</i> .....	79
<b>CHAPTER 4 – CONCLUSIONS AND FUTURE PERSPECTIVES .....</b>	<b>81</b>
4.1 CONCLUSIONS .....	82
4.2 FURTHER PERSPECTIVES .....	83
<b>ANNEXES .....</b>	<b>100</b>

# **Chapter 1 – Introduction**



## 1.1 A brief history of metallodrugs

Metals have been utilized in health treatments since ancient times <sup>1</sup>. But, mainly in the last century, an exponential development of new drugs matching metals and organic ligands and more specifically a few molecules that *per si* have already pharmacological effects, have appeared and been available for different health issues. Chemotherapy is still mainly depending on platinum drugs, although they are facing a more and more restricted use due to their toxicity and to spontaneous or acquired resistance <sup>1,2</sup>.

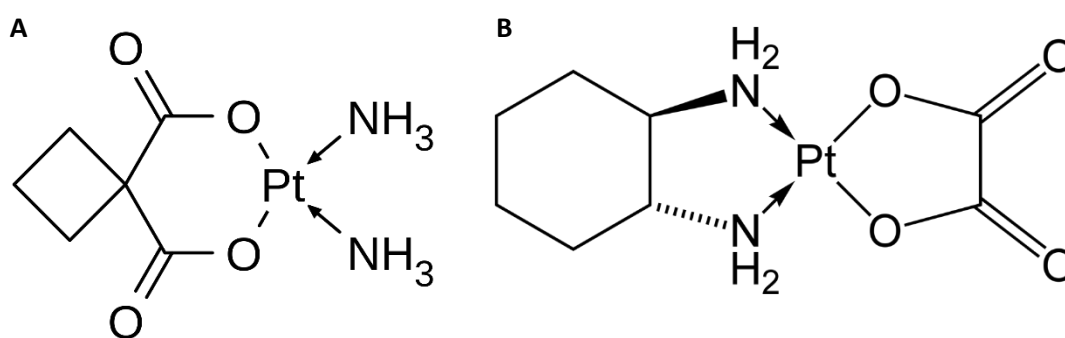


Figure 1: Structure of carboplatin (A) and oxaliplatin (B).

Within the ultimate purpose of overcoming these limitations, a vast number of other compounds with other metals have been emerging over the last years, in spite of only a very small number of these new compounds had reached clinical utility <sup>2</sup>. In particular, we can highlight different “platinum complexes” used in oncology <sup>3</sup>. Platinum complexes in the +4 oxidation state (Pt<sup>4+</sup>) started to appear soon the toxicity of cisplatin (Pt<sup>2+</sup>) became a major problem in cancer treatment. As octahedral Pt<sup>4+</sup> complexes are kinetically more inert than the parent Pt<sup>2+</sup> complexes, they are less toxic in bloodstream, but can be activated once they enter cancer cells <sup>2,4</sup>. Satraplatin (JM216) and LA-12 are the two best known examples of this type of complexes <sup>2</sup>.

Carboplatin, a Pt(II) complex, is a second generation platinum drug, considered a pro-drug for cisplatin, received FDA approval for a therapy combination in the treatment of ovarian cancer <sup>5</sup>. Other platinum derivatives have been synthesized and also received FDA approval, like oxaliplatin, in which the diaminocyclohexane ligand (DACH) plays an

important role in its cytotoxicity. This drug has been mainly used in patients who are intolerant to cis-Pt <sup>3,6</sup>.

Recently other platinum complexes have been synthesized, involving the combination of the metal ion (platinum) with other types of different ligands, in order to overcome the common platinum drugs side effects to improve their anti-cancer activity <sup>3</sup>. A good example of these new complexes are platinum complexes conjugated with sugars <sup>8</sup> like [Pt<sup>II</sup>Cl<sub>2</sub>(AcGlc-pyta)] which has shown less cytotoxicity (to normal cells) than cis-Pt <sup>2,7</sup>.

The synthesis of complexes/coordination compounds involving transitions metal ions and nonsteroidal anti-inflammatory drugs (NSAIDs) as ligands started in 1978 with the preparation of an acetylsalicylic acid (aspirin) copper(II) complex <sup>9</sup>. NSAIDs act as inhibitors of cyclooxygenase (COX) and in some cases their anti-inflammatory properties can be “improved” by the coordination to metal ions <sup>10</sup>. For example, the above acetylsalicylic acid copper(II) complex showed a more effective anti-inflammatory effect and lower ulcerogenicity and irritation in the digestive tract compared to aspirin itself <sup>11</sup>. This study was an important breakthrough because aspirin has no cyclooxygenase (COX) specificity, which means that, aspirin blocks the conversion of arachidonic acid into endoperoxide, catalysed by prostaglandin (PG) synthase (COX-2), stopping some steps of the inflammatory process, but also inhibiting COX-1 which is present in almost all tissues (stomach, kidneys, intestine, etc.) and its inhibition increases the risk of gastrointestinal bleeding and damage <sup>11–13</sup>.

It is very important to study the composition and structural features as well as the behaviour at biological level (cell surface binding and intracellular targets <sup>14</sup>) of that kind of complexes. For example, binding studies between this type of complexes and DNA or BSA/HSA are two of the most reported interaction studies <sup>15</sup>. However, RNA interactions have been much less investigated. Recently, this gap has been filled, taking the advantage that RNA offers a much more extensive structural diversity than DNA <sup>16</sup>. A recent study show that in *Saccharomyces cerevisiae* the cisplatin treatment demonstrated that platinum accumulates 4- to 20-fold more times in cellular RNA than in genomic DNA <sup>17</sup>.

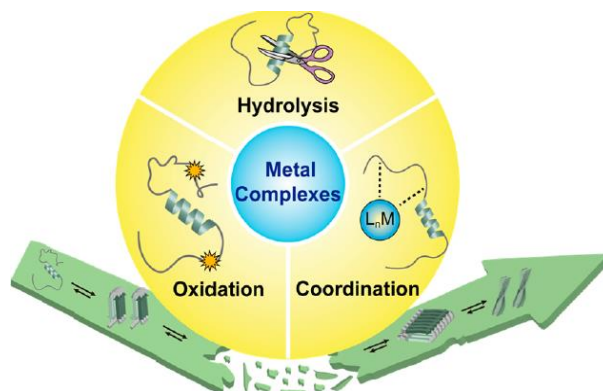


Figure 2: Strategies to control A $\beta$  aggregation by transition metal complexes. Adapted <sup>18</sup>.

In a completely new approach, some metal complexes have also been applied in studies of Alzheimer's disease. Three strategies have been proposed employing transition metal complexes towards modulation of A $\beta$  aggregation pathways, oxidative modification, hydrolytic cleavage of A $\beta$  as well as coordination to A $\beta$  <sup>18</sup>.

As we can see metal complexes can have various application. The metal ions by themselves can play a very important role on the drug design due to unique coordination environments, charge variation possibilities, Lewis acid properties, redox activity, etc. <sup>3</sup>.

### 1.1.1 The d-block metals – Biological Roles

The bonding established between metal ions and drugs (ligands) such as NSAIDs, is interesting in several aspects due to possible and frequent synergistic effects between the metal ion and the drugs themselves. An improvement is observed in the anti-ulcerous, anti-tumour and anti-bacterial activities, for example with copper, zinc, cobalt and manganese <sup>19</sup>. Over past years multiple metal ions have been tested in order to take advantage of this synergic effect. Among them, copper (Cu)<sup>20</sup>, zinc (Zn)<sup>21</sup>, iron (Fe)<sup>22</sup>, cobalt (Co)<sup>23</sup>, manganese (Mn)<sup>24</sup> and nickel (Ni)<sup>25</sup> have been the most utilized (or highlighted). As the thermodynamic stability constants of the referred complexes are basically invariant regardless the ligand type, their values can be ordered as follow:  $Mn^{2+} < Fe^{2+} < Co^{2+} < Ni^{2+} < Cu^{2+} > Zn^{2+}$ , which allows to identify copper(II) as one of the metal ions that forms the most stable complexes <sup>26</sup>.

Considering the above statements, it can be expected that, in this research field, those metal ions are the most used, and they are presented in the next sections, highlighting some of their biological features.

## I) Copper (Cu)

Copper plays a very important role in the human body, mostly because it allows many enzymes to function correctly. Copper is essential for keeping the strength of the skin, blood vessels and some tissues and is involved in the production of haemoglobin, myelin, and melanin. One of its most important characteristics is that it can act both as antioxidant and pro-oxidant centre. As an antioxidant copper neutralizes free radicals that occur naturally in the body and helps to prevent some of the damage that they can cause<sup>27</sup>. When acting as a pro-oxidant it can have pathological effects, such as neurodegenerative and hepatic disorders, that are related to the overload of copper ions, so, it is accepted that the damage observed in these disorders are a consequences of the pro-oxidant properties of this metal ion<sup>28</sup>. Additionally, copper also plays an important role in reducing inflammatory processes, and its role is achieved through the interference with the enzymatic activity of superoxide dismutase (SOD)<sup>29</sup>.

Cu(II), is a  $d^9$  electronic configuration ion, can be coordinated in a large variety of structures, from 4 to 6 coordination numbers, originating mono-, bi- or polynuclear type of complexes<sup>30</sup>. In what concerns to the ligands, besides NSAID's<sup>31–33</sup>, Schiff base<sup>34–39</sup>, phenanthroline<sup>40–42</sup> or pyridines<sup>43–48</sup> are common Cu(II) ligands.

## II) Zinc (Zn)

Zinc is a trace essential element with a minor plasma pool and a rapid turnover, being involved in several steps of the cellular metabolism, playing a role in respiration, immune functions, DNA synthesis, cell division, and others<sup>49,50</sup>. Although zinc is not a transition metal, by definition, it shows chemical properties similar to other transition metals. Because it possesses a full 3d level, *ie*, a  $3d^{10}$  electronic configuration, zinc complexes lack a ligand field energy stabilization, showing however a wide coordination flexibility). Consequently, these characteristics are critical in what concerns their catalytic roles in metalloenzymes, because of the capacity to assume different structures and coordination numbers, along with different possibilities of interactions with substrates.<sup>51</sup>

Variable coordination numbers/structures for Zn(II) complexes have been observed, although 4-coordination numbers, mainly in tetrahedral geometries, are the most



commonly found <sup>52</sup>, as they represent the optimal and least strained structures among zinc polyhedra <sup>53</sup>.

The tetrahedral geometry is adopted in coordination modes to fundamental metalloproteins, like zinc fingers (the most abundant class of zinc-binding proteins in humans <sup>54</sup>) or by metallo (Zn)-enzymes (10% of the human proteome are potentially zinc-binding *in vivo* <sup>54</sup>). Several polynuclear zinc(II) complexes have also been reported over the years <sup>55–57</sup>. As an example, a 2017 study reported that NSAID's, namely ibuprofen and naproxen, Zn-complexes, eased ulcerations caused by NSAID's themselves. Thus these authors have proposed that zinc supplementation during a NSAID therapy may have a helpful effect on ulcer prevention and healing by reducing the dose of the NSAID's and increasing its potency through the administration of the Zn-NSAID's complexes <sup>58</sup>. There are also some Zn-complexes that can inhibit the activity of specific proteins crucial for the DNA replication cycle. Polynuclear complexes of Zn (II) with flufenamic acid (flu), pyridine (py) or N,N,N',N'-tetramethylethylene (tmen), respectively  $[Zn_3(flu)_6(py)_2]$  and  $[Zn(flu)_2(tmen)]$ , can inhibit the catalytic activity of topoisomerase I <sup>59</sup>.

### III) Iron (Fe)

Iron has two main important features in the human body, that are the ability for participating in reversible oxidation/reduction and in radical reactions, and also a very important and fundamental role in vital biological processes/functions, as electron transport, neurotransmission, oxygen transport, DNA interactions, steroid hormones, etc. <sup>60</sup> As a redox-active metal centre, iron can originate reactive oxygen species (ROS), which lead to oxidative stress and initiation of signalling cascades that are both crucial for cell survival and cell death. Abnormal body accumulation of iron, and/or ROS formation is connected to an astounding number of traumas and chronic degenerative conditions, such as chronic obstructive pulmonary disease (COPD), for example <sup>61</sup>.

The electronic characteristics and the activation and transformation of substrates by different metalloproteins are correlated to the number and type of donor atoms and their geometric arrangements around the metal centre. In the case of iron, mainly as  $Fe^{2+}$  or  $Fe^3$ , coordination's compounds are commonly hexa-coordinated <sup>62</sup>.

Multiple DNA interactions with iron (II and III) complexes have been reported. For example, a Fe(III) complex with a Schiff base (2,3-dimethyl-1-phenyl-4- (2-hydroxy-3-methoxy benzylideneamino) -pyrazol-5-one showed good affinity with CT-DNA, the authors proposed intercalation as the interaction mode through the DNA minor groove <sup>63</sup>. Using that iron complex, a positive antimicrobial activity has also been showed while the isolated Schiff base was inactive <sup>63</sup>. This also has been verified for a complex with Fe(III) and mesalazine (5-aminosalicylic acid; 5-ASA) which has been tested against several species of bacteria, having showed a more intense antimicrobial activity than the parent drug (5-ASA) <sup>64</sup>.

#### **IV) Cobalt (Co)**

Cobalt is “the metal” of vitamin B12 (cobalamin), which plays an important role in mitosis. It is also important for the synthesis of amino acids and for some proteins involved in the formation of the myelin sheaths in nerve cells <sup>65</sup>. Cobalt ions participate in free-radical reactions, such as in the transformation of ribonucleotides into their corresponding deoxy derivatives <sup>66</sup>.

Cobalt can occur in different oxidation states from  $\text{Co}^{+1}$  to  $\text{Co}^{+5}$ , although the most common are  $\text{Co}^{+2}$  and  $\text{Co}^{+3}$  <sup>23,67</sup>.

Many cobalt (II) complexes with different NSAID's and N,N'-donor ligands (2,2'-bipyridylamine, 2,2'-bipyridine and 1,10- phenanthroline) have been reported and characterized. All the referred complexes interact with CT-DNA by an intercalation mode. They all exhibited more activity than the corresponding free ligands <sup>23</sup>. Also, some Co(II) complexes with a Schiff base and N,N'-donor ligands may also have the ability to cleave DNA plasmid (pBR-322 plasmids) in the presence of an oxidant ( $\text{H}_2\text{O}_2$ ), which can be attributed to hydroxyl free radicals formation from the metal complex and the oxidant reaction <sup>68,69</sup>.

#### **V) Manganese (Mn)**

Manganese (Mn) is also an essential element associated to various physiological processes. It is involved in enzymatic reactions and can act as a cofactor. Manganese plays a role as activator and cofactor in gluconeogenesis and in Krebs Cycle, respectively. Manganese ions are crucial in superoxide dismutase (SOD) activity. In humans, Mn-SOD is

a tetrameric enzyme with four subunits each one containing a  $\text{Mn}^{3+}$  ion in a complex with a distorted octahedral geometry (four N- and two O-donors atoms) <sup>26</sup>.

In the central nervous system (CNS), manganese ions act as a cofactor for glutamine synthetase (GS) <sup>70</sup>. Extreme exposure to manganese is linked to adverse psychiatric, cognitive and motor disorders, known as manganism, and it is also been involved in the pathogenesis of hepatic encephalopathy, where it can be a potential neurotoxin <sup>71</sup>.

In biological condition, manganese can be found in three oxidation states, Mn(II) (more common), Mn(III) and Mn(IV) <sup>66</sup>.

Mn(II) have a  $d^5$  electron configuration, easily building complexes with 6 coordination number. However these are often unstable interacting easily with other molecules/ligands which leads to alterations in their coordination spheres <sup>26</sup>. The consequences of these situations are the type of their interaction modes with specific enzymes, which are determined by the spatial arrangements of the atoms in a certain complex <sup>26</sup>. Three Mn (II) complexes containing mefenamic acid (mef), 2,2'-bipyridyl (bipy) and phenanthroline (phen) as ligands, exhibit a LOX-1 inhibitory activity higher than mefenamic acid by itself <sup>72</sup>. LOX-1 (lectin-like oxidized low-density lipoprotein receptor-1) is upregulated in several different types of cancer <sup>73</sup>. They concluded that a complex with two mefenamic acid ligands is capable of inhibiting the LOX-1 enzyme activity, while others with only one of this ligand (mef) tend to inhibit the enzyme activity uncompetitively <sup>72</sup>.

Additionally, it has also been reported that Mn(II) complexes with tolfenamic acid and N,N'-donor ligands (phen, pyridine, or 2,2'-bipyridylamine) and O-donors like  $\text{H}_2\text{O}$  or DMF, interact with CT-DNA, probably via intercalation mode <sup>24</sup>.

## **VI) Nickel (Ni)**

The biological role of nickel is not yet completely understood. In humans, it is found in the nucleic acids, particularly in RNA. Probably it has a role in stabilizing nucleic acids structures, and may help in the production of prolactin and so it is involved in human breast milk production <sup>74</sup>. Nickel is also found in the active sites of some metalloenzymes such as urease, glyoxalase I, lactate racemase, acireductone dioxygenase, etc. <sup>75</sup>. Ni(II) can be transported into cells through calcium channels and/or proteins like DMT-1 (divalent metal transporter 1) <sup>76</sup>.

As Ni(II) has a  $d^8$  electronic configuration it can form octahedral, tetrahedral or square-planar complexes <sup>66</sup>.

Several studies with nickel(II) complexes with different ligands have reported that the most probable, and found, interaction mode with CT DNA is by intercalation <sup>77,78</sup>. As an example, a study in 2013, reported that a Ni(II) complex with NSAID diclofenac (dicl) and 2,2'-dipyridylketoneoxime as ligands binds to CT-DNA by intercalation mode <sup>25</sup>. However, two neutral mononuclear Ni(II) complexes with diclofenac and bipy or 1,10-phen as ligands, *ie*, [Ni(dicl)<sub>2</sub>(bipy)] and [Ni(dicl)<sub>2</sub>(phen)] respectively, were observed to interact with CT-DNA in a different way, being so proposed that the type of interaction was a non-classical intercalative mode, that is by electrostatic or external groove-binding <sup>25</sup>.

## 1.2 Metal ions and ligands: Coordination chemistry

Aiming to improve the therapeutic action and/or to reduce the toxicity of some drug molecules, their coordination of bioactive molecules to metal ions is a very interesting strategy <sup>79,26</sup>.

The crystal field theory (CFT) was established to explain compounds electronic and structural formation. Although with strong limitations its statements keep being extremely useful. It is base in electrostatic interactions between the positively charged central metal ion and the electrons of the ligands, considered as negative point charges. Besides these electrostatic interaction repulsions between ligand electrons and  $d$  electrons of the metal have to be consider. The main point of this theory is focused on the initial five equal energetic  $d$  orbitals of the metal ion and how they are splitted, upon the presence of the “near” ligands, in two or more different energy levels, as illustrated in *figure 3* for an octahedral complex ( $t_{2g}$  and  $e_g$  sets of orbitals). Different ligands will cause different energy splits of the  $d$  orbitals ( $\Delta_{oct}$ ,  $\Delta_{tetrah}$ , etc.), which also depends on the metal ion, on its oxidation state and on the complex geometry. For example, 2,2'-bipyridine, originates a large  $\Delta_{oct}$  (strong field). CFT theory is mainly theoretical and essentially didactic, showing strong limitations. Discrepancies between empirical observations and theory created a need for considering instead the overlap of atomic/molecular orbitals, leading to the ligand field theory (LFT). This theory combines the approximate energies and wave functions of all the atomic orbitals to obtain the best approximations for the energies and wave

functions of complexes making use of “covalency” in the interactions between the metal ion and the ligand <sup>26,66,80</sup>.

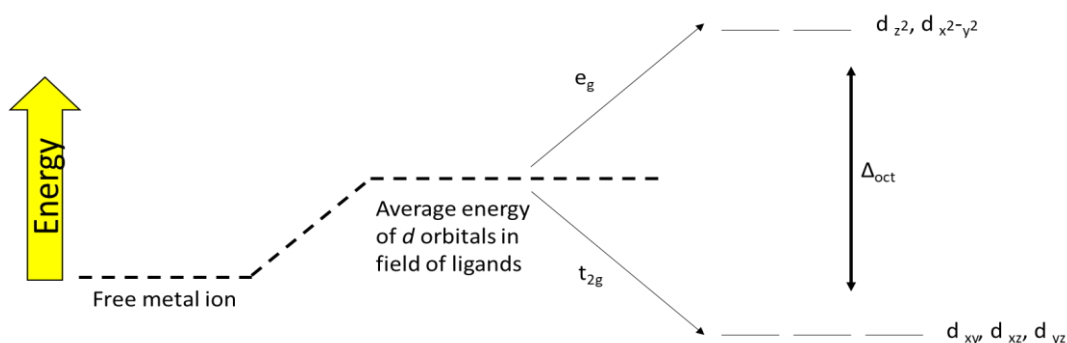


Figure 3: Crystal field d orbital splitting diagram in the formation of an octahedral complex. Adapted <sup>26,79</sup>.

### 1.2.1 N-donor ligands

Nitrogen donor ligands, usually heterocyclic molecules, coordinate to a great variety of metal ions, many of them functioning as typical bidentate, tridentate, etc, ligands <sup>81</sup>. For example, pyridine, a monodentate ligand, is one of the N-donor ligands more used in metal complexes. It can coordinate to all transition metals resulting in different coordination compounds in different oxidation states <sup>82</sup>. This fact is due to the nitrogen lone pair which gives to the pyridine ring its Lewis basic character (figure 4) <sup>82,83</sup>. Some other pyridine derivative ligands, mainly polypyridine systems, also deserve to be noticed, as can act as multidentate ligands. Common examples are: 2,2'-bipyridine, 1,10-phenanthroline and terpyridine.

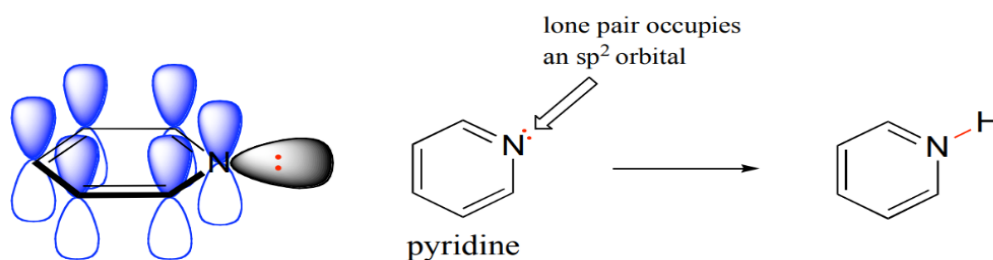


Figure 4: Pyridine ring and its nitrogen lone electron pair. Adapted <sup>82</sup>

### 1.2.2 NSAID's as O-donors

NSAIDs can be divided into different classes according to their chemical structures, appearing commonly grouped into salicylic, arylalkanoic, arylanthranilic and other carboxylic acid derivatives, aniline, p-aminophenol and enolic acid derivatives, pyrazolone, naphthylbutanone, oxicams, sulfonamides, and benzoxazocine derivatives<sup>84,85</sup>.

These compounds, mainly because of their carboxylic acid functional groups, can, after deprotonation, easily coordinate to metal ions in a great versatility of coordination modes, and consequently NSAID ligands are able to coordinate as mono, bidentate, or bridging ligands, in polynuclear complexes (figure 5)<sup>84-86</sup>.

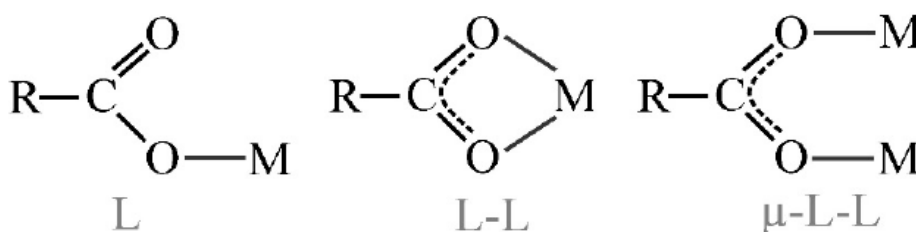


Figure 5: Types of coordination modes between a metal ion and the deprotonated carboxylic group. Adapted<sup>19</sup>.

In this work, NSAIDs ibuprofen and diclofenac, were used as ligands in the synthesis of new complexes (figure 6).

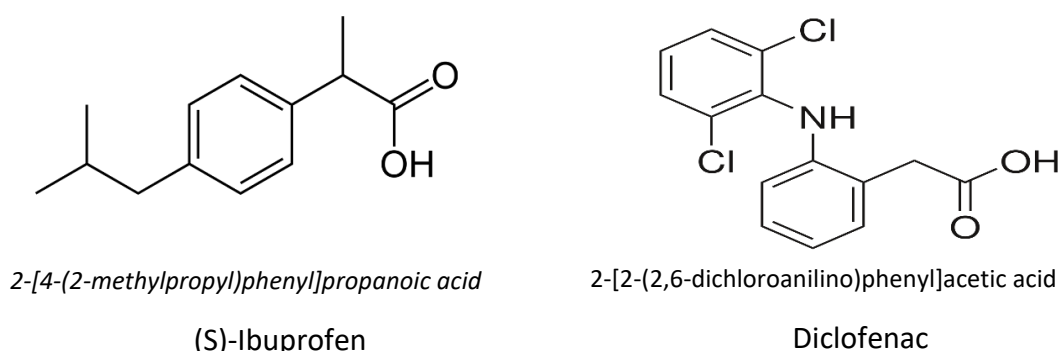


Figure 6: Structure of (S)-Ibuprofen and diclofenac.

There are few reports of metal complexes coordinated with monodentate NSAIDs. For example, naproxen and mefenamic acid act as monodentate ligands in complexes with Co(II) and Zn(II)<sup>86-89</sup>.

A far greater number of complexes show bidentate NSAIDs. Zn(II) complexes with mefenamic acid (Hpko) or other heterocyclic ligands, give rise to distinct carboxylate binding modes, monodentate in  $[\text{Zn}(\text{mef-O})_2(\text{Hpko-N,N'})_2] \cdot \text{EtOH}$ , bidentate in  $[\text{Zn}(\text{mef-O,O'})_2(\text{bipy})]$ , and both in  $[\text{Zn}(\text{mef-O})(\text{mef-O,O'})(\text{phen})(\text{H}_2\text{O})]$ <sup>89</sup>. The same coordination arrangements of a O-donor (tolf - tolfenamic acid) ligand is found in a mononuclear Mn(II) complex,  $[\text{Mn}(\text{tolf-O})(\text{tolf-O,O})(\text{phen})(\text{H}_2\text{O})]$ <sup>24</sup>.

On the other hand, Cu(II) complexes with several NSAIDs, such as ibuprofen, naproxen, tolmetin and diclofenac mainly leads to the dimeric  $[\text{Cu}_2\text{L}_4(\text{H}_2\text{O})_2]$  structures with the two copper(II) ions bridged by four carboxylate groups of the two NSAIDs, where each of them is a bridging bidentate ligand<sup>90</sup> (figure 7).

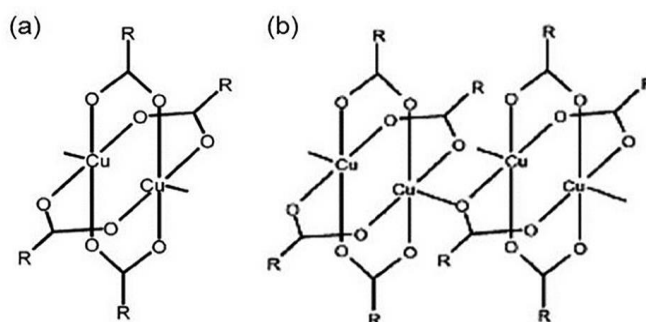


Figure 7: Paddle-wheel structural types involving  $\text{Cu}^{2+}$ . (a) Paddle-wheel dimer and (b) polymeric dimer. Adapted<sup>90</sup>

### 1.2.3 Complexes structure determination analytical techniques and spectroscopic studies

The determination of the structure of complexes can be accomplished by a series of spectroscopic methods and different analytical techniques, such as, X-ray diffraction, crucial to elucidate 3D structures, UV-Vis and CD (circular dichroism) spectrophotometry are useful to analysed the atoms distribution around the metal ion centre and to study the symmetry characteristics of the complex (chirality, isomers, etc.), another important technique is FTIR (Fourier transform infra-red) that can be used to explain the type of ligands coordination to the metal ion. Nuclear magnetic resonance (NRM) can also be sued with this same propose.

Other information's on the coordination compounds can be acquired with recourse to TGA (thermogravimetric analysis) and DTA (differential thermal analysis) <sup>19</sup>.

The complexes structural features, that is, coordination type and, numbers, geometry, redox states of the metal ions and ligands, the thermokinetics complexes behaviour, offers a wide range of targets that can and may be exploited <sup>91</sup>. Regarding to their observable or expected biological activity, structural aspects of these complexes bearing NSAIDs ligands (drugs) are interesting coordination compounds to target different biological molecules.

## 1.2 Molecular targets of the metal complexes

The most frequent form of DNA is B-DNA, with major and minor grooves that, although differing in many aspects (size, shape and hydrogen bonding sites), provide binding/interactions sites for different molecules (figure 8) <sup>92,93</sup>.

The success of some modes of chemotherapy lays on interactions between metallodrugs and DNA, for most cases. The example of cisplatin was revolutionary in treating different types of cancer, precisely because of these possibilities of DNA interaction. Then, in particular, cisplatin binds covalently to DNA, as is schematically illustrated in figure 9 <sup>94,95</sup>.

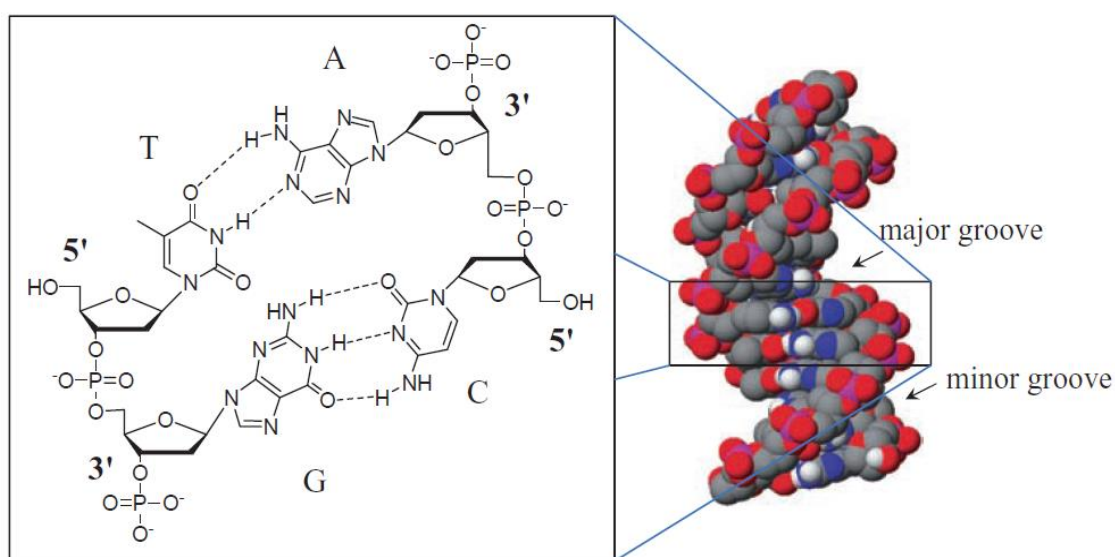


Figure 8: B-DNA form and its major and minor grooves. Adapted <sup>91</sup>.



DNA is consequently an exceptional target for metal ions. Firstly because of the negatively charged phosphate groups, several ions like,  $\text{Ca}^{2+}$ ,  $\text{Fe}^{2+}$ ,  $\text{Mn}^{2+}$ ,  $\text{Ni}^{2+}$ , and  $\text{Zn}^{2+}$ , interact with DNA neutralizing its charge, so some of these metal ions are essential for DNA structure stability<sup>95</sup>. Besides the most probable sites for these electrostatic interactions, that is the phosphate groups, some atoms of the heterocyclic nucleobases, N and/or O, as well, in minor extent, the hydroxyl groups of the sugars molecules scaffold are also adequate sites for interactions<sup>96</sup>.

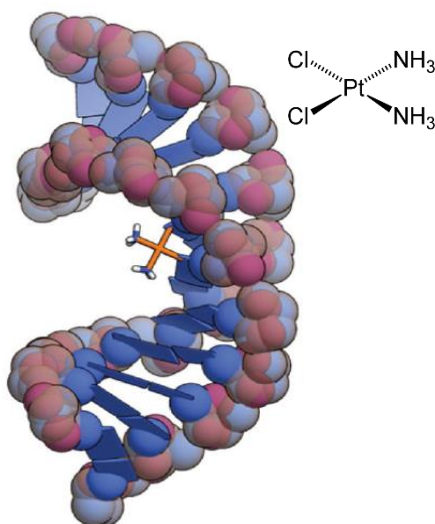


Figure 9: Adduct between cisplatin and DNA. Adapted<sup>93</sup>.

Concerning DNA-metal coordination compounds (drugs), the metal complex geometry and the spatial arrangement of its ligands, or their type, have an interesting influence on the binding activity of the drug<sup>92,97</sup>. It may cause certain changes in the DNA structure with inherent consequences at the biological level mechanism, such as transcription, replication and DNA repair processes<sup>98</sup>.

Some complexes with different N-donor ligands have been investigated, like lanthanide complexes with 2,2'-bipyridine<sup>99</sup>, cobalt (II) complexes with 2,2'-bipyridylamine, 2,2'-bipyridine and 1,10'-phenanthroline for which intercalation was the author's suggestion as the most possible DNA-binding mode<sup>23</sup>. In particular, some complexes show specific characteristics, for example, a palladium complex with 1,10'-phenanthroline showed higher anticancer activity against chronic myelogenous leukemia

cell lines that cisplatin<sup>100</sup>. There are also examples of dinuclear complexes, like terpyridine complexes with different metals (ruthenium, osmium, iron, and cobalt)<sup>101</sup>.

### 1.3.1 Binding modes of metal complexes to DNA

Metal complexes bind to the DNA helix through several different ways. In general, these modes can be divided into two main groups, that is, covalent and non-covalent binding<sup>92</sup>. In this last group (non-covalent binding) are clustered intercalation and groove binding, that used to be highlighted<sup>102,103</sup>.

#### Covalent binding

Covalent binding of a metal coordination compounds to the DNA chain is actually the cisplatin DNA-binding mechanism, which was only fully understood in 1995, by Lippard group, through the determination of the crystal structure of the adduct “cis-platin/DNA”. As the solvent environment plays an essential role in many biochemical processes in general, is expected to have a particular strong effect on the activation (hydrolysis) of cisplatin, as well as cisplatin derivatives<sup>104</sup>.

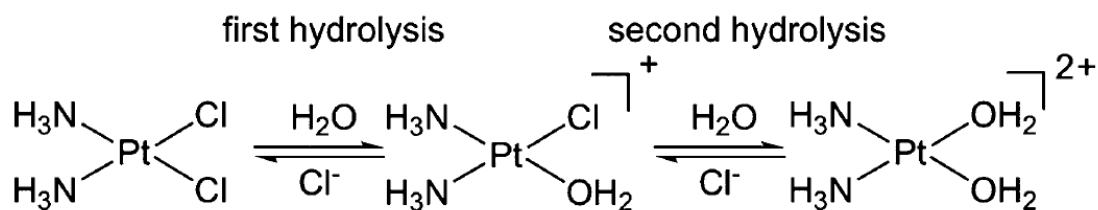


Figure 10: Cisplatin hydrolysis and formation of aqua-complexes. Adapted<sup>104</sup>.

The covalent binding is possible only after the hydrolysis of Pt–Cl bonds, in order to form a Pt–aqua complex (figure 10). This reaction occurs inside the cell because the extracellular chloride high concentration blocks the hydrolysis process. However, once inside the cell, as the chloride concentration is lower, Pt–Cl bonds hydrolyse, which, at first place gives rise to the mono-aqua product  $[\text{Pt}(\text{NH}_3)_2\text{Cl}(\text{OH}_2)]^+$ , followed by the formation of another aqua complex  $[\text{Pt}(\text{NH}_3)_2(\text{OH}_2)_2]^{2+}$ . These hydrolysed cisplatin complexes directly bind to DNA, through purine bases at the N7 position of either guanine (G) or adenine (A) in the dinucleotide sequences GG and AG to form interstrand cross-links and 1,2- or 1,3-intrastrand cross-links, thereby targeting the cell division process as its

primary mode of anticancer activity<sup>92,104–107</sup>. After the binding of the cisplatin, DNA duplex is significantly bent, provoking a change of its conformation, B-DNA to A-DNA<sup>103</sup>.

Another example of DNA-covalent binding by the same type of mechanism is the one carried out by phenanthriplatin, a cisplatin derivate. In this specific case, the binding to DNA involves, partial intercalation of the phenanthridine rings followed by Pt-Cl hydrolysis and N7 purine base bonding<sup>108</sup>. This mechanism is illustrated in figure 11.

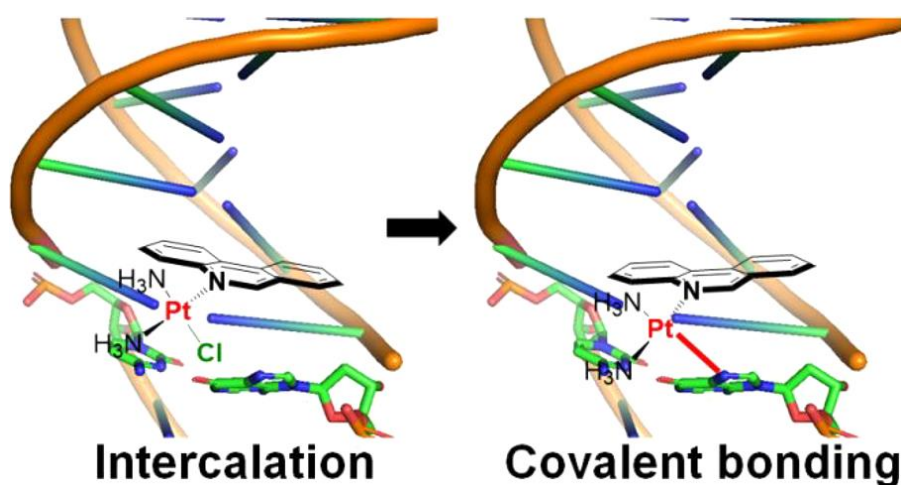


Figure 11: Phenanthridine DNA- binding mechanism. Adapted<sup>108</sup>.

### Non-covalent binding

In a different approach and by contrast with the DNA-covalent interaction described above, metal complexes can interact with DNA in a reversible and non-covalent manner. This type of interaction offers several possibilities to contribute to the binding, like hydrogen bonding,  $\pi$ - $\pi$  stacking, and hydrophobic interactions<sup>102</sup>.

One of the sub-types of a “non-covalent interaction” has already been slightly approached above, because as Manning’s polyelectrolyte theory affirms, the DNA negative can be compensated by small alkali cations<sup>92–96,98,102,109</sup>.

Other sub-types of non-covalent binding modes of metal complexes to DNA, are showed below<sup>107</sup>.

### Intercalation

Intercalation is anti-cooperative at adjacent sites, meaning that intercalators can only bind at alternative DNA base pairs. When an intercalator binds to one DNA base pair

its two neighbouring sites may continue unoccupied <sup>110,111</sup>. Essentially there are two modes of intercalation: classical intercalation and threading intercalation, both illustrated in figure 12 <sup>102,112</sup>.

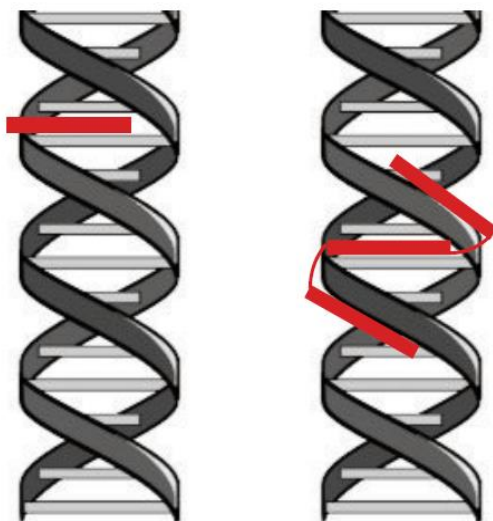


Figure 12: Two modes of DNA-intercalation. Left: classical intercalation; right: threading intercalation. Adapted <sup>101</sup>.

Classical intercalators simply bind to double-stranded DNA with their all aromatic rings inserted between two base pairs, that is, intercalation DNA site. Threading intercalators instead, interact simultaneously with both DNA grooves <sup>112</sup>. This binding mode is accomplished by the insertion of one of the ligands of the metal complex, usually a planar aromatic ring, into the DNA between two base pairs. Normally, full insertion of the intercalating ligand is observed in metal complexes with square-planar geometries <sup>113</sup>. Inserting one more variable, we can still have full or partial intercalation like is illustrated in figure 13, where dipyrrophenazine (dppz) ligand show classical full intercalation and 1,10-phenanthroline (phen) just has partial intercalation or “semi-intercalation” <sup>113</sup>.

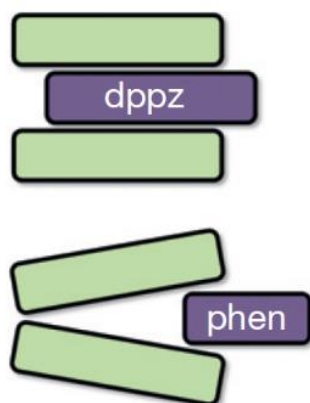


Figure 13: Two types of intercalation. Full and partial intercalation by the ligands dppz (dipyridophenazine) and phen (phenanthroline). Adapted <sup>113</sup>.

### Groove binding

Groove binding is another DNA binding mode for complexes, which is the association of the whole or a part of the complex with one of the grooves or with both of them. This association is carried out by a combination of different parameters like, electrostatic forces, van der Waals contacts, hydrophobic interaction and hydrogen bonding <sup>113</sup>. Once there is no free energy costs for this kind of binding, groove binders have bigger association constants than mere intercalators <sup>102</sup>.

Most of complexes bind to the minor groove especially to the A/T-rich sequences, because these A/T-rich sequences have greater electronegative potential than the G/C-ones and are more flexible (once they have only two hydrogen bonds between them). Essentially these characteristics make A/T-rich sites more “attractive” for the binding of complexes especially if they are positively charged compounds <sup>102,113</sup>.

### Telomeric DNA

With the consistent advance in cancer research and in anti-cancer metal compounds come the study of new targets, being telomeric DNA one of them. This region of DNA consists of a guanine-rich TTAGGG repeats folded into G-quadruplex structures or T-loops <sup>114</sup>. In every cell division, the telomeric DNA shortens and after a limited number of divisions the cell stop dividing and dies by apoptosis. However, by the action of the telomerase enzyme the length of the telomeric DNA can be maintained <sup>114</sup>. In the most part of tumours, this enzyme is overexpressed, which makes the cancer cells almost “immortal”,

once the missing biological signal of the telomerase don't allow the cells to kill themselves

102.

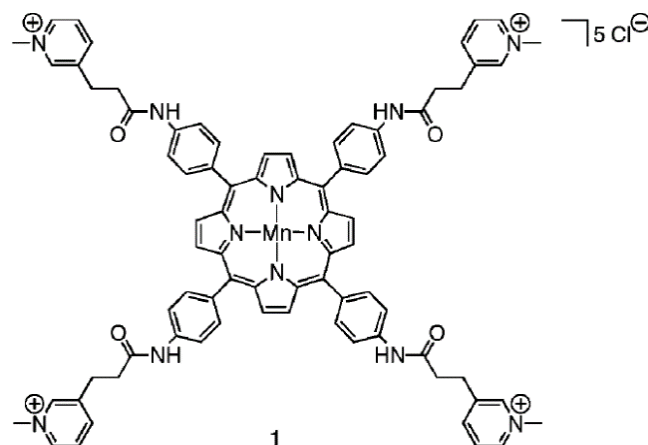


Figure 14: Structure of pentacationic manganese (III) porphyrin. Adapted <sup>115</sup>.

Once telomerase is very specific for the type of DNA organization in telomere (single-stranded overhang), G-quadruplexes are a very interesting target for metal complexes with the purpose of avoiding telomerase to maintain telomere lengths <sup>91,114</sup>. Consequently, here the crucial challenge in the drug design is the selectivity to G-quadruplexes instead of to DNA duplex. One of the best examples of this situation is the pentacationic complex manganese (III)-porphyrin (figure 14), which shows an exceptional 10000-fold selectivity for telomeric region over duplex DNA <sup>115</sup>.

### 1.3.2 Target proteins

For decades metallodrugs research was focus on DNA binding, which, as was described above, relies on the damage that metal complexes inflict on the DNA structure. However, metallodrugs can exert its effects on other molecules, proteins are one of these targets <sup>116</sup>. Of all the molecules present in living organisms, proteins are the most abundant and they constitute a very interesting target for metal complexes, once they are involved on almost every life process. As was been pointed before, there are some proteins that play key roles on cancer initiation and progression <sup>117</sup>. Topoisomerase role in cancer was already explained above, indeed there are metal complexes that bind to this protein and inhibit its

activity, which is another way to stop telomeres length maintenance <sup>59,116</sup>. Another interesting target are the kinases proteins, deregulation of these proteins are usually found on tumours and can be crucial for the survival and progression of cancer cells <sup>118</sup>. There are already a few metal complexes that were design with the purpose of binding to the ATP binding site of kinase proteins and act as its inhibitors <sup>119,120</sup>.

However, we can't look at proteins only as targets to fight cancer, they can also act as "self" drug delivery system. In this field, albumin (HSA) is one of the most interesting targets <sup>121</sup>. HSA is the most abundant protein on blood plasma (60% of the total protein content) and because of its features it can reversibly bind to drugs, and this binding enhance the drug biodistribution and bioavailability, it is already known that aspirin, ibuprofen, and warfarin benefit from this interaction <sup>116,122</sup>. This interaction has been exploited in Abraxane (FDA-approved oncologic drug), in this case HSA is responsible for the drug delivery, in fact, drug design has focused on this, several Pt(IV) were designed to bind to the fatty acids binding pocket of HSA <sup>123</sup>. When approaching the evaluation of small molecules affinity for albumins, bovine serum albumin (BSA) is usually selected as a trustworthy model, due to its structural similarity with human serum albumin (76%) <sup>124</sup>.

### **1.3.3 Spectroscopic studies for biological measurements**

Several techniques can serve the propose to study the interaction between metal complexes and biological targets such as DNA and HSA or BSA. For example, fluorescence spectroscopy can be used for study the binding of coordination compounds to HSA or DNA, and therefore calculate their binding constants. While HSA/BSA has intrinsic fluorescence, DNA has not, hence for this last biological target competitive assays has to be carried out, where ethidium bromide, usually serving as a probe, is used for competition intercalative assays <sup>125–127</sup>. UV-VIS spectrophotometry is another spectroscopic technique very often used in this type of studies <sup>128</sup>, allowing to observe the hyperchromic or hypochromic effects caused on the DNA structure by metal complexes <sup>129</sup>. Circular dichroism spectroscopy is also used with the same propose as UV/Vis spectroscopy, although allowing other specificities (mainly chiral features), because with this spectroscopic technique the binding to specific motifs can be measure (like  $\alpha$ -helix), both in DNA and BSA/HSA <sup>126</sup>.

## 1.4 Objectives

The main objective of this work was the synthesis and structure determination of new metal complexes with anti-tumoral properties. In order to obtain the novel metallodrugs, several synthesis with different transition metals (such as Cu, Co and Ni) combined with different ligands (such as NSAID's and pyridine derivatives) were performed. Studies regarding the capacity of the new metal complexes to interact with deoxyribonucleic acid (DNA) and bovine albumin (BSA) were performed by several spectroscopic techniques. *In vitro* studies to determine the cytotoxic activity and lipid peroxidation of the metal complexes on breast cancer cell lines vs non-tumoural cells were also undertaken. At last, this work allows us to evaluate the influence of the metal centre on the biological behaviour of the metal complexes.



## **Chapter 2 – Experimental Procedure**



## 2.1 Reagents and materials

ZnCl<sub>2</sub>, 2,2':6',2''-terpyridine (terpy), diclofenac sodium salt (diclo), deoxyribonucleic acid sodium salt, from calf thymus (CT-DNA) and S (+)-ibuprofen (ibu) were purchased from Sigma-Aldrich; 2,2'-bipyridine (bipy) and 2,2'-dipyridilamine (dipy) from Fulka; 1,10-phenanthroline (phen) from Alfa Aesar; CoCl<sub>2</sub>·6H<sub>2</sub>O from Panreac and CuCl<sub>2</sub>·2H<sub>2</sub>O from CARLO ERBA. All chemicals were reagent grade and were used as purchased without any further purification. Solvents (ethanol and methanol) were of analytical grade and had been used as received (from VWR chemicals). BSA was purchased from VWR™ and used without further purification.

## 2.2 Methods and instrumentation

Infrared (IR) spectra were recorded on a Mattson-7000 FT-IR spectrophotometer with samples prepared as KBr disks. UV-visible (UV-Vis) spectra were recorded on a GBC Cintra 303 spectrophotometer. Circular dichroism (CD) experiments were performed with a JASCO J-1500 CD spectrometer, at room temperature. Powder XRD data were obtained on a PANalytical Empyrean diffractometer, using K $\alpha$ (Cu) radiation with a curved graphite monochromator. Intensity data were collected by the step counting method (step 0.05°) in the range 3.5° < 2 $\theta$  < 50°. TGA were carried out under air, with a heating rate of 10 °C min<sup>-1</sup>, using a Shimadzu TGA-50 analyser. The total weight losses (%TG) have been calculated assuming final decomposition of the complexes, at the end of the experiments, to a mixture of oxides. C, H, and N elemental analyses were performed on a Leco CHNS-932 apparatus.

## 2.3 X-ray crystallography (single-crystal X-ray)

Crystalline samples were analysed using a Stemi 2000 stereomicroscope equipped with Carl Zeiss lenses. Crystals were mounted on a Hampton Research CryoLoops and data collected at 150 (2) K, or on a Bruker D8 QUEST, equipped with Mo-K $\alpha$  sealed tube ( $\lambda$  = 0.71073 Å), a multilayer TRIUMPH X-ray mirror with a PHOTON 100 CMOS detector, and a low-temperature system (Oxford Instruments Cryostrem 700+ Series), or collected on a Bruker X8 Kappa APEX II CCD area-detector diffractometer (Mo K $\alpha$  graphite-

monochromatic radiation,  $\lambda = 0.71073 \text{ \AA}$ ) equipped with a low temperature system (also from Oxford Cryosystems Series 700) remotely monitored using Cryopad software.

## **2.4. Synthesis of the complexes**

### **2.4.1 Synthesis of complex [Cu(ibu)(2,2'-dipy)Cl] (1)**

NSAID ibuprofen (99.2 mg; 0.5 mmol) was dissolved in methanol (10 mL) and deprotonated with KOH (30.1 mg; 0.5 mmol), after 1h stirring. This solution was added dropwise, simultaneously with a methanolic solution of 2,2'-dipyridylamine (85.4 mg, 0.5 mmol) to a stirred methanolic solution (20 mL) of  $\text{CuCl}_2 \cdot 2\text{H}_2\text{O}$  (84.9 mg; 0.5 mmol). The resultant mixture was stirred for 30 min and left for slow evaporation at room temperature. Green crystals of [Cu(ibu)(2,2'-dipy)Cl] were collected after one week.

### **2.4.2 Synthesis of complex [Ni(terpy)](dicl)<sub>2</sub>·8H<sub>2</sub>O (2)**

An ethanolic solution (10 mL) of the NSAID diclofenac (127.0 mg; 0.4 mmol) and 2,2':6',2''-terpyridine (93.1 mg; 0.4 mmol) was added dropwise to a stirred ethanolic solution (10 mL) of  $\text{NiCl}_2 \cdot 6\text{H}_2\text{O}$  (4.71 mg; 0.2 mmol). The resulting solution was stirred for half an hour and left to evaporate at room temperature. Dark orange crystals were obtained after 10 days.

### **2.4.3 Synthesis of complexes [M(dicl)<sub>2</sub>(2,2'-bipy)]; M = Co(II) and Ni(II), for (3) and (4)**

Complexes **3** and **4** have been prepared in a similar way to complex **2**, using 2,2'-bipyridine as the N,N'-donor ligand (62.5 mg, 0.6 mmol) and diclofenac as the NSAID (126.8 mg, 0.4 mmol) and  $\text{CoCl}_2 \cdot 6\text{H}_2\text{O}$  (46.9 mg, 0.2 mmol) for complex **3**, or  $\text{NiCl}_2 \cdot 6\text{H}_2\text{O}$  (48.3 mg, 0.2 mmol) for complex **4**. Light red (**3**) and blue (**4**) crystals were collected after 2 weeks.

### **2.4.4 Synthesis of complexes [M(dicl)<sub>2</sub>(1,10-phen)]; M = Co(II) and Ni(II) for (5) and (6)**

Complexes **5** and **6** were synthesised using the N,N'-donor ligand 1,10-phenanthroline (72.4 mg; 0.4 mmol) and diclofenac (126.8 mg; 0.4 mmol) and  $\text{CoCl}_2 \cdot 6\text{H}_2\text{O}$  (47.1 mg; 0.2 mmol) for complex **5**, and  $\text{NiCl}_2 \cdot 6\text{H}_2\text{O}$  (47.0 mg; 0.2 mmol) for complex **6**. Light red (**5**) and green (**6**) crystals were collected after 2 weeks.

## 2.5 Albumin binding studies

### 2.5.1 Experimental details

All experiments involving BSA have been performed in Tris-HCl/NaCl buffer solutions (5 mM Tris-HCl/50 mM NaCl buffer; pH 7.4). The concentration of the BSA was determined spectrophotometrically using an extinction coefficient  $43824 \text{ M}^{-1} \text{ cm}^{-1}$ <sup>130</sup>. Albumin binding studies were performed by UV-Vis, CD and fluorescence spectroscopies.

### 2.5.2 BSA interaction studies by UV-vis spectroscopy

The UV spectra of BSA were recorded at room temperature (cell path length=1 cm). The BSA/complexes interactions experiments were performed in the absence and in the presence of the complexes in different concentration. Each spectrum was baseline corrected with Tris-HCl/NaCl buffer.

### 2.5.3 BSA interaction studies by circular dichroism spectroscopy

In the DC experiments BSA concentration and the path length of the cell used were 0.3  $\mu\text{M}$  and 1 cm, respectively. The spectrometer was purged with  $\text{N}_2$  (g), at a flow of 7 L/min, prior and during to the experiment. Each spectrum was baseline corrected and taken as the average of five accumulations at a scan rate of  $100 \text{ nm min}^{-1}$  with a response time of 4s, and a bandwidth set on 0.50 nm.

CD results are presented in terms of the mean residue ellipticity (MRE), in  $\text{deg.cm}^2.\text{dmol}^{-1}$  according to the following equation<sup>131</sup>:

$$MRE = \frac{\text{ObservedCD (mdeg)}}{C_p.n.l.10} \quad (\text{Equation 1})$$

where  $C_p$  is BSA molar concentration,  $n$  is the number of amino acid residues (583 for this protein) and  $l$  the path-length (1 cm). To calculate the  $\alpha$ -helix contents of the free and altered BSA, the following equation was used<sup>131</sup>:

$$\alpha - \text{helix (\%)} = \frac{MRE_{208} - 4000}{33000 - 4000} \times 100 \quad (\text{Equation 2})$$

where  $MRE_{208}$  stands for the observed value of MRE, 4000 is the MRE value of the  $\beta$ -form and random coil conformation cross, and 33000 the MRE value of the  $\alpha$ -helix of the pure protein, all the MRE values at 208 nm.

#### 2.5.4 BSA interaction studies by fluorescence spectroscopy

BSA owe its intrinsic fluorescence to the two tryptophan residues (Trp-134 and Trp-212) <sup>132</sup>. The interaction between the metal complexes and BSA can be monitored by the quenching of this fluorescence upon the addition of complexes. The spectra's were recorded on a Jasco Spectrofluorometer FP-8300 fluorometer, excitation bandwidth set at 5nm; emission bandwidth set at 5 nm; sensitivity low; excitation wavelength 295.0 nm; at a scan speed 200 nm/min.

The results can be analysed by the Stern–Volmer equation (*equation 3*).

$$\frac{F_0}{F} = 1 + K_{sv}[Q] \text{ (Equation 3)}$$

where  $F_0$  and  $F$  are fluorescence intensities of free BSA and in the presence of the quencher (complexes) respectively, at different concentrations  $[Q]$ , which can be used to calculate the Stern-Volmer quenching constant ( $K_{sv}$ ) <sup>133</sup>. The value of  $K_{sv}$  can be obtained directed from the slope of the obtained lines calculated by equation 3.

### 2.6 Interaction with CT-DNA

#### 2.6.1 Experimental details

All experiments involving CT-DNA were performed in Tris-HCl/NaCl buffer solution (5 mM TRIS-HCl/50 mM NaCl buffer; pH 7.4), at room temperature. The purity of CT-DNA solutions was confirmed by UV absorbance at 260 nm and 280 nm ( $A_{260}/A_{280}$ ), ratio, considering that a value of 1.81 which is indicative that a CT-DNA solution was sufficiently free of protein. The CT-DNA concentration was calculated from the UV absorbance intensity, at 260 nm, as follows  $1,0 = 50 \mu\text{g/mL}$  <sup>134</sup>.

#### 2.6.2 EB competitive studies by fluorescence spectroscopy

Competitive studies with ethidium bromide (EB) for each of the synthesised complexes have been carried out by fluorescence spectroscopy in order to examine whether the complex can displace EB from its CT-DNA – EB adduct. The CT-DNA – EB adduct was prepared by adding equal volumes of 0.36 mM EB and 1.15 mM CT-DNA solutions, in Tris-HCl/NaCl buffer (5 mM TRIS-HCl/50 mM NaCl buffer; pH 7.4). The “interaction effect” of the complexes with the DNA-EB was studied by adding fixed volumes of increasing

concentrations of the complexes to CT-DNA – EB solution. The spectra's were recorded on a Jasco Spectrofluorometer FP-8300 fluorometer; excitation bandwidth set at 5nm; emission bandwidth set at 5 nm; sensitivity low; excitation wavelength 295.0 nm; at a scan speed 200 nm/min.

### **2.6.3 CT-DNA interaction studies by circular dichroism spectroscopy**

CT-DNA/complexes interaction studies were also analysed by circular dichroism at room temperature. The CD-spectrometer was purged with N<sub>2</sub>(g) prior and during the experiments (flow rate = 7 L/min). Each spectrum was baseline corrected and taken as the average of five accumulations at a scan rate of 100 nm min<sup>-1</sup> with a response time of 4s, and a bandwidth set on 0.50 nm. The CT-DNA concentration was 100 µM, except for interactions with complexes (1) and (2) which were 50 µM (1cm cell path length).

### **2.6.4 CT-DNA interaction studies by UV-vis spectroscopy**

The spectra of CT-DNA were recorded at room temperature (cell path length=1 cm). The CT-DNA/complexes interactions experiments were performed in the absence and in the presence of the complexes in different concentration. Each spectrum was baseline corrected with Tris-HCl/NaCl buffer.

## **2.7 *In vitro* biological assays**

### **2.7.1 Materials**

RPMI 1640 medium, human epidermal growth factor, cholera toxin, bovine insulin, hydrocortisone and MTT(3,4,5-dimethylthiazolyl- 2–2,5-diphenyl-tetrazolium bromide) were purchased from Sigma-Aldrich (St. Louis, MO, USA). Dulbecco's Modified Eagle's Medium (DMEM:Ham's F12 medium (1:1)), L-glutamine, sodium bicarbonate, fetal bovine serum (FBS) and antibiotic/antimycotic were purchase from Biochrom, Berlin, Germany. Horse serum was purchased from GIBCO (Life Technologies Corporation, CA, USA). All other chemicals used were of analytical grade.

### **2.7.2 Cell culture**

MCF-7, an estrogen receptor (ER)-positive human breast epithelial adenocarcinoma cell line and MDA-MB-231, a triple negative human breast adenocarcinoma cell line, were

obtained from the American Type Culture Collection (ATCC) and used between passages 83-98 and 70-86, respectively. MCF-12A cell line, a non-tumorigenic epithelial cell line, was also obtained from ATCC and used between passages 28-34. Cells were maintained in a humidified atmosphere of 5% CO<sub>2</sub>-95% air and were grown in RPMI 1640 supplemented with 2 mM L-glutamine, 10 mM sodium bicarbonate, 15% heat-inactivated FBS and 1% antibiotic/antimycotic (MCF7 and MDA-MB-231 cells); DMEM:Ham's F12 medium (1:1) supplemented with 20 ng/ml human epidermal growth factor, 100 ng/mL cholera toxin, 0.01 mg/mL bovine insulin, 500 ng/mL hydrocortisone, 5% heat-inactivated horse serum and 1% antibiotic/antimycotic (MCF-12A). Culture medium was renewed every 2-3 days, and the culture was split every 7 days. For the determination of viability and oxidative stress cells were seeded on 24-well culture dishes (2 cm<sup>2</sup>; Ø 16 mm; TPP®, Trasadingen, Switzerland) and used after 5 days (90% confluence).

### **2.7.2 MTT assay**

After a 24 h-exposure of the cells to increasing concentrations of the complexes (10–100 µM), 50 µL of MTT solution (5 mg/mL) was added to each well and the cells were further incubated for 3 h at 37 °C. Afterwards, the MTT solution was removed and the cells were lysed by the addition of 200 µL of dimethyl sulfoxide (DMSO) followed by plate shaking for 10 min at room temperature. Optical density (OD) for the solution in each well was determined at both 540 and 660 nm. OD at 660 nm corresponds to unspecific light absorption and was subtracted from the OD at 540 nm to give the OD value specific to formazan crystals derived from MTT cleavage, which is proportional to the number of viable cells with active mitochondria. Results are presented as number of viable cells (in % of control) (n=6).

### **2.7.3 TBARS assays**

Cells were exposed to the highest complex's concentration tested in the MTT assay (50 or 100 µM) for 24h, and oxidative stress was determined by lipid peroxidation (malondialdehyde). At the end of the 24h-treatment period the reaction was started by addition of 50% (w/v) trichloroacetic acid (TCA) to each sample, followed by a centrifugation for 2 min at 10000 rpm. Then, 1% 2-thiobarbituric acid was added to the



supernatant and the reaction was carried out in a boiling water bath for 40 min. A pink-coloured complex was quantified spectrophotometrically at 535 nm.

## **2.8 Statistical analysis**

The results are expressed as Mean  $\pm$  SD from 6 similar experiments, each one performed in triplicate. Student's "t-test" was used to determine the level of significance and the following values \*  $P < 0.05$ , calculated compared to control unless stated otherwise.



## **Chapter 3 – Results and discussion**



Within this work we were able to synthesise six new different complexes that can be divided into two different groups. The complexes (1) and (2) will be discussed individually, and because of their structural similarities, complexes (3) to (6) were clustered together in a second group.

### 3.1. Complex [Cu(Ibu)(2,2'-dipy)Cl] (1)

#### 3.1.1 Synthesis

The synthesis of complex (1) was performed as described in detailed in section 2. (2.4.1). Briefly, a methanolic solution of ibu was added dropwise and simultaneously with a methanolic solution of 2,2'-dipyridylamine to a stirred methanolic solution of  $\text{CuCl}_2 \cdot 2\text{H}_2\text{O}$ .

#### 3.1.2 Single crystal structure

Complex (1) was unveiled by single-crystal X-ray diffraction analysis and formulated as  $[\text{Cu}(\text{Ibu})(2,2'\text{-dipy})\text{Cl}]$ , crystallizing in the monoclinic space group  $P2_1$ . More crystallographic data are shown in annex I. The asymmetric unit is composed of two complex units, each containing a molecule of ibuprofen bidentated (O,O) to the metal centre, one molecule of 2,2'-dipyridylamine coordinated to Cu(II) ion, also in a bidentated mode by two N-atoms, and a chloride ion acting as a charge balancing ion. The Cu(II) metal centre is then pentacoordinated with the coordination sphere  $\{\text{CuO}_2\text{N}_2\text{Cl}\}$  resembling a pyramidal quadrangular geometry (figure 16). The powder X-ray diffraction pattern of complex (1) prepared in this work agrees well with the powder X-ray diffraction calculated from the single crystal X-ray data (figure 15).

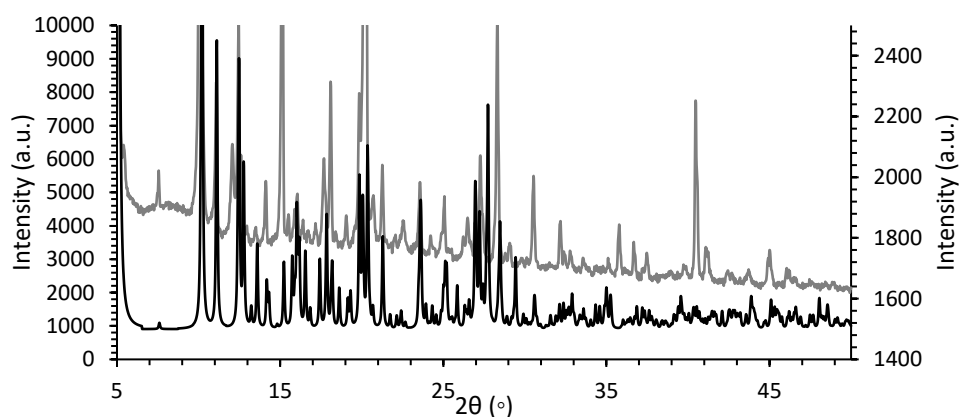


Figure 15: Experimental and by crystal X-ray data XRD graph for complex (1). Black line = single crystal X-ray data; Grey line = Complex (1)

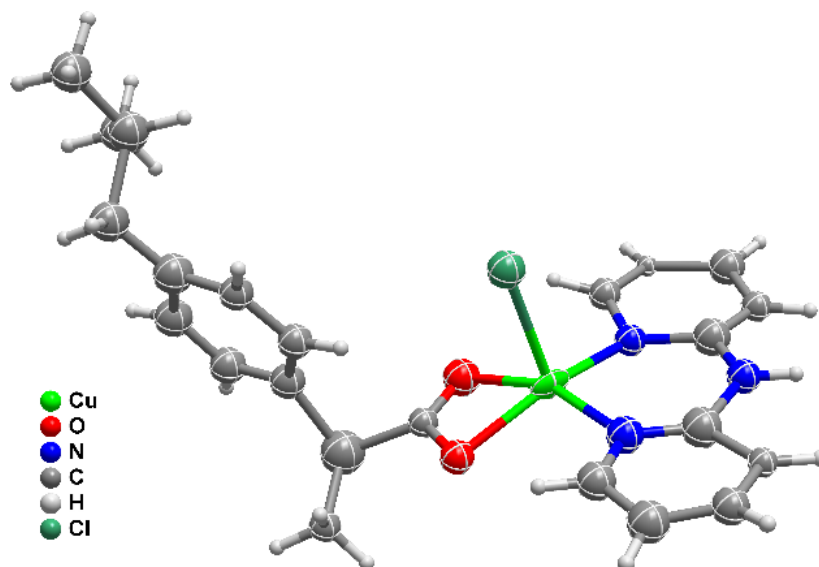


Figure 16: Representation of the complex  $[\text{Cu}(\text{Ibu})(2,2'\text{-dipy})\text{Cl}]$  (1) showing all atoms represented as small spheres with arbitrary radius. The asymmetric unit is composed of two  $[\text{Cu}(\text{Ibu})(2,2'\text{-dipy})\text{Cl}]$  units.

### 3.1.3 Infrared spectra

The most important spectral bands of the ligands and complex (1), that provide information regarding the type of functional groups, are listed in Table 1.

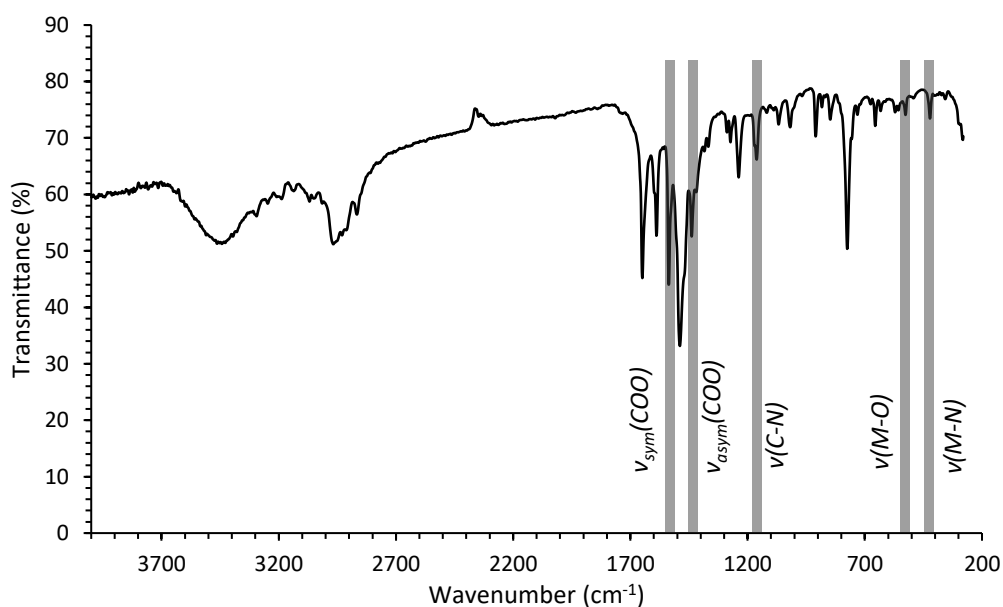


Figure 17: IR spectra of complex (1) with all the relevant peak highlighted.

According to literature <sup>20</sup>, the difference between the asymmetric peak of carboxylate and the symmetric peak ( $\Delta\nu = \nu_{\text{asym}}(\text{COO}) - \nu_{\text{sym}}(\text{COO})$ ) of this same group give us information about its coordination mode, if this difference is lower than  $200 \text{ cm}^{-1}$  the coordination between the metal and the carboxylate ligand is bidentate. In the IR spectra of complex (1) (figure 17) the  $\Delta\nu = 150 \text{ cm}^{-1}$ , so the ibuprofen is probably bidentate to the copper ion. The absence of the strong band  $\nu(\text{C=O}) = 1700 \text{ cm}^{-1}$  also supports the fact that the coordination is bidentate. The presence of the peak  $\nu(\text{C-N}) = 1162 \text{ cm}^{-1}$  in complex's spectra confirms that the coordination is through all the nitrogen atoms of the N-donor molecule. In the same way the absence of the peak  $\nu(\text{C=N}) = 1604 \text{ cm}^{-1}$  also comes to confirms that. For complex (1) lower intensity bands like  $\nu(\text{M-N})$  and  $\nu(\text{M-O})$  are also present at 422 and  $526 \text{ cm}^{-1}$ , respectively, proving again the coordination of both the 2,2'-dipyridylamine and the ibuprofen molecule.

Table 1: The characteristic IR absorption frequencies ( $\text{cm}^{-1}$ ) of the free ligands and complex (1).

Assignment	Ibu	2,2'-dipy	$[\text{Cu}_2(\text{Ibu})_2(2,2'\text{-bipy})_2\text{Cl}_2]$
$\nu_{\text{sym}}(\text{COO})$	1538	-	1538
$\nu(\text{C-N})$	-	-	1162
$\nu_{\text{asym}}(\text{COO})$	1417	-	1438
$\nu(\text{C=O})$	1706	-	-
$\nu(\text{M-N})$	-	-	422
$\nu(\text{C=N})$	-	1604	-
$\nu(\text{M-O})$	-	-	526

### 3.1.4 Elemental and thermogravimetric analysis

Elemental analysis (C,H,N) confirmed the chemical composition of the complex, and as is presented in table 3, the values obtained through EA analysis are in good agreement with the ones that were calculated (Table 2).

Table 2: Elementary analysis data for complex (1). “AE” = obtained values; “Cal” = calculated values base on the chemical formula from single crystal X-ray.

Complex	Carbon %		Hydrogen (%)		Nitrogen (%)	
	AE	Cal	AE	Cal	AE	Cal
(1)	50.4	49.8	4.7	5.1	8.7	7.9

Figure 18 shows the results of the thermogravimetric analysis performed on complex 1. The data characteristic of the thermal decomposition was collected in table 3. The TG and DTG curves of complex 1 show that compound is thermally stable in the temperature range of 24-130 °C. A further increase in temperature causes a four-stage decomposition. In the first place, complex 1 loses 54 mg, which represents 4.9 % of the sample, that can be attributed to the loss of two molecules of water. The second stage is up to 310 °C and represents the degradation of 1 molecule of 2,2-dipyridylamine and the 2 chloride ions, which represents 28.3% of the sample mass, the last step occurring up to 750 °C and is attributed to the other 2,2-dipyridylamine molecule and the 2 ibuprofen molecules representing 53.3% of the sample and is up to 750 °C. Further heating gives CuO (observed 12.5 %, calculated 15.8 %) as the final product.

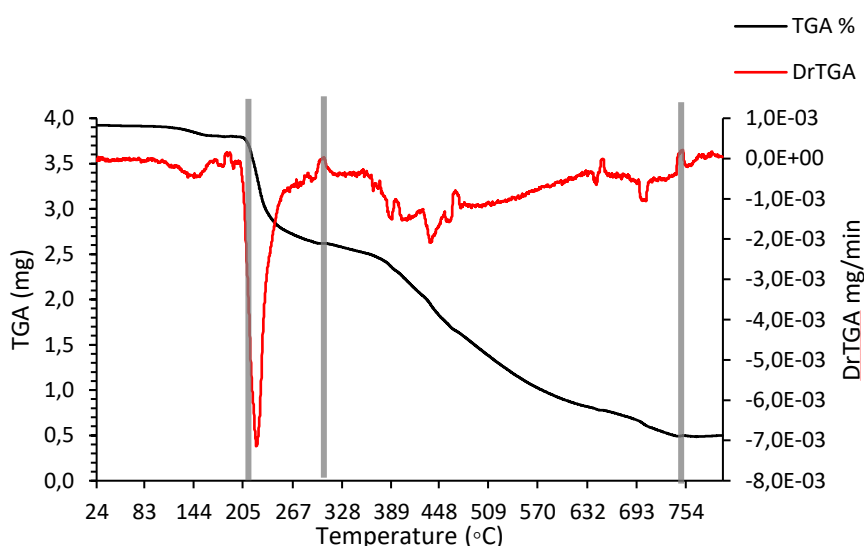


Figure 18: TGA/DSC results for complex 1.



Table 3: TG analysis data for complex (1). “AE” = obtained values; “Cal” = calculated values base on the chemical formula from single crystal X-ray.

Complex (1)	Stage 1 (%)		Stage 2 (%)		Stage 3 (%)		Stage 4 (%)	
	<i>TG</i>	<i>Cal</i>	<i>TG</i>	<i>Cal</i>	<i>TG</i>	<i>Cal</i>	<i>TG</i>	<i>Cal</i>
	4,9	5,3	28,3	24,5	53,3	54,5	12,5	15,8

## 3.2 BSA interaction studies

### 3.2.1 Fluorescence quenching and binding constant

For macromolecules, fluorescence measurements can provide information of the binding at the molecular level of small molecular substances to proteins, such as the binding mechanism, binding mode, binding constant, intermolecular distances, etc. Thus, the intrinsic fluorescence of proteins can supply significant information regarding their structure and dynamics and is often considered in the study of protein folding and association reactions <sup>135,136</sup>. It should be noted that the intrinsic fluorescence of protein is very sensitive to its microenvironment. When local surrounding of protein is slightly altered, its intrinsic fluorescence becomes significantly weakened, and factors such as protein conformational transition, biomolecular binding, etc., should be responsible for such weakening <sup>137</sup>.

BSA fluorescence comes from the three amino acid residues with intrinsic fluorophore groups present in the protein, i.e. tryptophan (Trp), tyrosine (Tyr), and phenylalanine (Phe). Actually, the fluorescence of BSA comes almost completely from Trp and Tyr, since phenylalanine has a very low quantum yield <sup>138</sup>. When a small molecule binds to BSA, it may trigger changes in the intrinsic fluorescence intensity due to alterations in the microenvironment of the Trp/Tyr residues. The participation of each residue in this process can be further distinguished by different excitation wavelengths: with 280 nm fluorescence of albumin comes from both tryptophan and tyrosine residues, whereas 295 nm wavelength excites only tryptophan residues <sup>139,140</sup>.

Figure 19 shows the effect of complex (1) concentration on the fluorescence intensity of BSA at  $\lambda_{ex}=295$  nm. As can be seen, it is clear that the presence of complex (1)

quenches the fluorescence intensity of BSA (up to 59.6 %). The maximum fluorescence emission is reached at 342.5 nm and quenching was accompanied by a small shift in maximum intensity of emission towards greater wavelengths (342 nm to 345 nm). This shift reflects an increase in the hydrophobicity of the microenvironment nearby the tryptophan residues as a consequence of complex binding <sup>122</sup>. This same behaviour has previously been observed in the interaction between other Cu-NSAIDs and BSA <sup>31,141–143</sup>.

As indicated in Figure 19, the Stern-Volmer plot obtained for complex 1 is linear and this fact allows us to calculate the value of  $K_{sv} = 1.54 \times 10^4 \text{ M}^{-1}$ . The binding strength of any drug to serum albumin is the main factor for availability of that drug to diffuse from the circulatory system to target tissues <sup>144</sup>. The linear plot obtained (figure 19 – inset) is indicative that only one type of quenching mechanism is involved, it can be static or dynamic, however, for more conclusive results further studies are needed. For example, performing this same experiment at different temperatures can show us with more certainty if the quenching mechanism is dynamic or static, this because if the quenching is static an increase in temperature leads to a lower stability of the complex bound to the protein which leads to a decrease in the quenching constant, on the other hand if the quenching mechanism is dynamic, at higher temperatures the quenching constant increases <sup>122</sup>. The  $K_{sv}$  for complex (1) is indicative that the interaction between these metal complexes and the BSA is moderately strong <sup>122</sup>.

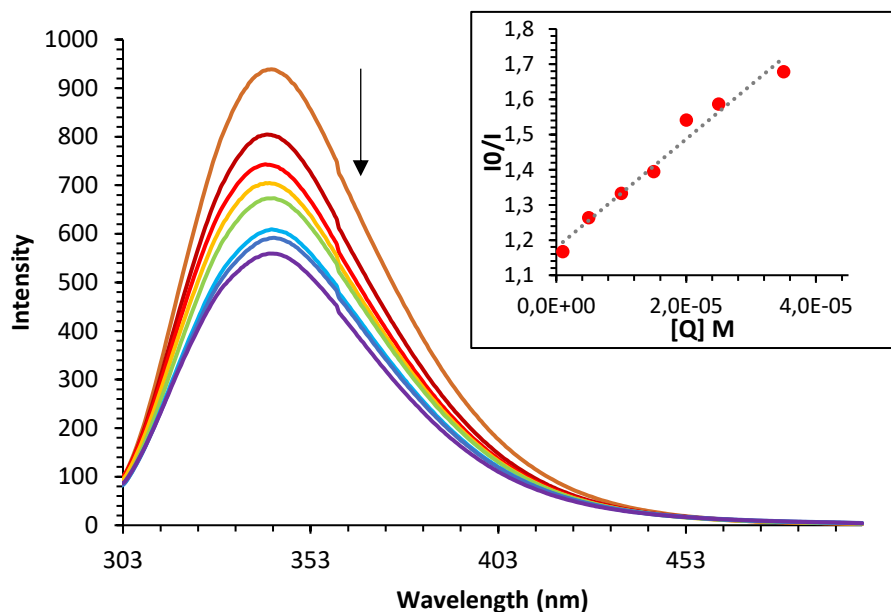


Figure 19: The fluorescence quenching spectra of BSA in the presence of various concentrations of complex (1) at  $\lambda_{\text{ex}} = 295 \text{ nm}$  and  $[\text{BSA}] = 5 \mu\text{M}$ . Arrow indicates the change upon increasing the complex concentration ( $R=0.2$ ;  $R=1$ ;  $R=2$ ;  $R=3$ ;  $R=4$ ;  $R=5$ ;  $R=6$ ;  $R=7$ ). The plot  $F_0/F$  versus  $[Q]$  according with the Stern-Volmer equation is depicted in the inset.

### 3.2.2 Circular Dichroism spectroscopic studies

When drugs bind to a protein, the intermolecular forces responsible for maintaining the secondary and tertiary structures can be altered, resulting in a conformational change in the protein <sup>145</sup>. CD technique is particularly suited to provide information on the specific binding of small substrates to chiral macromolecules <sup>145</sup>. Therefore, in this work the conformational alteration in BSA as a result of binding with metal complexes was monitored using CD spectroscopy.

As reported in literature the CD spectra of native BSA exhibited two negative bands at 208 and 222 nm which are typical characterization of the  $\alpha$ -helical structure of proteins. These negative peaks are the contribution from the  $\pi \rightarrow \pi^*$  (208 nm) and  $n \rightarrow \pi^*$  (222 nm) transitions of the peptides in the  $\alpha$ -helix <sup>131,146</sup>. As depicted in Figure 20, complex (1) was able to reduce the two negative bands of the native BSA along with a slight red peak shift. This phenomenon clearly indicates decrease in the  $\alpha$ -helical content of the protein. Herein, we have calculated the  $\alpha$ -helical content of free and bound BSA with complex (1) calculated from MRE values at 208 nm using the equation (2) as discussed in section 2.5 (table 4). According to quantitative analysis, native  $[\text{BSA}] = 0.25 \mu\text{M}$  have about 37% of  $\alpha$ -helical

content and complex (1) was able to reduce this percentage in about 6 and 7 % for R=0.5 and R=1.0, respectively.

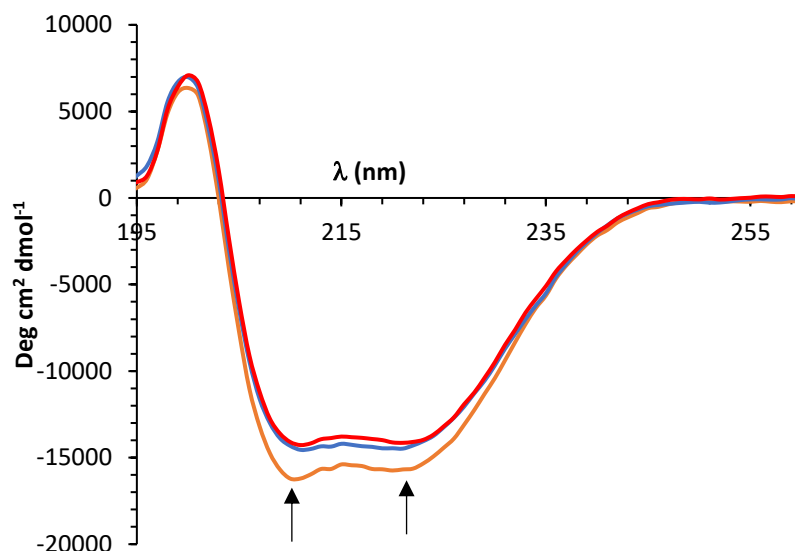


Figure 20: CD spectra of BSA in the presence of various concentrations of complex 1. Arrow indicates the change upon increasing the complex concentration. ([BSA]= 0.25  $\mu$ M; R=0.5; R=1).

The decreased in the  $\alpha$ -helical content suggest that the complexes induce a slight unfolding of the polypeptides, and once secondary structure reflects the local conformations within a polypeptide chain and are mostly defined by hydrogen bonds, the results suggest that this hydrogen bonds are disturbed by complex (1)<sup>147,148</sup>. These conformational changes may also increase the exposure of some hydrophobic regions that were previously buried<sup>148</sup>. Another Cu-NSAID's complexes have showed a different effect, increasing the  $\alpha$ -helix content of BSA<sup>149</sup>.

Table 4:  $\alpha$ -helix content in free [BSA]=0.25  $\mu$ M (Ratio=0) and in the presence of different ratios of complex (1).

Ratio=[Complex]/[BSA]	$\alpha$ -Helix %
0	37.0
0,5	31.0
1	30.2

### 3.2.3 UV absorption spectra

UV-visible absorption spectroscopy can be used to further explore the structural changes of protein and to investigate protein-ligand complex formation. UV-Vis spectra of BSA exhibit two absorption peaks at 198 and 280 nm, the first peak is due to the transitions of  $\pi \rightarrow \pi^*$  of BSA's characteristic polypeptide backbone and the second one corresponds to the aromatic ring amino acids<sup>150,151</sup>.

This technique is also useful to confirm the possible quenching mechanism of complex (1). If a dynamic quenching is present the interaction between the quencher and the protein does not result in any changes in the BSA absorption spectra, on the other hand, in a static quenching the absorption spectra of BSA will be significantly affected<sup>122,152</sup>.

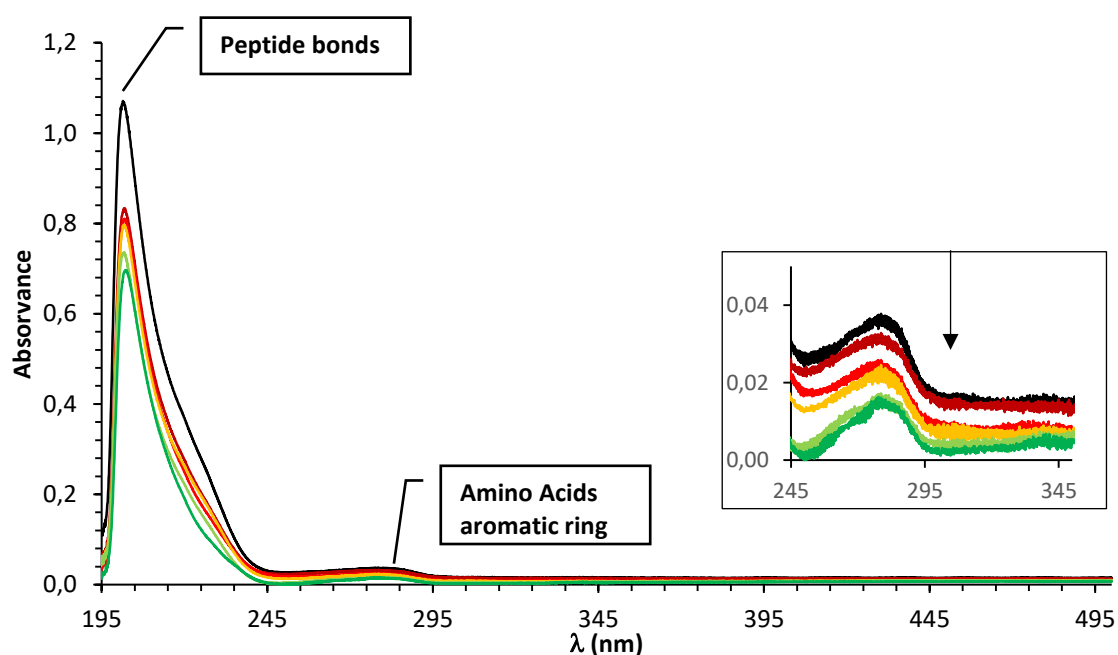


Figure 21: UV-visible absorption spectra of BSA in the presence and absence of complex (1). Arrow indicates the change upon increasing the complex concentration ([BSA]= 0.47  $\mu$ M; R=0.2; R=2.1; R=10.6; R=21.3; R=53.1).

In figure 21 we can observe that the 198 nm peak decreases upon the addition of the complexes which indicates perturbation on the protein secondary structure (peptide bonds), the changes in the 280 nm peak are slightest and indicate that the surrounding environment of the aromatic rings of the amino acids was altered. These findings are

characteristic of a static interaction between BSA and complex (1) <sup>122</sup>, confirming the results obtain in section 3.2.1 by tryptophan emission-quenching studies.

### 3.3 CT-DNA interaction studies

#### 3.3.1 Competitive DNA-Binding studies

Ethidium bromide (EB) is commonly used to probe drug binding to the DNA structure, which can tell us if the drugs can intercalate between the DNA base pairs and how strongly this type of interactions is <sup>153</sup>. EB is a well-known intercalator, the binding of EB to double strand DNA increase its fluorescence intensity at 600 nm, this phenomenon is due to the strong intercalation of the planar phenanthridinium ring between the DNA base pairs <sup>154</sup>.

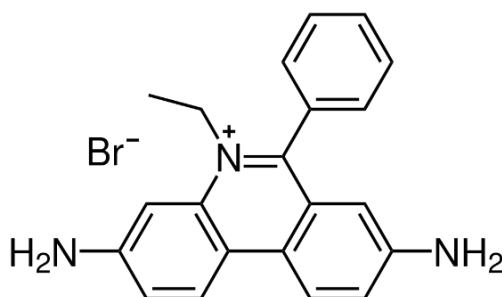


Figure 22: Structure of ethidium bromide [(3,8-diamino-5-ethyl-6-phenyl phenanthridinium bromide)].

Upon the addition of the metal complexes, if they intercalate with the DNA base pairs, they will compete with the EB for the intercalation sites and the displacement of the EB from the intercalative sites will create a decreasing in the intensity of the fluorescence <sup>154</sup>. The result of this experiment is presented on Figure 23. The addition of complex (1) to CT-DNA pre-treated with EB leads to a quenching of the fluorescence intensity which indicate that complex (1) compete with EB in the intercalation with DNA and displace this dye from DNA. This shows that complex (1) bind to DNA at by intercalation <sup>154</sup>.

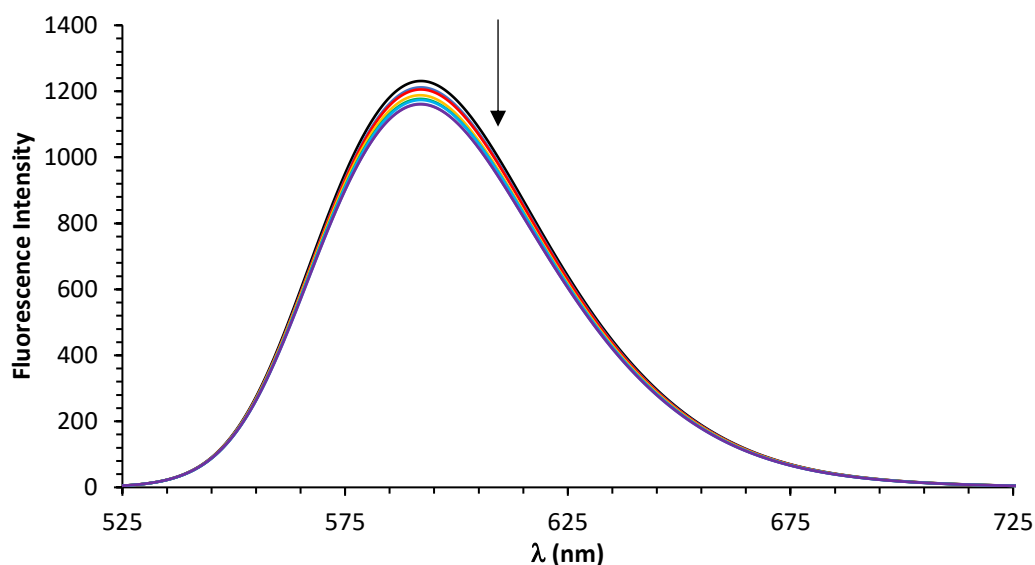


Figure 23: Effect of addition [complex (1)]=1-30  $\mu$ M on the fluorescence intensity of the CT-DNA bound ethidium bromide (EB). Arrow show the effect of complex (1) on the EB-DNA adduct fluorescence.

### 3.3.2 UV-Vis absorption spectroscopic studies

The UV-Vis absorption spectroscopy is one of the most used techniques to study the interaction between coordination compounds and DNA, this interaction can be explored based on the differences of the absorption spectra before and after the addition of the metal complexes. The spectra of free DNA in the UV region exhibit one intense absorption band at 256 nm, which can be attributed to  $\pi \rightarrow \pi^*$  intraligand transitions <sup>155</sup>.

A decreased in the absorbance (hypochromic effect=5,24%) and a bathochromic shift (0.4-0.9 nm) is observed in figure 24, these two effects are characteristics of molecules that bind to DNA by intercalation <sup>156</sup>. This study represents one more evidence that complex (1) act as intercalator of the DNA chains.

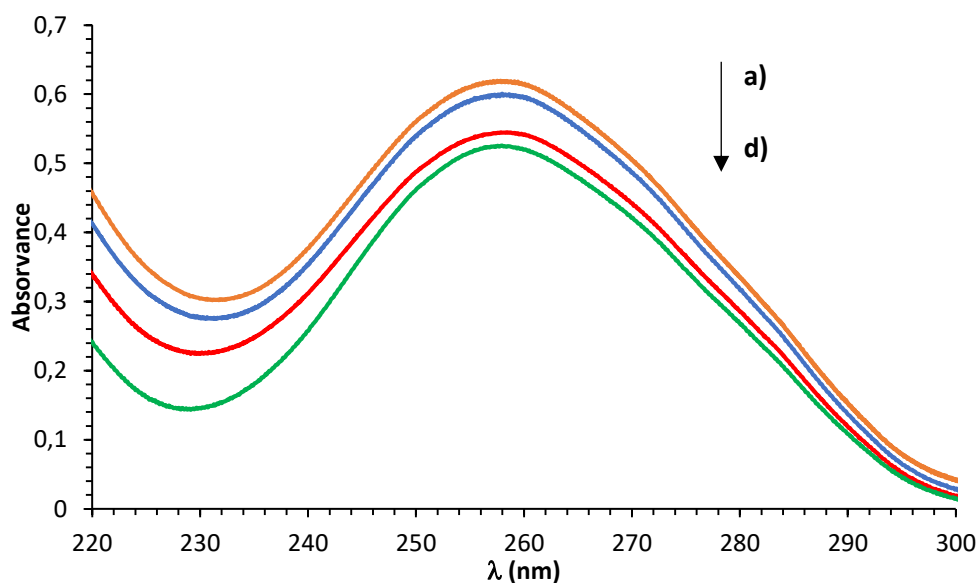


Figure 24: UV spectra of CT-DNA in the absence (a) and presence of different concentrations of complex (1). ([CT-DNA] = 0.5  $\mu$ M; [Complex (1)] = b-5  $\mu$ M; c-15  $\mu$ M; d-30  $\mu$ M).

### 3.4 *In vitro* biological assays

Breast cancer can be classified into different subtypes depending on their molecular features, they can be divided into hormone receptor positive tumours (regarding to estrogen receptor (ER) or progesterone receptor (PR)), HER-2/Neu (Human Epidermal growth factor Receptor 2) amplified tumours, and the ones that don't express ER, PR and do not have the oncogene HER-2/Neu amplified, this last group is known as triple-negative breast cancer (TNBC), because of the three missing molecular markers <sup>157</sup>.

All the biological assays were done in three different cell lines, MCF-7, MDA-MB-231 and MCF-12A (non-tumour cell line). MCF-7 is ER-positive and PR-positive, is poorly aggressive and non-invasive cell line, considered to have low metastatic potential <sup>158</sup>. On the other hand, MDA-MB-231 is a triple-negative breast cancer cell line, very aggressive and is associated to a highly invasive behaviour <sup>157,159</sup>.

#### 3.4.1 MTT assay

MTT results revealed a concentration dependent cytotoxicity response, observed for the three cell lines, after the 24h exposure to different concentrations (10 and 50  $\mu$ M) of complex (1) – Figure 25. In particular, it was possible to confirm that the copper coordination compound presented higher cytotoxicity, in comparison with the tumoral



cells, to the non-tumoral line (MCF-12A). The results are similar to others reported in literature<sup>160</sup> regarding the *in vitro* cytotoxicity of copper complexes to MCF-7 cells. Mašković et. al (2018) reported a Cu(II) complex that reveal the lowest IC<sub>50</sub> when tested on MDA-MB-231 compared to several tumoral cell lines<sup>161</sup>. However, most of the cytotoxic studies do not test the cytotoxicity of the complexes in non-tumoral cells.

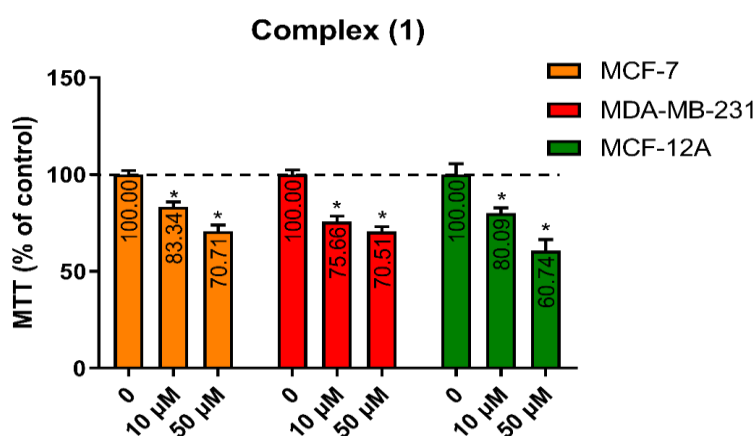


Figure 25: Cytotoxicity assessment by MTT assay induced by complex (1). The cells were exposed to different concentrations of each complex for 24h. \*p<0,05 vs control.

### 3.4.2 TBARS assay

It well known that oxidative stress caused by the increasing of ROS (reactive oxygen species) or other free radical species may play an important part in the treatment of cancer with chemotherapeutic drugs<sup>162–164</sup>. Cells are continuously producing ROS as a consequence of their metabolic processes, however, the balance between the prooxidant and antioxidant levels keeps the biological equilibrium of the redox states in the cell<sup>163</sup>. It's well known that high levels of ROS can inflict direct damage to the lipids (oxidative stress)<sup>165</sup>. The reaction that translates the lipid damage is call lipid peroxidation (LPO), and it can be described as the process under which free radicals attack lipids, especially polyunsaturated fatty acids (cellular membrane lipids)<sup>163</sup>. Most chemotherapeutics increase the intracellular levels of ROS, for example cisplatin or doxorubicin, involve both ROS-dependent and ROS-independent pathways<sup>166</sup>.

As illustrated in figure 26, MDA (malondialdehyde) is one of the secondary products resulting from lipid peroxidation and it can be used as a biomarker for lipid oxidation <sup>162</sup>. The TBARS (thiobarbituric acid reactive substances) assays is a quantification method to determinate the MDA concentration. The reaction of TBA with MDA gives rise to MDA-TBA<sub>2</sub> and this adduct can be detected by calorimetry <sup>165</sup>.

Lipid peroxidation is one of the most studied consequences inflicted by ROS generation in cell membrane structure and function. It is also known that the lipid hydroperoxides and oxygenated products of lipid degradation, as well as initiators (i.e., ROS), can contribute to cell proliferation, signal transduction cascade, differentiation and apoptosis <sup>160</sup>.

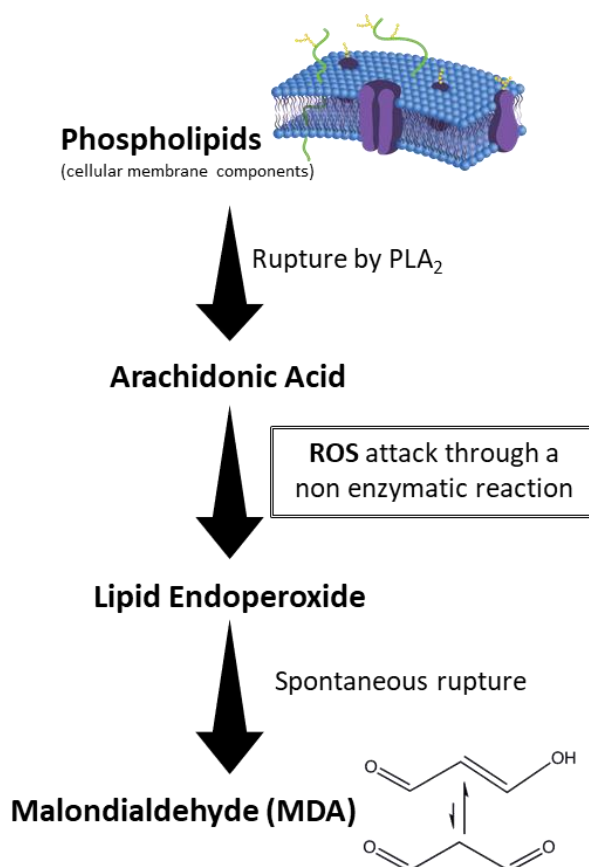


Figure 26: Principal steps in the formation of MDA. PLA<sub>2</sub> – Phospholipase A<sub>2</sub>. Adapted from <sup>162</sup>.

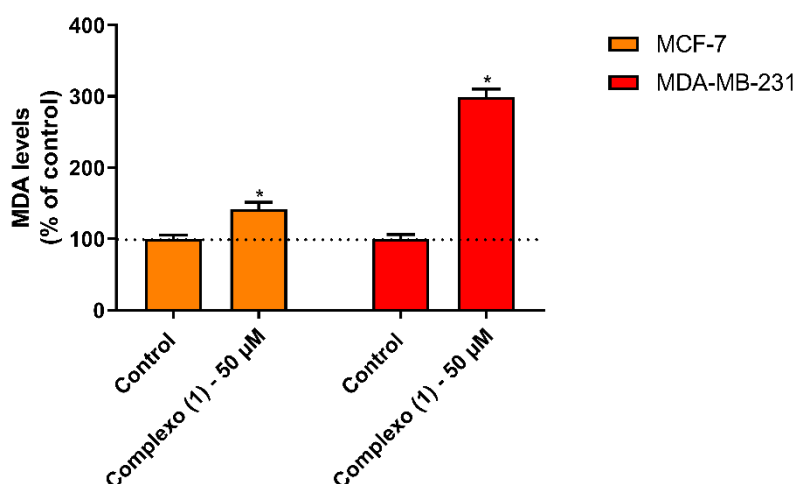


Figure 27: Lipid peroxidation levels of the cell lines after 24h treatment with complex (1). \* $p < 0,05$  vs control (t-test).

Therefore, in this work, we have studied the value of LPO (MDA levels in %) in MCF-7 and MDA-MB-231 cells exposed to complex (1) using the TBARS method (figure 27). Overall, the results showed that MDA levels increased significantly after 24h exposure of both cell lines to complex 1 (values compared with control). However, the MDA levels were significantly higher, when both cells were compared, in MDA-MB-231 line after complex exposure. The TBARS results correlated well with the MTT study. Complex (1) seems to have the ability to disrupt the redox homeostasis (TBARS assay) of this cell lines which appears to be the reason of the decreased in the cell viability (MTT assay).

There is a thin line between the role of ROS in cancer progression and cancer cell death, and this line is called redox homeostasis. Like normal cells, the cancer cells also need to maintain their own redox homeostasis, moderate levels of ROS may promote proliferation and support survival. However, if the levels of ROS exceed a certain level, LPO products induce signalling for cancer cells apoptosis<sup>167,168</sup>.

With this in mind, this assay suggests that complex (1) promote lipid peroxidation by increasing the oxidative stress levels which reduce cell viability, however this doesn't exclude that other mechanisms may act<sup>169</sup>.

### 3.5. Complex [Ni(terpy)<sub>2</sub>](diclof)<sub>2</sub>·8H<sub>2</sub>O (2)

#### 3.5.1 Synthesis

The synthesis of complex (2) was performed as described in detailed in section 2. (2.4.1). Briefly, a methanolic solution of diclofenac was added dropwise and simultaneously with a methanolic solution of 2,2':6',2''-Terpyridine to a stirred methanolic solution of NiCl<sub>2</sub>·6H<sub>2</sub>O.

#### 3.5.2 Single crystal structure

Complex (2) was unveiled by single-crystal X-ray diffraction analysis and formulated as [Ni(terpy)<sub>2</sub>](diclof)<sub>2</sub>·8H<sub>2</sub>O crystallizing in the orthorhombic space group *Pbcn*. More crystallographic data is shown on annex I. The metal centre in complex (2) presents an octahedral geometry, arising from its coordination to two terpyridines ligands coordinated by 3 nitrogen atoms to the central Ni(II) ion. The remaining part of this complex is composed of two deprotonated diclofenac molecules, that act as counterions, and 8 crystallization waters molecules which help stabilize the crystal structure by providing with several intermolecular hydrogen interactions (Figure 29). The powder X-ray diffraction pattern of complex (2) prepared in this work agrees well with the powder X-ray diffraction calculated from the single crystal X-ray data (figure 28).

Although complex (2) is not a metallodrug, since diclofenac is not coordinated with the metal ion, but as was obtained during the course of the work, all studies were performed.

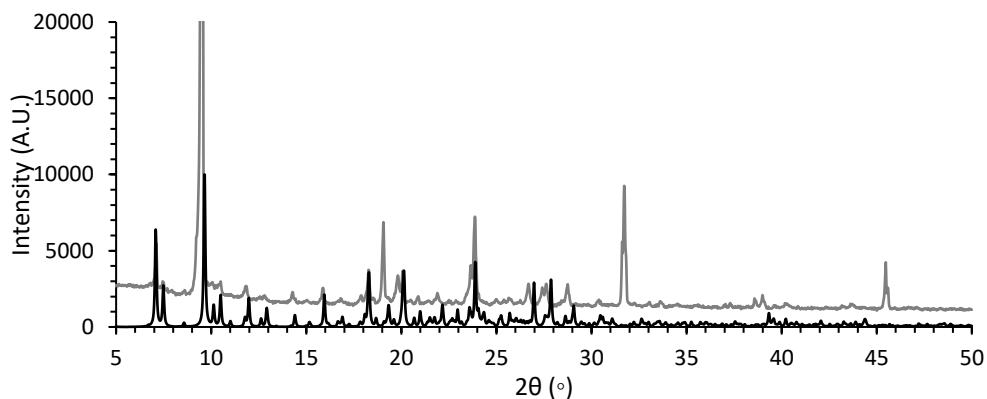


Figure 28: Experimental and by crystal X-ray data XRD graph for complex (2). Black line = single crystal X-ray data; Grey line = Complex (2)

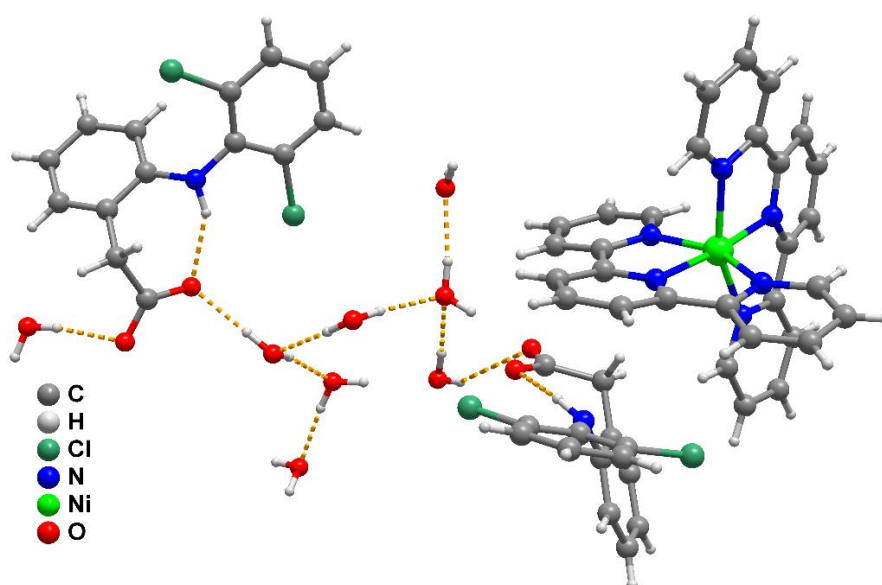


Figure 29: Asymmetric unit of [Ni(terpy)<sub>2</sub>](diclof)<sub>2</sub>·8H<sub>2</sub>O (2) showing all atoms represented as small spheres with arbitrary radius.

### 3.5.3 Infrared spectra

The most significant spectral bands of the ligands and complex (2), that provide information regarding the type of functional groups, are listed in Table 5. Complex (2) IR spectra (figure 30) present the peak  $\nu(\text{C-N})=1159\text{ cm}^{-1}$  which confirms the coordination of the N-donor molecule, the absence of the peak  $\nu(\text{C=N})=1604\text{ cm}^{-1}$  confirm that and proves that the coordination is through all the N atoms. Regarding to lower intensity bands like  $\nu(\text{M-N})$  and  $\nu(\text{C-Cl})$  they are also present at  $414$  and  $775\text{ cm}^{-1}$ , respectively, proving again the terpyridine coordination and the presence of the diclofenac molecule. The  $\nu_{\text{O-H}}(\text{H}_2\text{O})=3421\text{ cm}^{-1}$  is due to the presence of the 8 hydration waters.

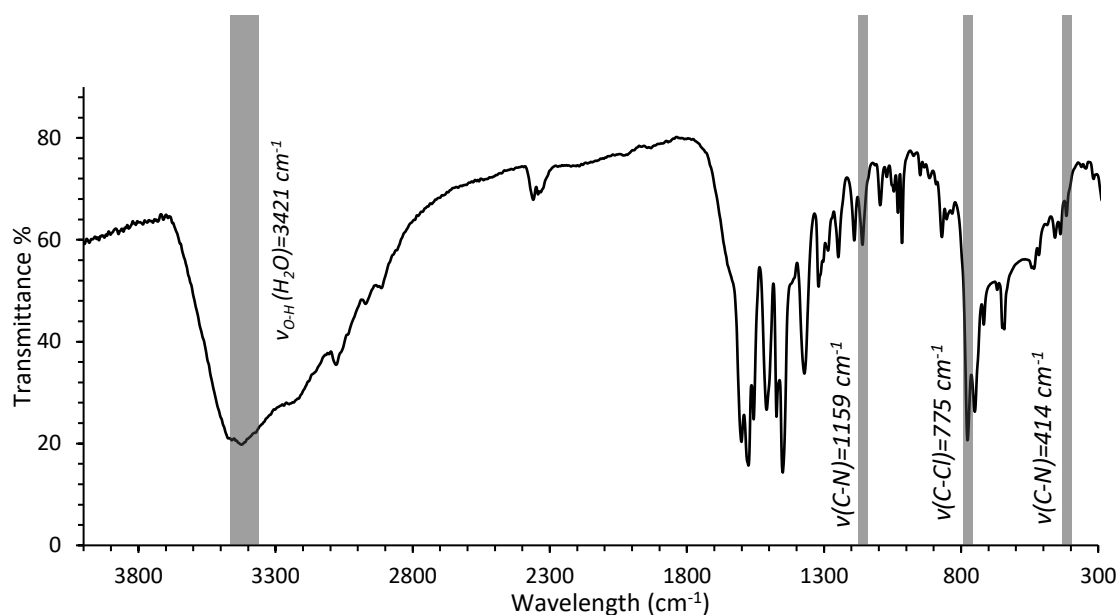


Figure 30: IR spectra of complex (2) with all the relevant peak highlighted.

Table 5: The characteristic IR absorption frequencies ( $\text{cm}^{-1}$ ) of the free ligands and complex (2).

Assignment	diclof	Terpy	$[\text{Ni}(\text{terpy})_2](\text{diclof})_2 \cdot 8\text{H}_2\text{O}$
$\nu_{\text{O-H}}(\text{H}_2\text{O})$	-	-	3421
$\nu_{\text{sym}}(\text{COO}^-)$	1556	-	-
$\nu_{\text{asym}}(\text{COO}^-)$	1399	-	-
$\nu(\text{C=O})$	1573	-	-
$\nu(\text{C=N})$	-	1579	-
$\nu(\text{C-N})$	-	-	1159
$\nu(\text{C-Cl})$	745	-	775
$\nu(\text{M-N})$	-	-	414

### 3.5.4 Elemental and thermogravimetric analysis

Elemental analysis (C,H,N) confirmed the chemical composition of complex (2), and as is presented in table 6, the values obtained through EA analysis are in good agreement with the ones that were calculated (Table 6).

Table 6: Results of the elementary analysis. “AE” are the values obtain from the analysis and “Cal” are the calculated values based on the chemical structure given by the x-ray.

	<b>Carbon %</b>		<b>Hydrogen (%)</b>		<b>Nitrogen (%)</b>	
	<b>AE</b>	<b>Cal</b>	<b>AE</b>	<b>Cal</b>	<b>AE</b>	<b>Cal</b>
<b>Complex (2)</b>	52,9	52,6	4,0	4,7	8,7	8,5

TG and DSC analysis of complex (2) are show in figure 31 and the decomposition percentages are in table 7. It's TG graphic can be divided into 3 stages, the first step represents the loss of 11.9% of the sample mass, which is the thermal degradation of the 10 molecules of H<sub>2</sub>O, the second one can be attributed to the loss of the 2 molecules of terpyridine and the 2 molecules of diclofenac which corresponds to the loss of 81.6% of the sample mass. The last heating from 655 °C up to 800 °C give the final decomposition product, NiO (observed 8.1 %, calculated 5.8 %).

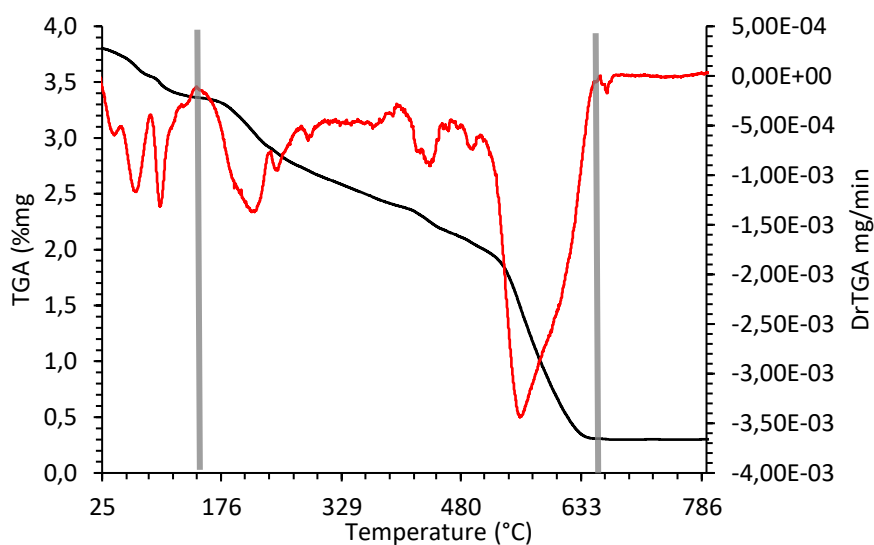


Figure 31: TGA/DSC results for complex (2).

Table 7: Results of the TGA analysis. Comparison between the “TG” values, obtain by the analysis and the “Cal” that were calculated based on their chemical structure.

	Stage 1 (%)		Stage 2 (%)		Stage 3 (%)	
	TG	Cal	TG	Cal	TG	Cal
Complex (2)	11.9	13.9	78.6	81.6	8.1	5.8

### 3.6 BSA Interaction studies

#### 3.6.1 Fluorescence quenching studies

Fluorescence spectroscopy, as was described above, can be used to study the conformational changes of the protein by the measurement of intrinsic fluorescence of two tryptophan residues (Trp-134 and Trp-212) <sup>132</sup>. The interaction between the metal complexes and BSA can be monitored by the quenching of this fluorescence upon the addition of complexes.

Complex (2) exhibit a very high fluorescence intensity at lower concentrations (Annex II) and

for that reason the interactions with BSA were only preformed with three concentrations of this complex and because of this limitation the  $K_{sv}$  was not calculated.

Figure 32 shows the effect of complex (2) on the fluorescence intensity of BSA at  $\lambda_{ex}=295$  nm. As can be seen, it is obvious that the presence of complex (2) quenches the fluorescence intensity of BSA (up to 9 %). The maximum fluorescence emission is reached at 342.5 nm and quenching was accompanied by a small shift in maximum intensity of emission towards greater wavelengths (342 nm to 345 nm). As was observed for complex (1), this shift reflects changes on the microenvironment of the tryptophan residues resulting from the complex binding <sup>122</sup>.



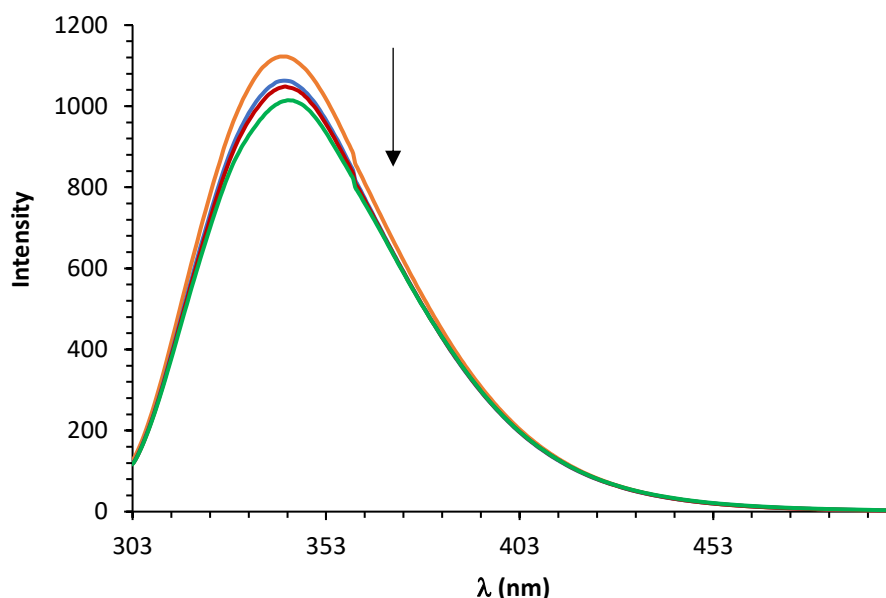


Figure 32: The fluorescence quenching spectra of BSA in the presence of various concentrations of complex (2) at  $\lambda_{\text{ex}} = 295 \text{ nm}$  and  $[\text{BSA}] = 6.5 \mu\text{M}$ . Arrow indicates the change upon increasing the complex concentration ( $R=0.02$ ;  $R=0.04$ ;  $R=0.06$ ).

### 3.6.2 Circular Dichroism spectroscopic studies

The results observed from the interaction between complex (2) and BSA are represented in Figure 33. Complex (2) was able to reduce the two negative bands of the native BSA and cause a slight peak shift. Herein, we have calculated the  $\alpha$ -helical content of free and bound BSA with complex (2) (table 8) calculated from MRE values at 208 nm using the equation (2) as discussed in section 2.5. According to quantitative analysis, native  $[\text{BSA}] = 0.25 \mu\text{M}$  have about 37.2% of  $\alpha$ -helical content and complex (2) was able to reduce this percentage in about 4.6 and 6.8 % for  $R=1$  and  $R=2$ , respectively.

The decreased in the  $\alpha$ -helical content suggest that the complex induces a certain unfolding of the polypeptides, and once this secondary structure are mainly defined by hydrogen bonds, the results suggest that this hydrogen bonds are disturbed by complex (2)<sup>147,148</sup>. Beyond these conformational changes, complex (2) may also increase the exposure of some hydrophobic regions that were previously buried<sup>148</sup>.

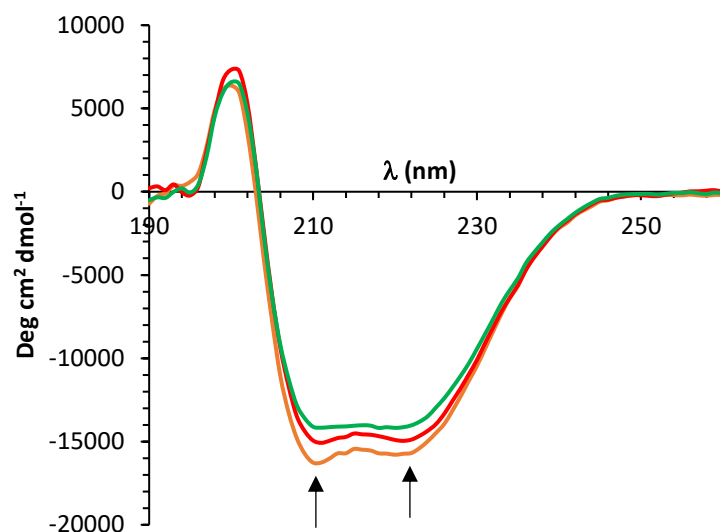


Figure 33: CD spectra of BSA in the presence of various concentrations of complex (2). Arrow indicates the change upon increasing the complex concentration. ([BSA]= 0.25  $\mu$ M; R=1; R=2).

Table 8:  $\alpha$ -helix content in free BSA at 0.25  $\mu$ M (Ratio=0) and in the presence of different ratios of complex (2)

Ratio=[Complex]/[BSA]	$\alpha$ -Helix %
0	37.2
1	32.6
2	30.4

### 3.6.3 UV-Vis absorption spectroscopic studies

The results in figure 34 show that complex (2) can disturb the peptide bonds and the aromatic ring of the amino acids in the BSA molecule. The 198 nm peak decreases upon the addition of the complexes due to the perturbation of the secondary structure (peptide bonds), the changes in the 280 nm peak are slightest and indicate that the surrounding environment of the aromatic amino acids was altered <sup>122</sup>, this phenomenon is indicative of a static mechanism <sup>122,152</sup>.

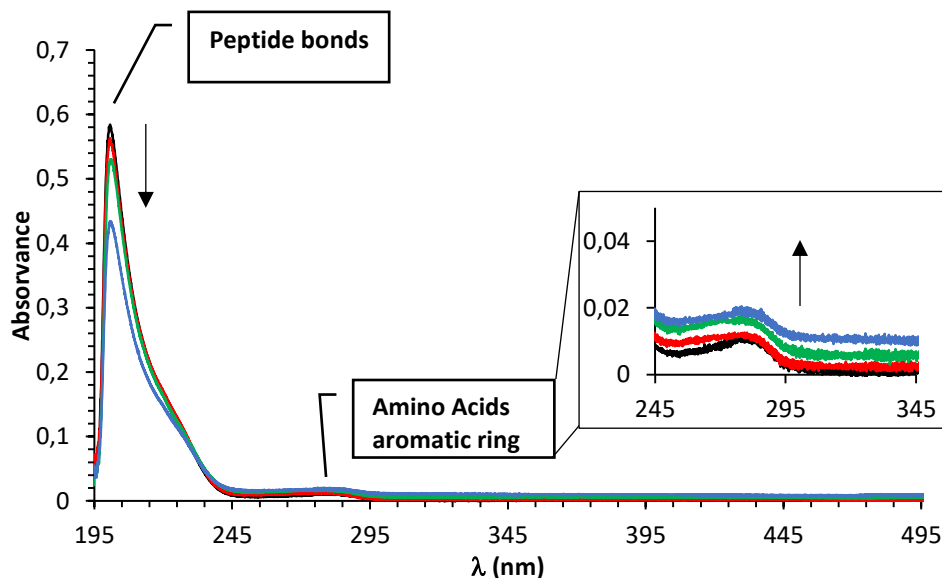


Figure 34: UV-visible absorption spectra of [BSA]=0.16  $\mu$ M in the absence (black line) and presence of complex (2). (R=0.1;R=0.9;R=25)

### 3.7 CT-DNA interaction studies

#### 3.7.1 Competitive DNA-Binding studies

The result of this competitive experiment is presented on figure 35. The addition of complex (2) to CT-DNA pre-treated with EB leads to a quenching of the fluorescence intensity which indicate that this complex competes with EB for the intercalation with DNA and displace this dye from DNA. This shows that, as was suggested before, complex (2) bind to DNA at by intercalation <sup>154</sup>.

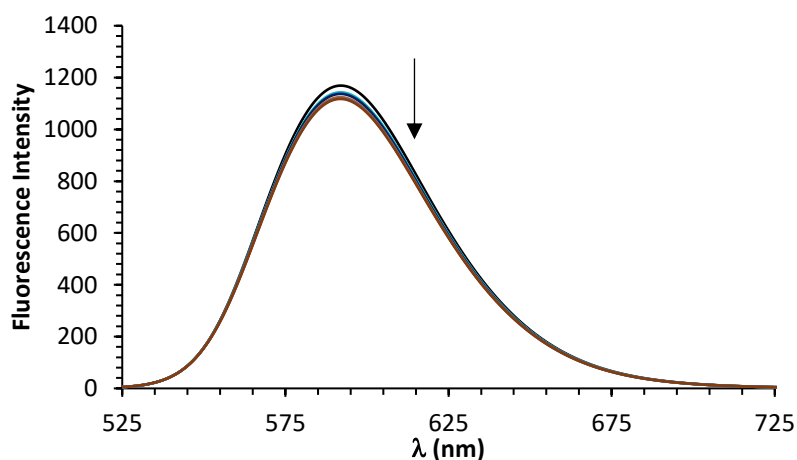


Figure 35: Effect of addition [complex (2)]=0.5-35  $\mu$ M on the fluorescence intensity of the CT-DNA bound ethidium bromide (EB)

### 3.7.2 UV-Vis absorption spectroscopic studies

The UV absorption studies is commonly used to study the interaction between coordination compounds and DNA, as was pointed above.

In figure 36 is observable a decreased in the absorbance (hypochromic effect=31.7%), this phenomenon is characteristic of molecules that bind to DNA by intercalation <sup>156</sup>. This is further evidence that complex (2) act as intercalator of the DNA.

Other Ni(II)-NSAID complexes with nitrogen-donor heterocyclic ligands cause the same changes upon their addition to DNA and intercalation is its most likely the binding mode, which was also evaluated through other studies <sup>170</sup>. There still are other Ni(II)-NSAID complex that shows a hyperchromic effect of DNA UV spectra, but did not interact with DNA through intercalation <sup>171</sup>.

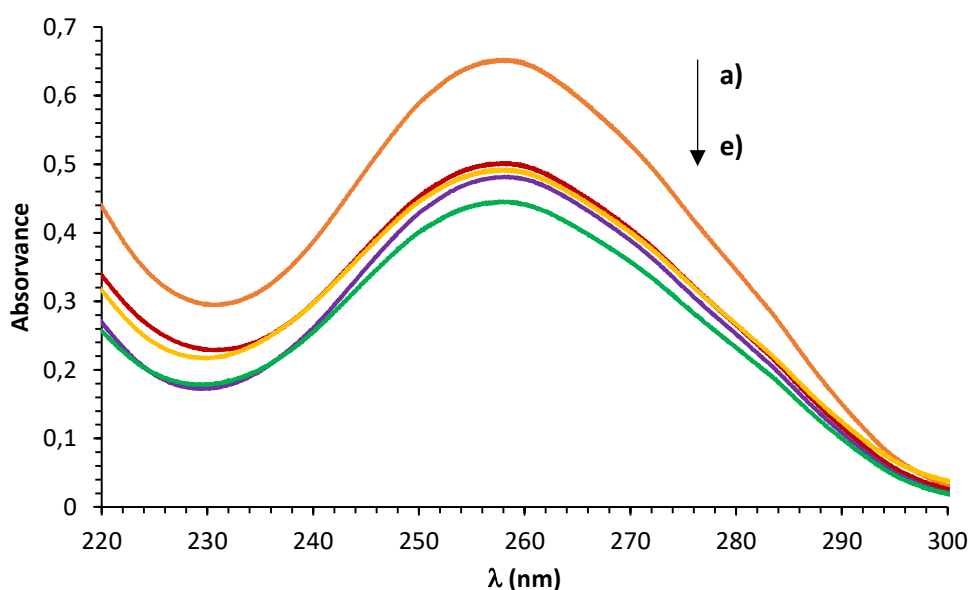


Figure 36: UV spectra of CT-DNA in the absence (a) and presence of different concentrations of complex (2). (a-[CT-DNA] = 0,5 μM, b- 2 μM; c- 4 μM; d- 7 μM, e- 35 μM). The arrow shows the absorbance changes upon increasing concentrations of the complex.

### 3.8 *In vitro* biological assays

#### 3.8.1 MTT assay

The MTT assays were performed under the same conditions used for complex (1).

The results of the cytotoxic activity obtained for complex (2) on MCF-7 and MDA-MB-231 cells revealed low anticancer activity (Figure 37) especially regarding the MCF-7 cell line. On the other hand, complex (2) presented higher cytotoxicity, when compared with cancer cell lines, for the non-tumoral cells (MCF-12A).

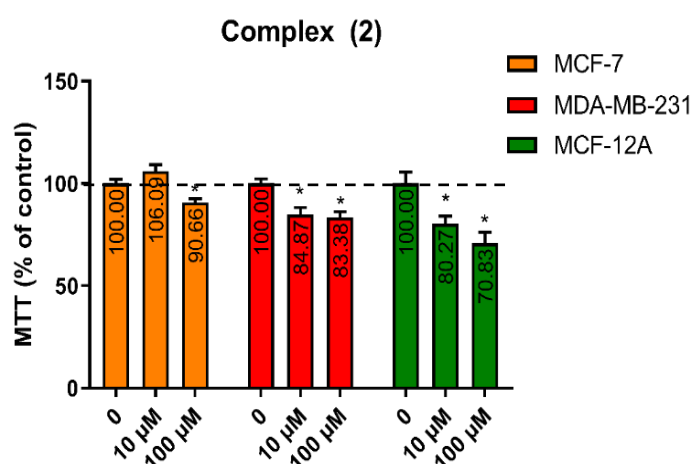


Figure 37: Cytotoxicity assessment by MTT assay induced by complex (2). The cells were exposed to different concentrations of each complex for 24h. \* $p < 0,05$  vs control.

#### 3.8.2 TBARS assays

As can be seen in figure 38 the MDA levels measured after the MCF-7 cells being 24h exposure to complex (2) were not significantly different from the values of the control. This fact is consistent with the results obtained by the MTT assay, regarding the same cell line, in which the metal complex was able to only decrease around 10% the cell viability. This result leads us to conclude that the small decrease on the cell viability of MCF-7 cells is not due to oxidative stress, this was already observed for other metal complexes that have antiproliferative and proapoptotic activities and do not trigger the redox cascade pathway<sup>172,173</sup>. TBARS results for the MDA-MB-231 cell line revealed higher MDA levels (in comparison with the control and with the MCF-7 line), meaning that lipid peroxidation may be behind the decrease on cell viability of the MDA-MB-231 cell line.

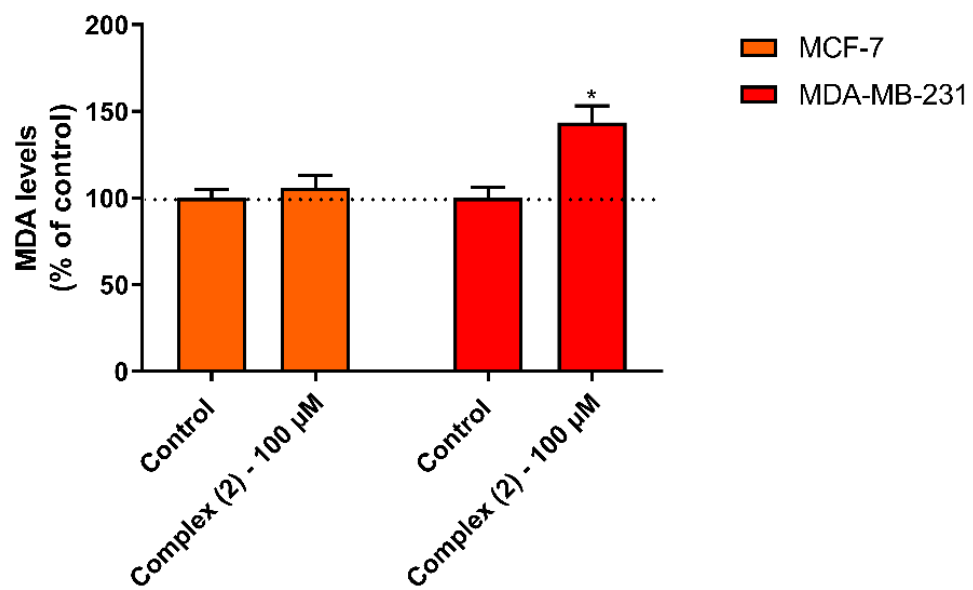


Figure 38: Lipid peroxidation levels of the cell lines after 24h treatment with complex (2). \* $p < 0,05$  vs control (t-test).

### 3.9 Complexes [M(diclo)<sub>2</sub>(2,2'-bipy)] (M<sup>2+</sup> = Co<sup>2+</sup>(3) or Ni<sup>2+</sup>(4))

#### 3.9.1 Synthesis

The synthesis of complex (3) and (4) was performed as described in detailed in section 2. (2.4.1). Briefly, an ethanolic solution of diclofenac was added dropwise and simultaneously with a methanolic solution of 2,2-bipyridine to a stirred methanolic solution of CoCl<sub>2</sub>·6H<sub>2</sub>O (3) or NiCl<sub>2</sub>·6H<sub>2</sub>O (4).

#### 3.9.2 Single crystal structures

Complex (3) and Complex (4) were both unveiled by single-crystal X-ray diffraction analysis and were formulated as [M(diclo)<sub>2</sub>(2,2'-bipy)] (where M<sup>2+</sup> = Co<sup>2+</sup>(3) or Ni<sup>2+</sup>(4)) crystallizing in the monoclinic space group *I*2/*a* (Figure 39). Since both compounds have the same structural features, a more detailed description will be provided only for complex (3). The asymmetric unit is composed of half a 2,2'-bipyridine molecule, one diclofenac molecule and half metal centre. This metal centre is hexacoordinated with a highly distorted octahedral geometry, being coordinated to two diclofenac.

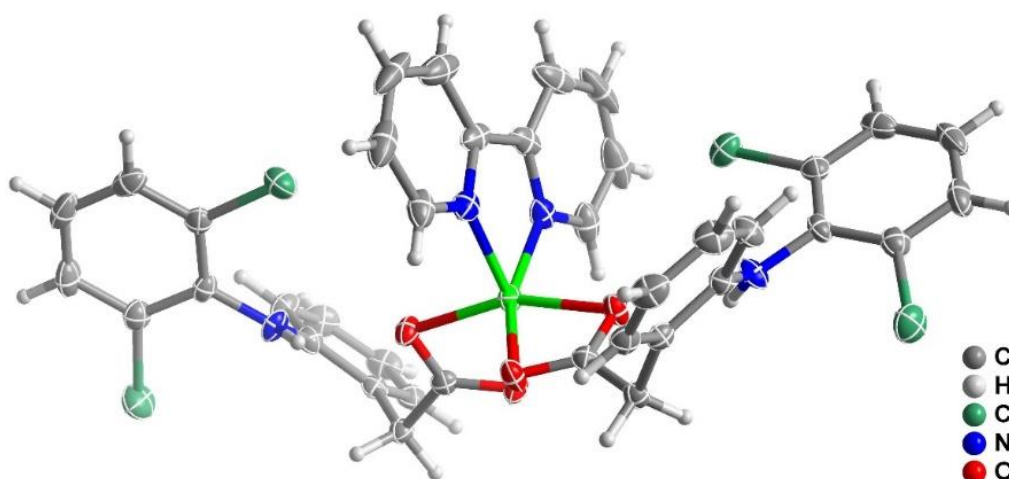
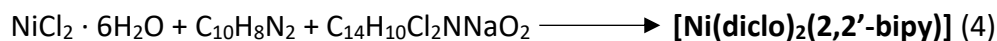
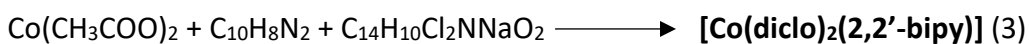
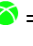



Figure 39: Crystal Structure of [M(diclo)<sub>2</sub>(2,2'-bipy)] (where M<sup>2+</sup> = Co<sup>2+</sup>(3) or Ni<sup>2+</sup>(4)) showing all non-hydrogen atoms represented as thermal ellipsoids drawn at the 50% probability level and hydrogen atoms as small spheres with arbitrary radius. The asymmetric unit is composed of only half of the represented complex, with the remaining atoms being generated by symmetry.

Complex (3)  = Cobalt; Complex (4)  = Nickel

As we can see from Figure 40, there are  $\pi$ - $\pi$  interactions between 2,2'-bipyridine aromatic rings ( $d = 3,5016(1) \text{ \AA}$ ) and between the diclofenac aromatic rings ( $d = 3,6339(1) \text{ \AA}$ ). This is indicative of the intercalator potential of this complex with a DNA, as it is positioned at distances that are analogous to the distance between the nitrogenous bases of DNA which is  $3.4 \text{ \AA}$  <sup>174</sup>.

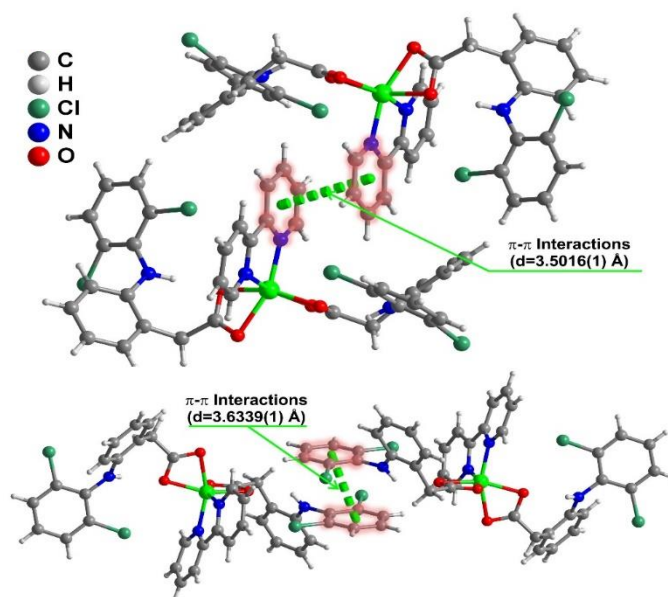


Figure 40: Packaging diagram of complex (3) and (4) showing the interactions (dashed line in the figure;  $\pi$ - $\pi$  interaction) between various structural units of the complexes.

### 3.10 Complexes $[M(\text{diclo})_2(1,10\text{-phen})]$ ( $M^{2+} = \text{Co}^{2+}(5)$ or $\text{Ni}^{2+}(6)$ )

#### 3.10.1 Synthesis

The synthesis of complex (5) and (6) was performed as described in detailed in section 2. (2.4.1). Briefly, an ethanolic solution of diclofenac was added dropwise and simultaneously with a methanolic solution of 1,10-phenatroline to a stirred methanolic solution of  $\text{CoCl}_2 \cdot 6\text{H}_2\text{O}$  (3) or  $\text{NiCl}_2 \cdot 6\text{H}_2\text{O}$  (4).

#### 3.10.2 Single crystal structures

The structural features of complex (5) and complex (6) were also unveiled by single-crystal X-ray diffraction, showing similarities to complexes (3) and (4) (see next for more detail). These compounds were formulated as  $[M(\text{diclo})_2(1,10\text{-phen})]$  (where  $M^{2+} = \text{Co}^{2+}(5)$  or  $\text{Ni}^{2+}(6)$ ) crystallizing in the same monoclinic space group  $I2/a$  (Figure 41). As for



previously, since both complexes have the same crystalline structure, only complex (5) is described here. The asymmetric unit in these complexes contain half of the 1,10-phenantroline molecule, one diclofenac molecule and half of metal centre. This metal centre as also a highly distorted octahedral geometry, being coordinated to two diclofenac molecules and to one 1,10-phenantroline molecule that is coordinated by two nitrogen atoms.

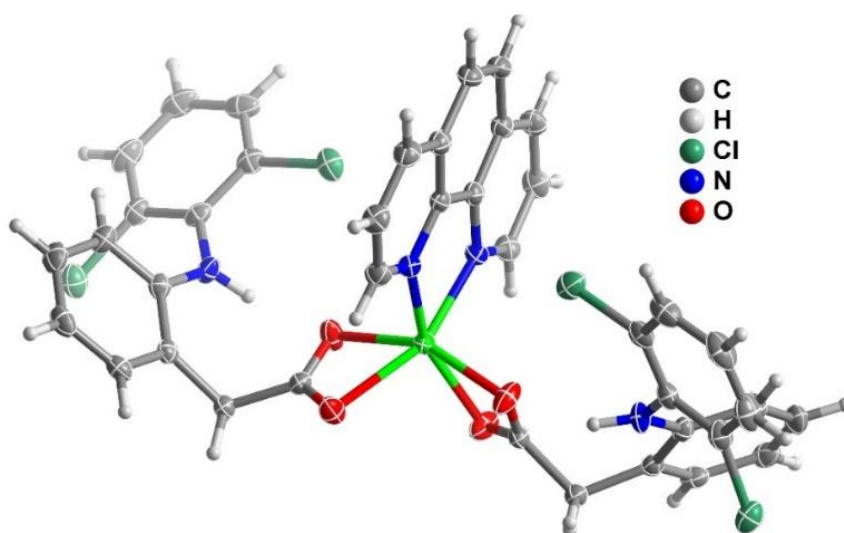
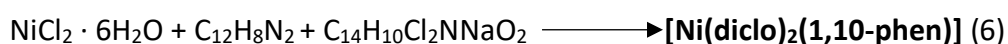
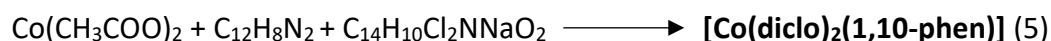




Figure 41: Crystal Structure of  $[\text{M}(\text{diclo})_2(1,10\text{-phen})]$  (where  $\text{M}^{2+} = \text{Co}^{2+}$ (5) or  $\text{Ni}^{2+}$ (6)) showing all non-hydrogen atoms represented as thermal ellipsoids drawn at the 50% probability level and hydrogen atoms as small spheres with arbitrary radius. The asymmetric unit is composed of only half of the represented complex, with the remaining atoms being generated by symmetry. Complex (5)  = Cobalt; Complex (6)  = Nickel

As was observed for complexes (3) and (4), also complex (5) and (6) present  $\pi$ - $\pi$  interactions between 1,10-phenantroline aromatic rings ( $d = 3,6222(2) \text{ \AA}$ ) and between the diclofenac aromatic rings ( $d = 3,7366(2) \text{ \AA}$ ) (Figure 42). This is indicative of the intercalator potential of this complex with a DNA, as it is positioned at distances that are analogous to the distance between the nitrogenous bases of DNA which is  $3.4 \text{ \AA}$  <sup>174</sup>.

As represented in figure 39 and 41, these complexes share similar features. All compounds crystallize in the monoclinic  $I2/a$  space group, with the only difference being in the co-ligand used: 2,2'-bipyridine for (3) and (4) or 1,10-phenantroline molecule for (5)

and (6). This is evidence of the similarity between these complexes structure and that, therefore, we can study the influence of metallic centre and ligands since their structure/geometry is not a variable in this equation. More information related to the crystal data are presented in table 9. Powder X-ray diffraction analysis were also performed, which allowed us to confirm that the complex pairs (complexes (3) and (4); complexes (5) and (6)) have the same diffractogram as compared to the ones generated by their single-crystal X-ray data, which confirms the representativeness of the entire sample obtained and its purity. All the XRD spectra are on figure 42 to 46.

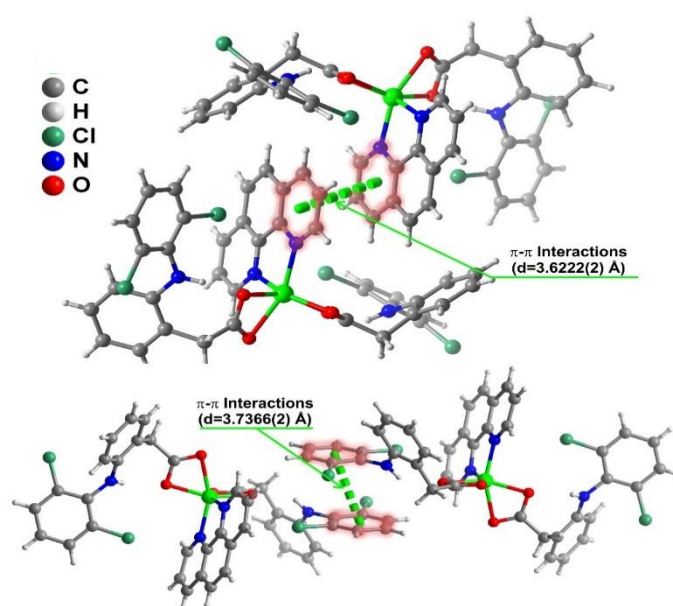


Figure 42: Packaging diagram of complex (5) and (6) showing the interactions (dashed line in the figure;  $\pi$ - $\pi$  interaction) between various structural units of the complexes.

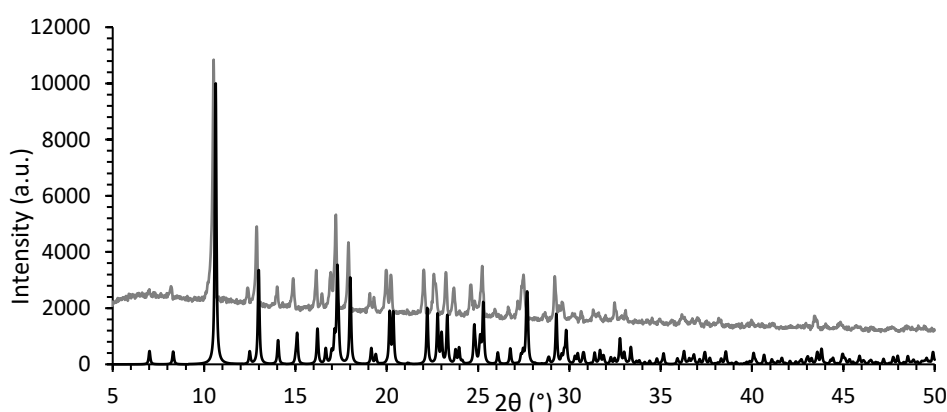


Figure 43: Experimental and by crystal X-ray data XRD graph for complex (3). Black line = single crystal X-ray data; Grey line = Complex (3).

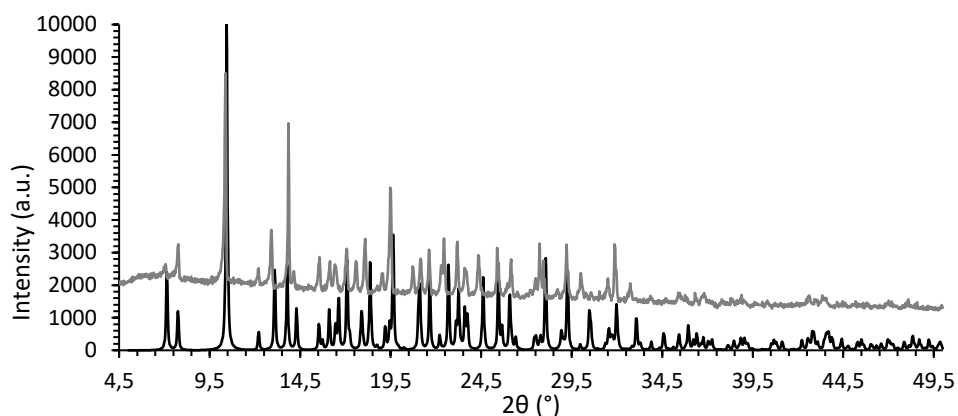


Figure 44: Experimental and by crystal X-ray data XRD graph for complex (4). Black line = single crystal X-ray data; Grey line = Complex (4).

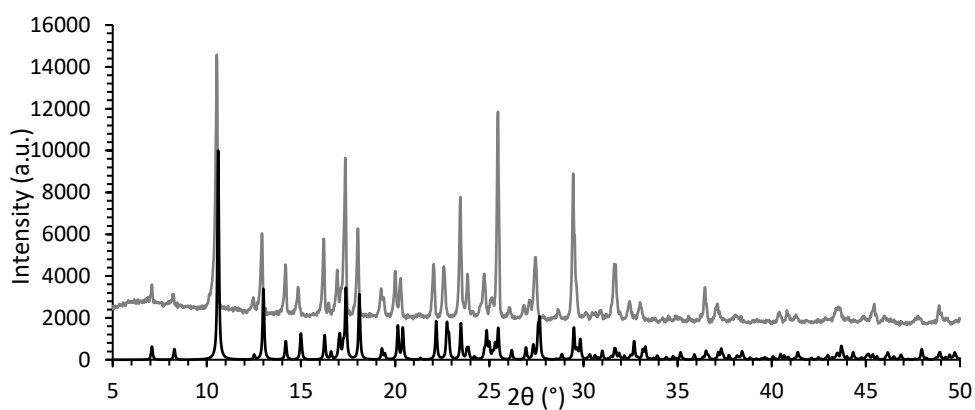


Figure 45: Experimental and by crystal X-ray data XRD graph for complex (5). Black line = single crystal X-ray data; Grey line = Complex (5)

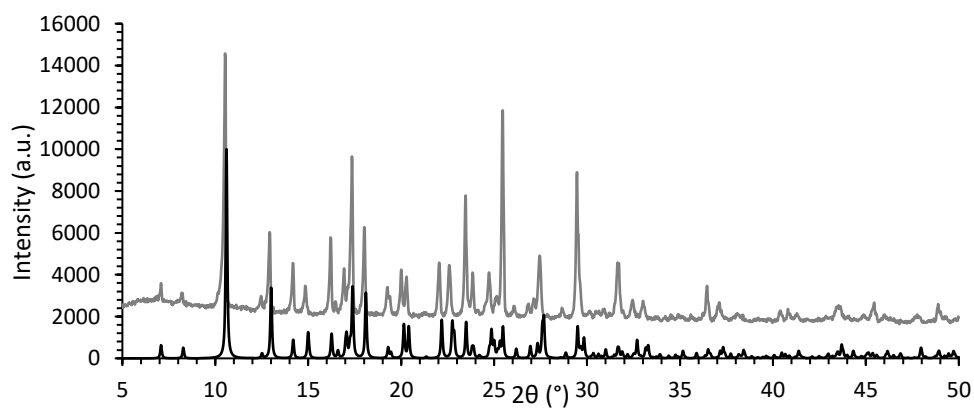


Figure 46: Experimental and by crystal X-ray data XRD graph for complex (6). Black line = single crystal X-ray data; Grey line = Complex (6)

Table 9: Crystal data collection and structure refinement details

	Complex 3	Complex 4	Complex 5	Complex 6
<b>Formula</b>	C <sub>20</sub> H <sub>10</sub> ClN <sub>4</sub> CoO <sub>4</sub>	C <sub>20</sub> H <sub>10</sub> ClN <sub>4</sub> NiO <sub>4</sub>	C <sub>40</sub> H <sub>28</sub> Cl <sub>4</sub> CoN <sub>4</sub> O <sub>4</sub>	C <sub>40</sub> H <sub>28</sub> Cl <sub>4</sub> NiN <sub>4</sub> O <sub>4</sub>
<b>Formula weight</b>	464.70	464.46	829.42	829.18
<b>Temperature / K</b>	150(2)	150(2)	150(2)	150(2)
<b>Crystal system</b>	<b>Monoclinic</b>	<b>Monoclinic</b>	<b>Monoclinic</b>	<b>Monoclinic</b>
<b>Space group</b>	<b>I2/a</b>	<b>I2/a</b>	<b>I2/a</b>	<b>I2/a</b>
<b><i>a</i> / Å</b>	11.8082 (9)	11.7935 (3)	11.3114 (6)	11.3506 (13)
<b><i>b</i> / Å</b>	11.7278 (8)	11.8095 (3)	12.8361 (6)	12.7840 (14)
<b><i>c</i> / Å</b>	25.233 (2)	24.9864 (9)	24.8738 (14)	24.737 (3)
<b><math>\alpha</math> / °</b>	90	90	90	90
<b><math>\beta</math> / °</b>	93.386 (4)	93.360 (2)	95.708 (2)	95.469 (3)
<b><math>\gamma</math> / °</b>	90	90	90	90
<b>Volume / Å<sup>3</sup></b>	3488.2 (5)	3474.01 (18)	3593.6 (3)	3573.1 (7)
<b>Z</b>	8	8	8	8
<b><math>\mu</math>(Mo K<math>\alpha</math>) / mm<sup>-1</sup></b>	1.18	0.92	1.28	1.27
<b>Crystal type</b>	Red Block	Blue Plate	Red Block	Green Block
<b>Crystal size / mm</b>	0.17×0.06×0.06	0.12×0.11×0.04	0.24×0.19×0.09	0.17×0.16×0.16
<b><math>\theta</math> range (°)</b>	2.87 – 25.38	2.44 – 25.39	1.64 – 29.23	2.82 – 25.36
<b>Index ranges</b>	-14 ≤ <i>h</i> ≤ 13	-13 ≤ <i>h</i> ≤ 14	-15 ≤ <i>h</i> ≤ 15	-13 ≤ <i>h</i> ≤ 13
	-14 ≤ <i>k</i> ≤ 14	-14 ≤ <i>k</i> ≤ 14	-17 ≤ <i>k</i> ≤ 17	-15 ≤ <i>k</i> ≤ 15
	-30 ≤ <i>l</i> ≤ 30	-26 ≤ <i>l</i> ≤ 30	-34 ≤ <i>l</i> ≤ 28	-29 ≤ <i>l</i> ≤ 29
<b>Collected Reflections</b>	20425	16152	49229	23241
<b>Independent Reflections</b>	3192 ( <i>R</i> <sub>int</sub> = 0.089)	3208 ( <i>R</i> <sub>int</sub> = 0.031)	4888 ( <i>R</i> <sub>int</sub> = 0.029)	3267 ( <i>R</i> <sub>int</sub> = 0.028)
<b>Completeness to <math>\theta = 25.24</math></b>	99.9%	99.9%	100%	99.6%
<b>Final <i>R</i> indices [<i>I</i> &gt; 2<math>\sigma</math>(<i>I</i>)]</b>	<i>R</i> 1 = 0.0621	<i>R</i> 1 = 0.0297	<i>R</i> 1 = 0.0287	<i>R</i> 1 = 0.0323
	<i>wR</i> 2 = 0.1058	<i>wR</i> 2 = 0.0675	<i>wR</i> 2 = 0.1058	<i>wR</i> 2 = 0.11328
<b>Final <i>R</i> indices (all data)</b>	<i>R</i> 1 = 0.0823	<i>R</i> 1 = 0.0400	<i>R</i> 1 = 0.0343	<i>R</i> 1 = 0.0351
	<i>wR</i> 2 = 0.1279	<i>wR</i> 2 = 0.0709	<i>wR</i> 2 = 0.1138	<i>wR</i> 2 = 0.1167
<b>Largest diff. peak and hole / eÅ<sup>-3</sup></b>	0.51 and -0.63	0.47 and -0.39	0.49 and -0.45	0.50 and -0.52

$$^a R1 = \sum ||F_o| - |F_c|| / \sum |F_o|$$

$$^b wR2 = \sqrt{\sum [w(F_o^2 - F_c^2)^2] / \sum [w(F_o^2)^2]}$$

$$^c w = 1 / \left[ \sigma^2(F_o^2) + (mP)^2 + nP \right] \text{ where } P = (F_o^2 + 2F_c^2) / 3$$

### 3.11 Infrared spectra

The most significant spectral bands of the ligands and complex (3), (4), (5) and (6) that provide information regarding the type of functional groups, are listed in table 10.

As already been said, the difference between the asymmetric peak and the symmetric peak of the carboxylate group give us information about its coordination mode. All IR spectra of the complexes show a difference ( $\Delta\nu = \nu_{\text{asym}}(\text{COO}^-) - \nu_{\text{sym}}(\text{COO}^-)$ ) inferior to  $200 \text{ cm}^{-1}$ ,  $106$  and  $126 \text{ cm}^{-1}$  for complex (3) and (4) respectively, and  $130$  and  $127 \text{ cm}^{-1}$  for complex (5) and (6), respectively. So the diclofenac molecule is probably bidentate to the metal centre in all the four complexes, the absence of the strong band  $\nu(\text{C}=\text{O}) = 1700 \text{ cm}^{-1}$  also supports this feature. The peak  $\nu(\text{C}-\text{Cl}) = 760 \text{ cm}^{-1}$  also proves the presence of diclofenac molecules on the complex. The presence of the low intensity peaks like  $\nu(\text{M}-\text{N}) = 410$  and  $\nu(\text{C}-\text{N}) = 1160 \text{ cm}^{-1}$  validates the coordination between the nitrogen atoms of the N-ligands with the metal ion, at the same time the absence of the peak  $\nu(\text{C}=\text{N}) = 1500 \text{ cm}^{-1}$  is also proof that the N-donor molecules are coordinated to the metal ion. Complex (6) presents the moderate band  $\nu_{\text{O}-\text{H}}(\text{H}_2\text{O})$  due to the presence of solvent residues on the crystals sample. All the data regarding to the IR spectra of the complexes are exposed in table 10 and in figure 47 – 50.

Table 10: The characteristic IR absorption frequencies ( $\text{cm}^{-1}$ ) of the free ligands and complex (3) to (6).

Assignment	diclo	2,2-bipy	(3)	(4)	1,10-phen	(5)	(6)
$\nu_{\text{sym}}(\text{COO}^-)$	1556	-	1554	1550	-	1554	1550
$\nu_{\text{asym}}(\text{COO}^-)$	1399	-	1448	1424	-	1424	1424
$\nu(\text{C}=\text{O})$	1573	-	-	-	-	-	-
$\nu(\text{C}=\text{N})$	-	1528	-	-	1504	-	-
$\nu(\text{C}-\text{N})$	-	-	1166	1168	-	1168	1168
$\nu(\text{C}-\text{Cl})$	745	-	763	763	-	762	754
$\nu(\text{M}-\text{O})$	-	-	543	547	-	547	547
$\nu(\text{M}-\text{N})$	-	-	412	410	-	402	445

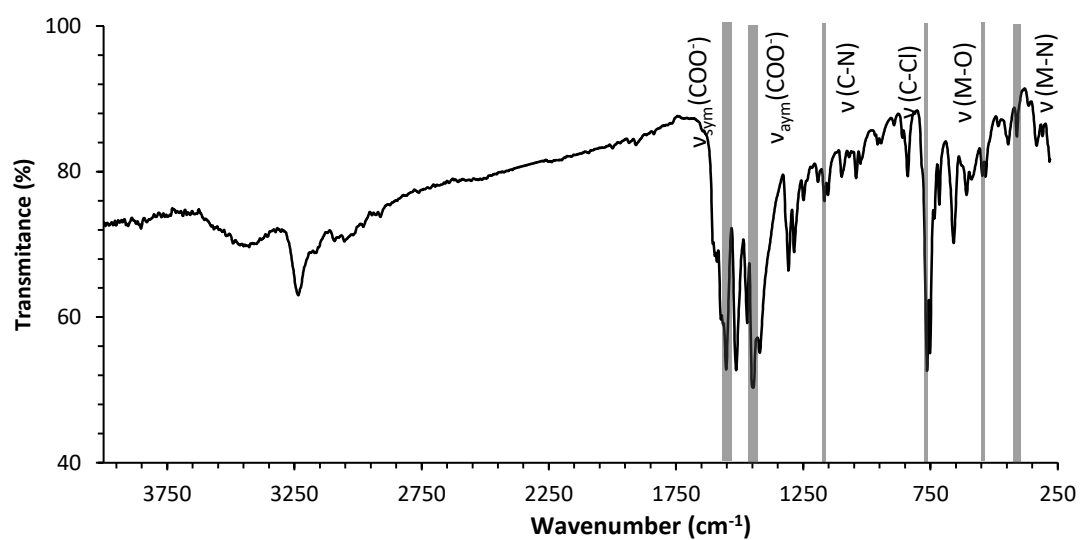


Figure 47: IR spectra of complex (3) with all the relevant peak highlighted.

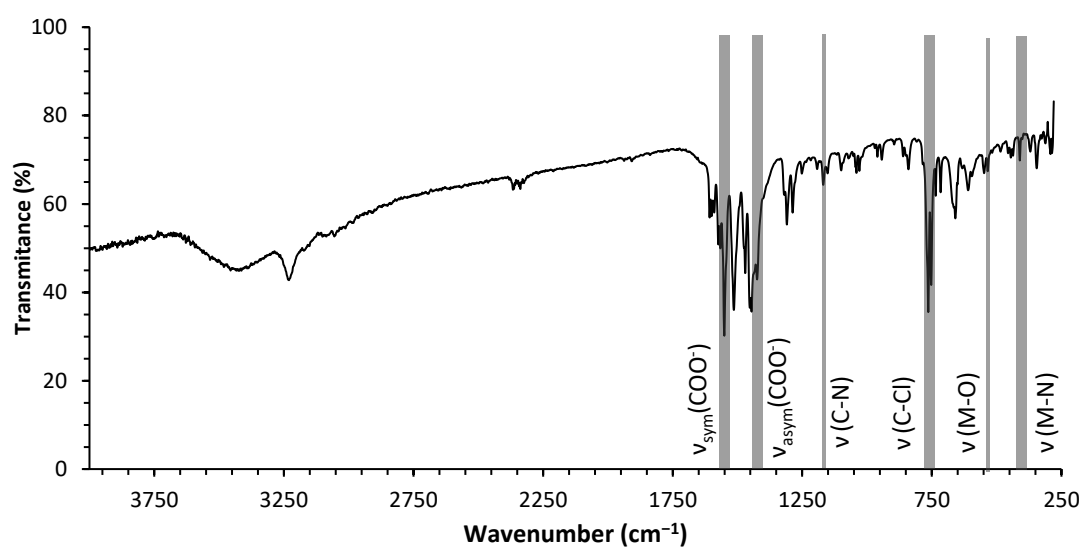


Figure 48: IR spectra of complex (4) with all the relevant peak highlighted.

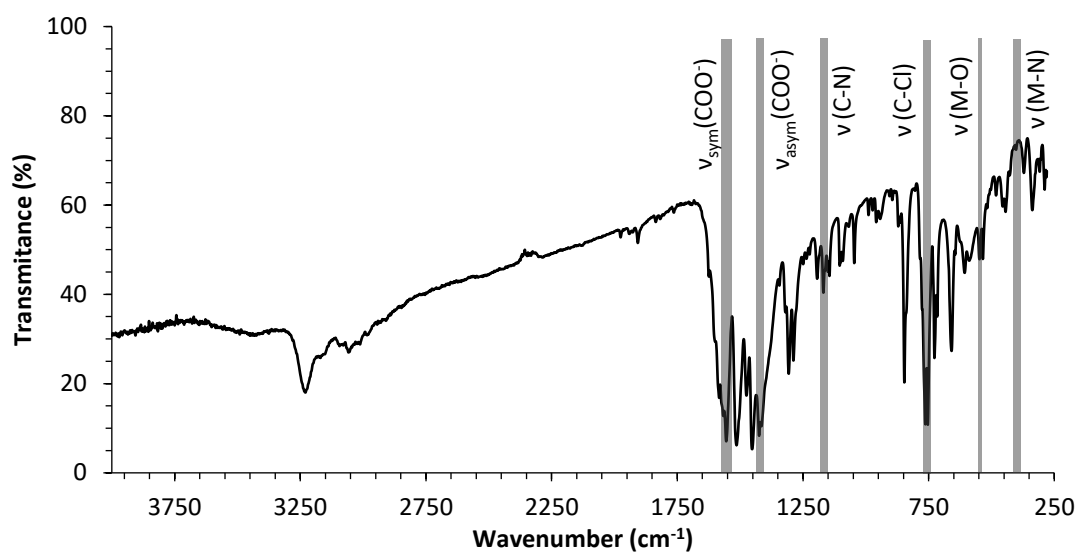


Figure 49: IR spectra of complex (5) with all the relevant peak highlighted.

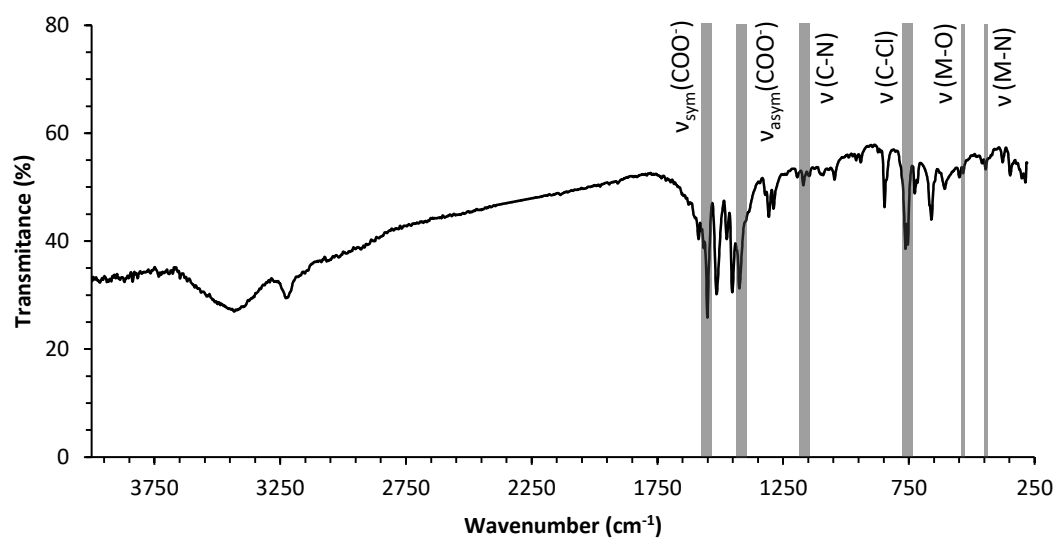


Figure 50: IR spectra of complex (6) with all the relevant peak highlighted.

### 3.12 Elemental and thermogravimetric analysis

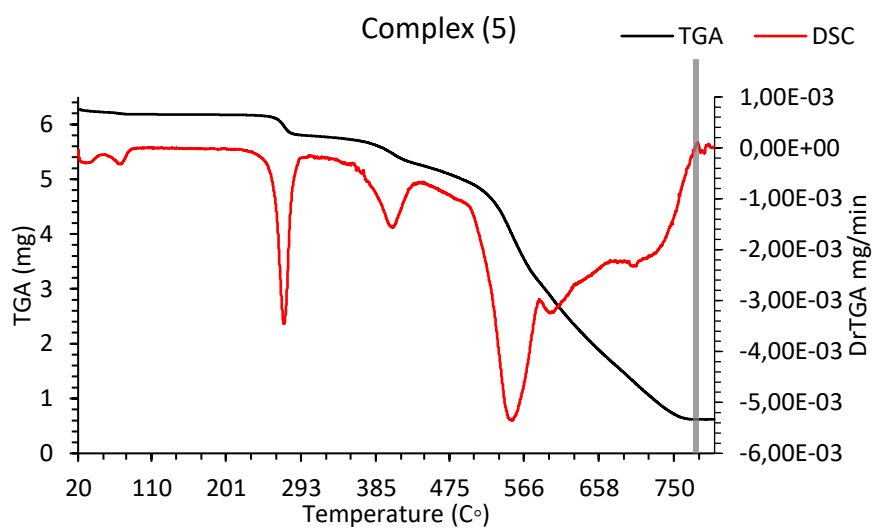
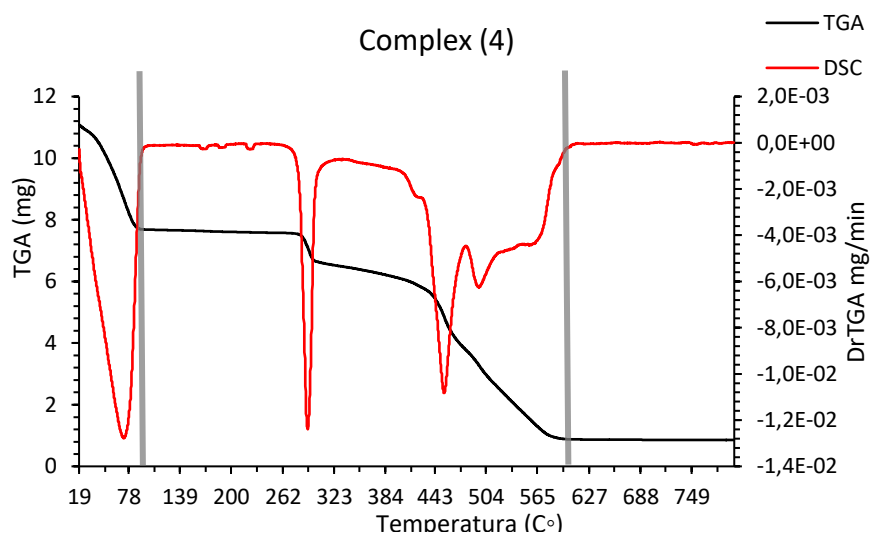
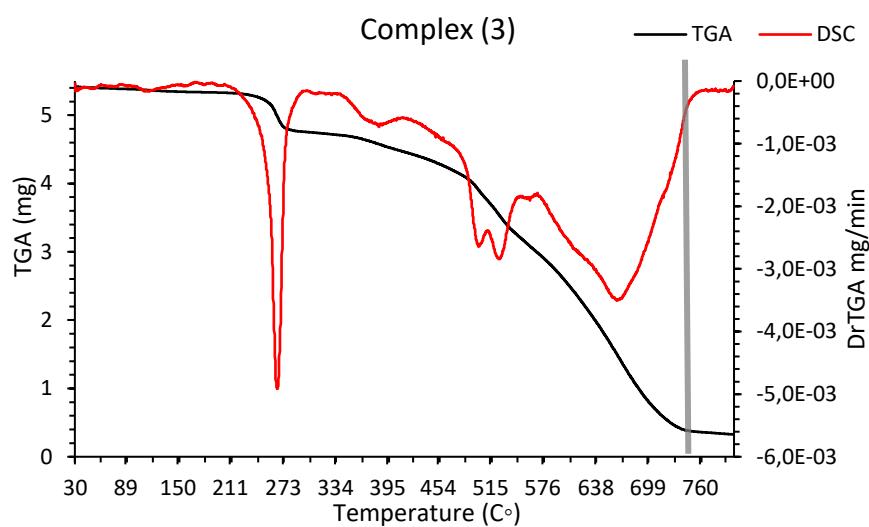
Elemental analysis (C,H,N) confirmed the chemical composition of the complexes, and as is presented in table 11, the values obtained through EA analysis are in good agreement with the ones that were calculated.

Table 11: Elementary analysis data for complex (1). "AE" = obtained values; "Cal" = calculated values base on the chemical formula from single crystal X-ray.

Complex	Carbon (%)		Hydrogen (%)		Nitrogen (%)	
	<i>AE</i>	<i>Cal</i>	<i>AE</i>	<i>Cal</i>	<i>AE</i>	<i>Cal</i>
(3)	56.2	56.5	3.86	3.50	7.54	6.94
(4)	55.4	56.5	3.60	3.50	7.31	6.94
(5)	58.9	57.9	3.72	3.40	7.23	6.76
(6)	59.0	57.9	3.51	3.40	7.34	6.76

Figure 51 shows the results of the thermogravimetric analysis performed on complex (3), (4), (5) and (6). The data characteristic of the thermal decomposition was collected in table 12. The TG and DTG curves of the complexes show that they are stable until  $\pm 380$  °C, except for complex (4) where the first stage can be attributed to the loss of two molecules of ethanol. A further increase in temperature causes a two-stage decomposition. In the first place, the complexes lose the respective ligands molecules (NSAIDs and two molecules of the N-donor) which represents the biggest % of the sample weight. Further heating gives to the final product, nickel oxide (NiO) in case of complex (4) and (6) and cobalt oxide (CoO) in case of complex (3) and (5).





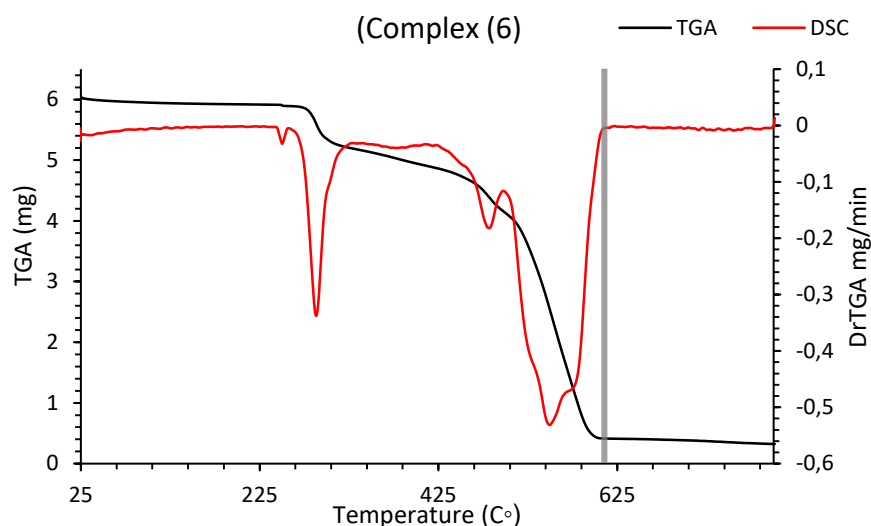


Figure 51: TGA/DSC results for complex (3) to (6).

Table 12: Results of the elementary analysis. “AE” are the values obtain from the analysis and “Cal” are the calculated values based on the chemical structure given by the x-ray.

	Stage 1 (%)		Stage 2 (%)		Stage 3 (%)	
	TG	Cal	TG	Cal	TG	Cal
Complex (3)	93.8	92.7	6.40	9.28	-----	
Complex (4)	11.1	10.3	81.1	83.2	7.81	8.31
Complex (5)	90.2	92.9	9.84	9.01	-----	
Complex (6)	93.3	93.2	6.73	9.01	-----	

With all this evidence, we can move on to interaction studies and *in vitro* studies with the certainty that, within each pair, the only variable between the complexes is the central metal and thus we can evaluate the influence of the metal ion and the N-donor ligands on the behaviour of a metal complex.

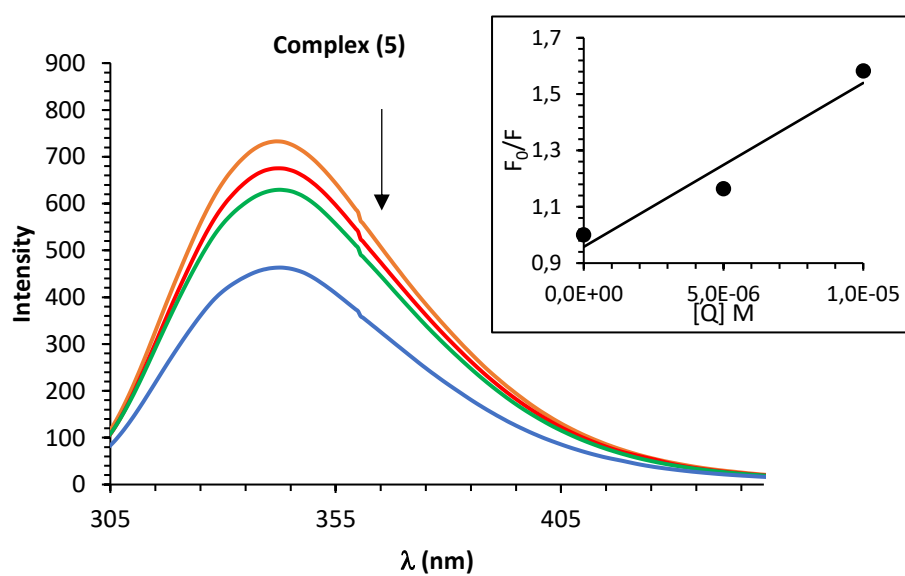
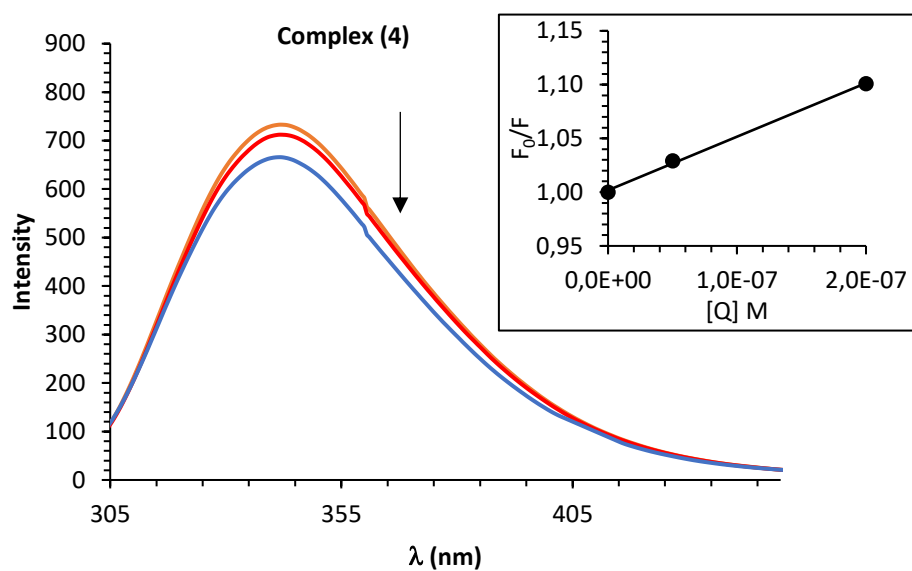
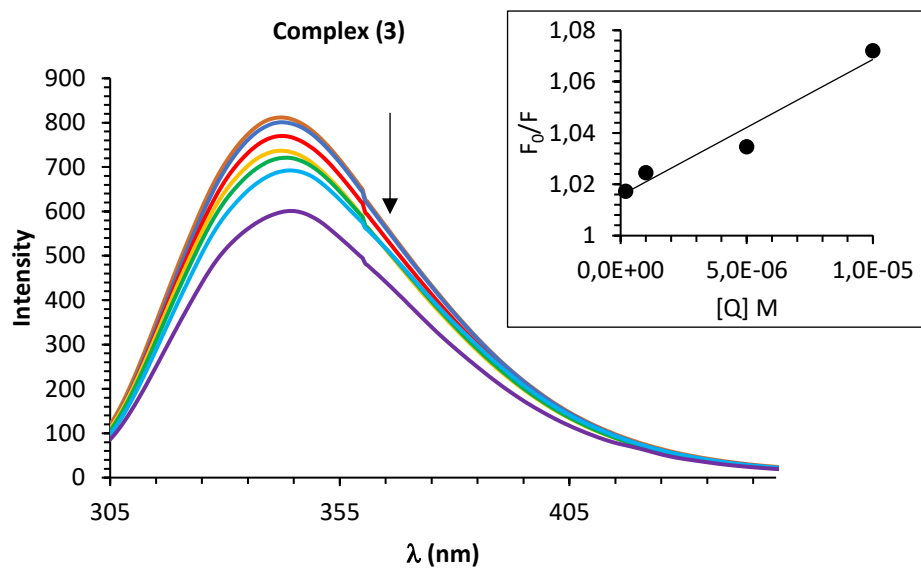
### 3.13 BSA interaction studies

#### 3.13.1 Fluorescence quenching studies

As already shown for the complexes discussed earlier, the interaction between the complexes and BSA was evaluated by fluorescence.

Complex (4) exhibit a very high fluorescence intensity at lower concentrations (Annex III) and because of that the interaction with BSA was only preformed with two concentrations of this complex, and for this reason its  $K_{sv}$  was not calculated.

Figure 52 shows the effect of these four complexes on the fluorescence intensity of BSA at  $\lambda_{ex}=295$  nm. As can be seen, it is obvious that the presence of the complexes quenches the fluorescence intensity of BSA. The quenching was accompanied by a small shift, all of this evidence reflects changes on the microenvironment of the tryptophan residues resulting from the complex interaction <sup>122</sup>. This can be analysed by the Stern–Volmer equation (*equation 3*). The  $K_{sv}$  values obtain are presented on table 13 and show that complex (3) and (5) bind to BSA with more strength that complex (6). The linearity of the plots (figure 52 – inset) are indicative that only one type of quenching mechanism is involved, it can be static or dynamic <sup>122</sup>.



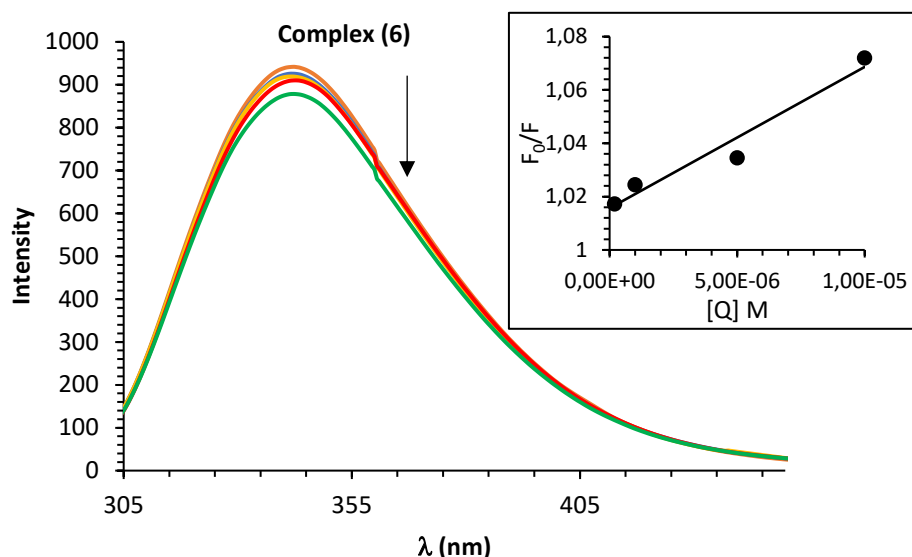


Figure 52: The fluorescence quenching spectra of BSA in the presence of various concentrations of complexes at  $\lambda_{ex} = 295$  nm and  $[BSA] = 3 \mu M$ . Arrow indicates the change upon increasing the complex concentration. Complex (3) - ( $R=0.02$ ;  $R=0.07$ ;  $R=0.3$ ;  $R=3.3$ ;  $R=6.7$ ;  $R=10$ ); Complex (4) - ( $R=0.02$ ;  $R=0.07$ ); Complex (5) - ( $R=0.07$ ;  $R=1.7$ ;  $R=3.3$ ); Complex (6) - ( $R=0.07$ ;  $R=0.33$ ;  $R=1.67$ ;  $R=1.33$ ). The plots  $F_0/F$  versus  $[Q]$  according with the Stern-Volmer equation are depicted in the insets.

Table 13: Quenching constant ( $K_{sv}$ ) for the interactions of complex (3), (5) and (6) with BSA.

Complex	$K_{sv} (M^{-1})$
(3)	$1,01 \times 10^4$
(5)	$5,29 \times 10^4$
(6)	$5,30 \times 10^3$

### 3.13.2 Circular Dichroism spectroscopic studies

The results observed from the interaction between these four complexes and BSA are represented in Figure 53. All complexes were able to reduce the two negative bands of the native BSA and cause a slight peak shift. Herein, we have calculated the  $\alpha$ -helical content of free and bound BSA with the complexes (table 14) calculated from MRE values at 208 nm using the equation (2) as discussed in section 2.5. According to quantitative analysis, native  $[BSA]=0.25 \mu M$  have about 34.6% (average) of  $\alpha$ -helical content and complex (3) and (6) was able to reduce this percentage in about 4.6 and 6.8 % respectively, for  $R=1$ , complex (4) and (5) cause a higher decrease in about 14.5 and 11.7 %, respectively, for  $R=1$ . These results show that all the four complexes were capable to change the secondary structure of BSA significantly at higher concentrations.

This phenomenon is due to the unfolding of the polypeptides which happens because of the disturbance in the hydrogen bonds caused by the metal complexes <sup>147,148</sup>.

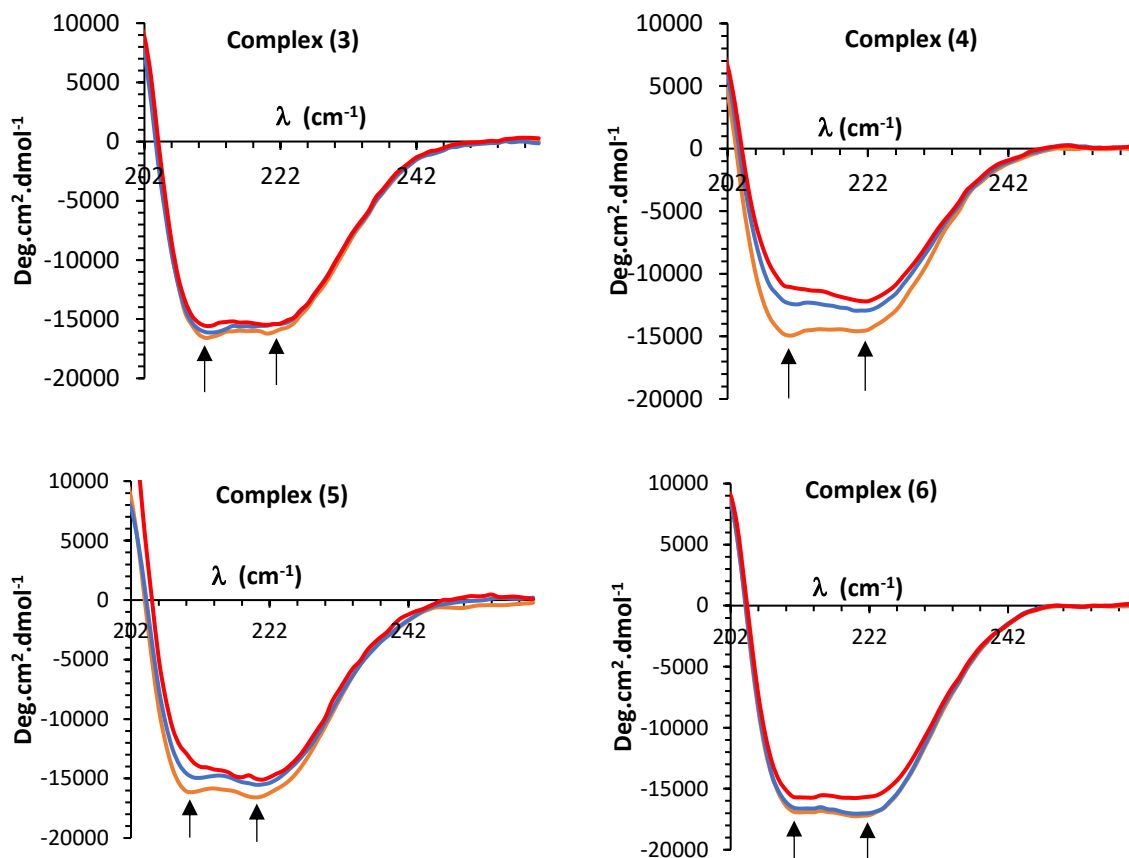


Figure 53: CD spectra of BSA in the presence of various concentrations of complex (3), (4), (5) and (6). Arrows indicates the change upon increasing the complex concentration. ([BSA]= 0.25  $\mu$ M; R=0.5; R=1).

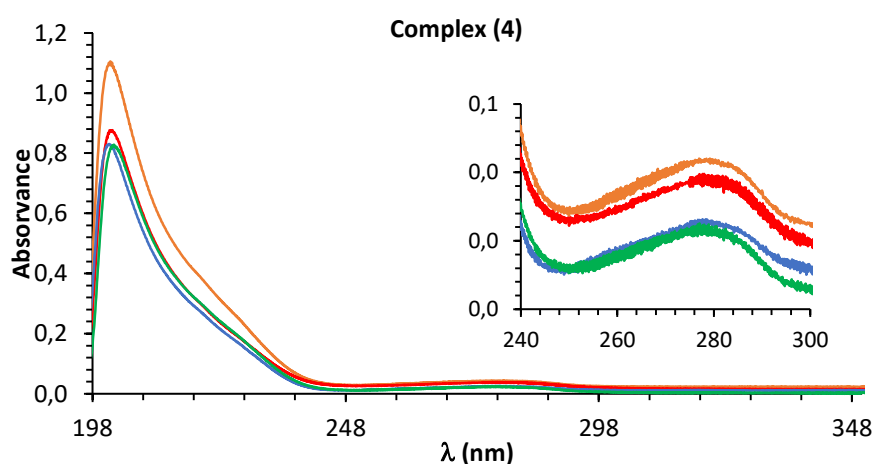
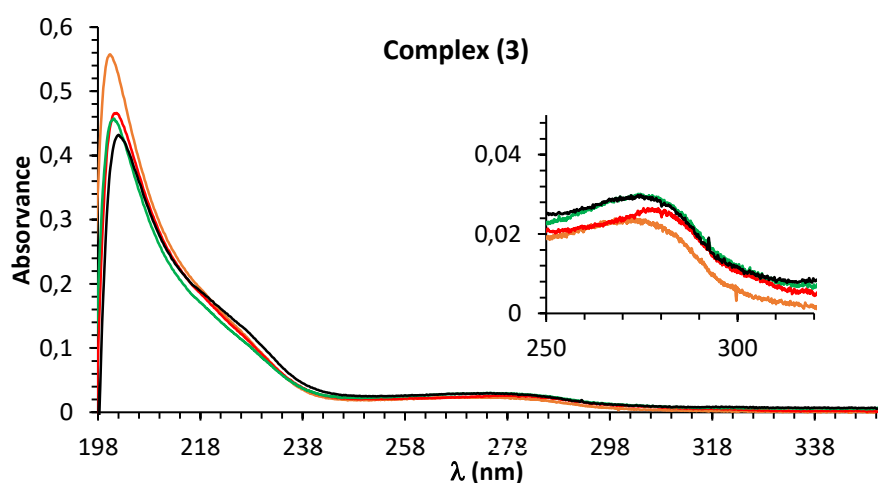
Table 14:  $\alpha$ -helix content in free BSA at 0,25  $\mu$ M (R=0) and in the presence of different ratios of complex (3) to (6).

Ratio	Complex (3)	Complex (4)	Complex (5)	Complex (6)
R=0	36.1	32.7	35.1	34.6
R=0.5	35.0	23.9	29.4	34.3
R=1	32.7	18.2	23.4	30.7

### 3.13.3 UV-Vis absorption spectroscopic studies

As previously discussed UV-Vis is a simple method that can be used to distinguish between the two possible quenching mechanisms, static or dynamic, by which the metal complexes interact with BSA <sup>122</sup>.

The results in figure 54 show that all complexes can disturb the peptide bonds and the aromatic ring of the amino acids in the BSA molecule. The 198 nm peak decreases upon the addition of the complexes due to the perturbation of the peptide bonds which reflects on changes in the secondary structure, as was seen on the DC studies – section 3.12.2. The changes in the 280 nm peak are slightest and indicate that the surrounding environment of the aromatic amino acids was altered <sup>122</sup>, this phenomenon is indicative of a static mechanism <sup>122,152</sup>. By the fluorescence quenching studies (figure 54) we were able to conclude that only one type of mechanism is present, this comes to confirm that the mechanism may be static.



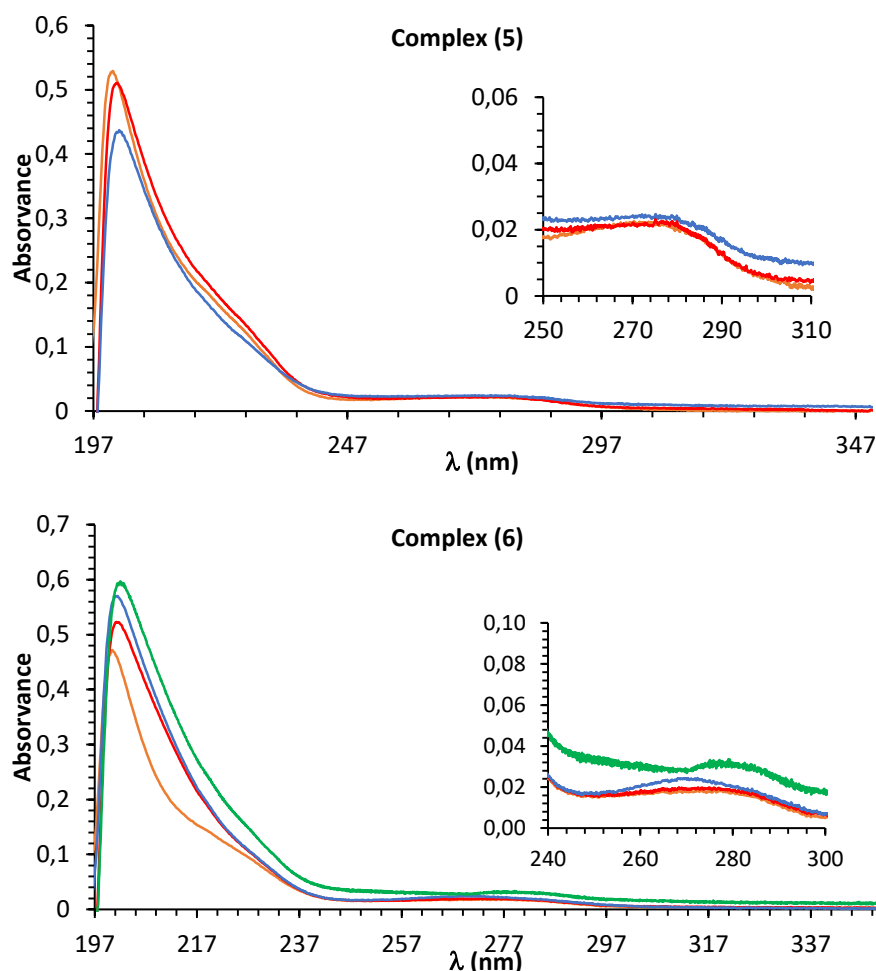


Figure 54: UV-visible absorption spectra of [BSA] in the absence (orange line) and presence of the four complexes. (Complex (3) – [BSA] = 0.5  $\mu$ M; R=20; R=40; R=100); (Complex (4) – [BSA] = 0.47  $\mu$ M; R=0.02; R=0.05; R=21); (Complex (5) – [BSA] = 0.46  $\mu$ M; R=0.11; R=1.1); (Complex (6) – [BSA] = 0.4  $\mu$ M; R=12; R=50; R=74);

### 3.14 CT-DNA interaction studies

#### 3.14.1 Circular Dichroism spectroscopic studies

Circular dichroism is a very sensitive technique that can be used to record conformational changes in CT-DNA structure. The CD spectra of CT-DNA exhibit two characteristic bands, a positive one at 275 nm and a negative one at 240 nm that are characteristic of the B-DNA form in solution <sup>175</sup>. The positive band is due to the base stacking interactions and the negative one is due to right-handed helicity of DNA <sup>176</sup>.

Different interactions between small molecules and the DNA show different perturbations in the CD spectra of the DNA, for example, simple groove binding or electrostatic interactions show very small perturbations or no perturbation at all on the



base stacking and helicity bands <sup>176</sup>. While intercalation cause significant changes in both bands <sup>100</sup>.

By the data showed in figure 55 its clear that the addition of the complexes causes an decreased on both bands, meaning that all four complexes induced disturbance on DNA base stacking and DNA right-handed helicity, by the literature this tell us that the complexes might interact with the DNA double strands in a intercalative way <sup>176,177</sup>.

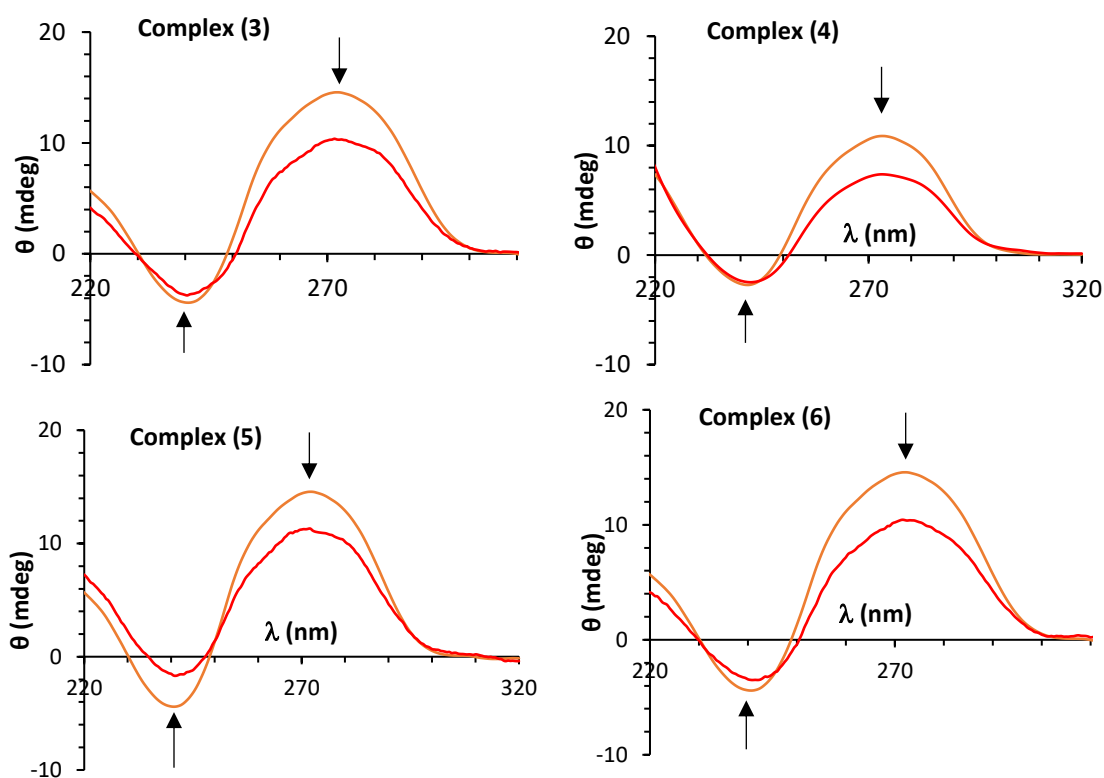


Figure 55: Circular dichroism spectra of [CT-DNA]=100  $\mu$ M in the absence and presence the complexes. [Complex (3)] - 0.05  $\mu$ M; [Complex (4)] - 0.1  $\mu$ M; [Complex (5)] - 0.05  $\mu$ M; [Complex (6)] - 0.2  $\mu$ M;

### 3.14.2 Competitive DNA-binding studies

Upon the addition of complexes to CT-DNA–EB adduct a quenching of the fluorescence intensity was observed (Figure 56), which indicate that these complexes compete with EB for the intercalation with DNA and they displace this dye from DNA. This shows that, as was suggested before, that complex (3), (4), (5) and (6) probably interact with DNA by intercalation <sup>154</sup>.

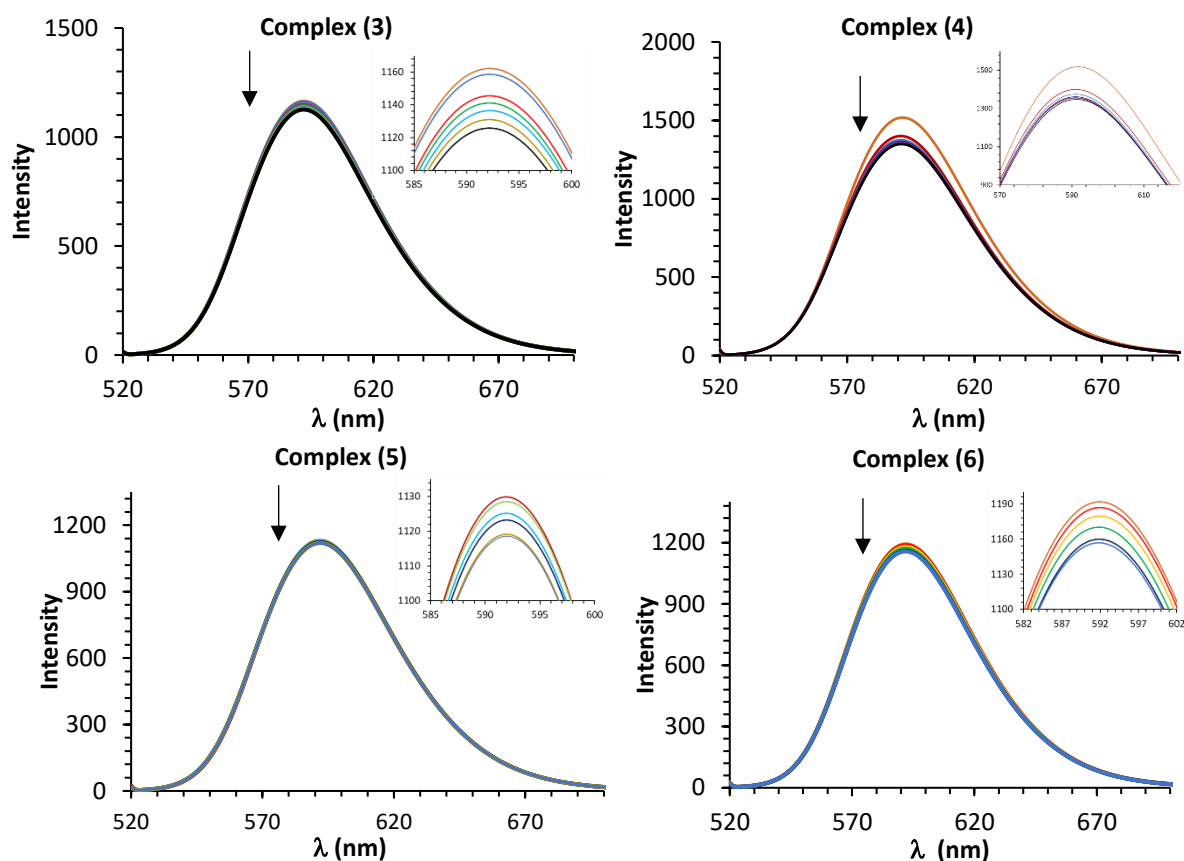


Figure 56: Effect of addition of complex (3), (4), (5) and (6) on the fluorescence intensity of the CT-DNA bound ethidium bromide (EB). The arrows show the tendency upon the addition of increasing concentrations of the complexes. [Complex (3)] – 0.05  $\mu$ M; 0.2  $\mu$ M; 1  $\mu$ M; 10  $\mu$ M; 20  $\mu$ M; 30  $\mu$ M; [Complex (4)] – 0.1  $\mu$ M; 0.25  $\mu$ M; 1  $\mu$ M; 2  $\mu$ M; 7.4  $\mu$ M; 14.8  $\mu$ M; [Complex (5)] – 0.05  $\mu$ M; 1  $\mu$ M; 5  $\mu$ M; 10  $\mu$ M; 29.6  $\mu$ M; [Complex (6)] – 0.05  $\mu$ M; 0.2  $\mu$ M; 1  $\mu$ M; 20  $\mu$ M; 30  $\mu$ M; Zoom of the quenching zone are displayed in insets.

### 3.14.3 UV-Vis absorption spectroscopy studies

In figure 57 is observable a decreased in the absorbance of the complexes UV-spectra, a hypochromic effect, this phenomenon is characteristic of molecules that bind to DNA by intercalation<sup>156</sup>. This constitute another evidence that these complexes bind to DNA through intercalation, which confirms the findings discuss above. This experiment was only preformed for complex (3) and (6). As shown in all DNA interaction assays, all complexes behave the same way, in figure 57 are only represented the interaction for complex (3) and (6), but the hypochromic effect found for these complexes is probably representative of the behaviour of complexes (4) and (5).

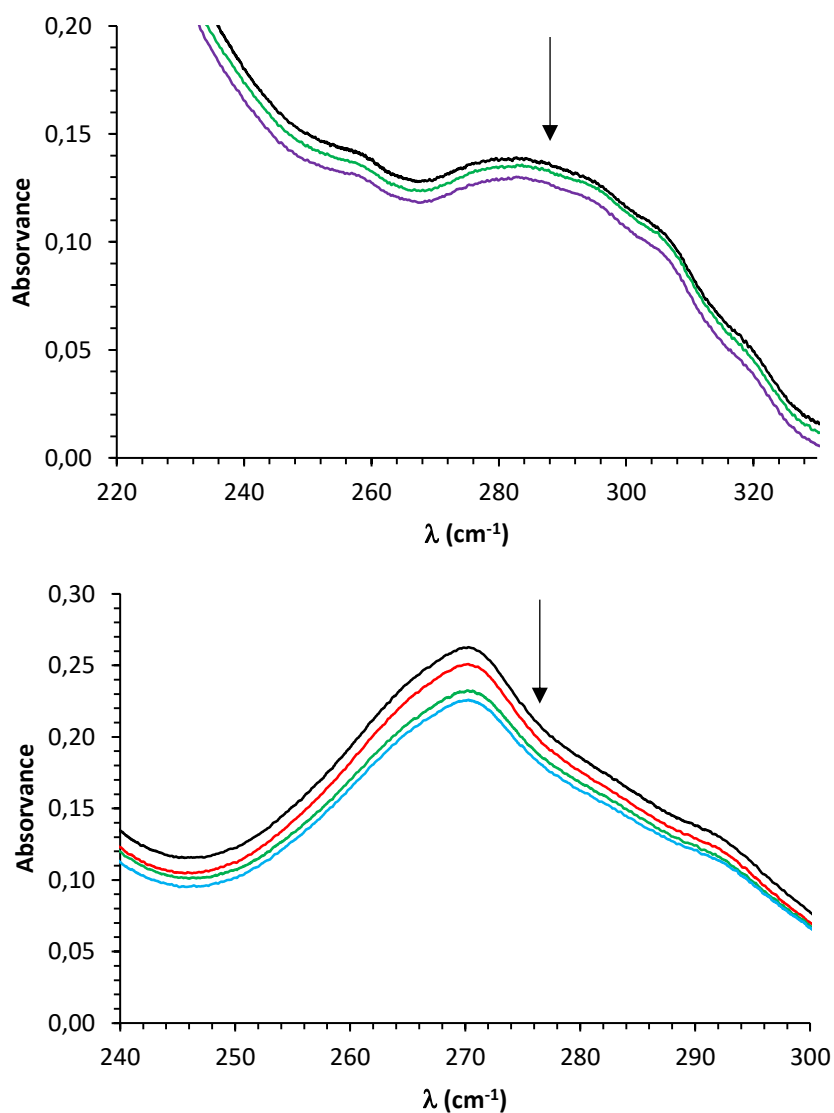


Figure 57: UV spectra of complex (3) and (6) (black line) with increasing concentrations of CT-DNA. The arrows show the effect upon the addition of CT-DNA. [Complex (3)]=20  $\mu\text{M}$ ; [CT-DNA]=10  $\mu\text{M}$ ; 20  $\mu\text{M}$ ; [Complex (6)]= 20  $\mu\text{M}$ ; [CT-DNA]=10  $\mu\text{M}$ ; 15  $\mu\text{M}$ ; 25  $\mu\text{M}$ ;

### 3.15 *In vitro* biological assays

#### 3.15.1. MTT assay

The cytotoxicity of all the four Co and Ni complexes (3-6) was tested on the MCF-7, MDA-MB-231 and MCF-12A cell lines by exposing them for 24h to the medium containing the complex at concentrations 10 and 100  $\mu\text{M}$ . As can be seen in figure 58 the cytotoxicity of the four complexes was different between them and different for each cell line under study.

Regarding to the MCF-7 cell line, complexes (4) and (6) were not able to significantly decrease their cell viability at any of the tested concentrations. On the other hand, complexes (3) and (5) were able to significantly decreased cell viability for the highest concentration (100  $\mu$ M). The main difference between compounds (4) and (6) and compounds (3) and (5) is the nature of metallic centre, the former are nickel complexes and the last ones have cobalt, this fact prompted us to search studies where the type of the metal could be related with the development and progression of tumours. The search revealed that some studies have suggested that heavy metals such as cadmium and nickel can function as endocrine disruptors by mimicking the action of estrogen. As a result, these metals are often referred to as metalloestrogens <sup>178,179</sup>. Since estrogen itself plays an important role in the development and progression of the disease, the ability of metalloestrogens to bind to and activate the estrogen receptors suggests that these compounds may also contribute to the development of breast cancer <sup>180</sup>. Once the MCF-7 cells are ER positive (estrogen receptor positive) and the compounds (4) and (6) are nickel complexes we must considered the possibility of they act as metalloestrogens. However more (and different) biological assays will be needed to validate this hypothesis.

The MTT results obtained for the MDA-MB-231 cell line revealed a concentration dependent cytotoxicity effect for the complexes (3), (4) and (5). Data obtained for complex 6 revealed a significant increase of the cell viability for the same cell line. MDA-MB-231 cell line is known as triple-negative breast cancer (TNBC), because of the three missing molecular markers, and therefore no relationship between cell viability and nature of metal centre was expected.

Regarding to the non-tumoral line (MCF-12A) it was possible observed that complexes (4) and (5) revealed a concentration dependent cytotoxicity effect towards the normal cells. As can be seen this effect is more pronounced for complex (4). On the other hand, complexes (3) and (6) did not cause any significant change on MCF-12 cellular viability.

Combination of the MTT results obtained for the four complexes, regarding tumoral and non-tumoral lines, allow us to conclude that complex (3) shows selectivity (is cytotoxic to both tumoral lines but present almost no toxicity regarding normal cells).

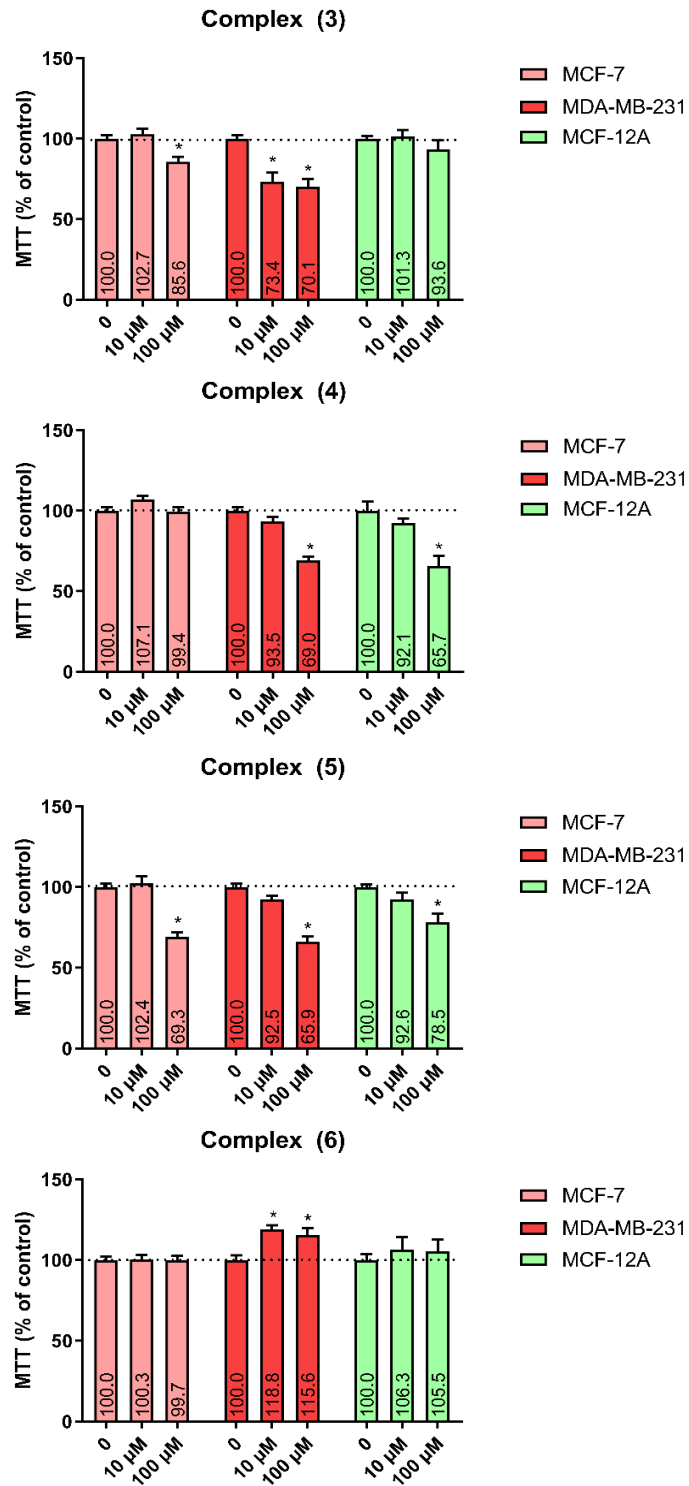


Figure 58: Cytotoxicity assessment by MTT assay induced by complex (3), (4), (5) and (6). The cells were exposed to different concentrations of each complex for 24h. \* $p < 0,05$  vs control.

### 3.16.2. TBARS assay

As previously mentioned, the results obtained by TBARS assay gives information about the lipid peroxidation promoted by the metal complexes, and conclusions can be made about its role on cancer cell death. In figure 59 are presented the results obtained for complexes (3) to (6). For the MCF-7 cell line, only complexes (4) and (5) increased significantly the levels of lipid peroxidation. This increase was much more evident to complex (5) which can be well correlated with the MTT results, once this complex was the one that exhibited the higher decreased on cell viability. On the other hand, and although complex (4) also promoted an increase of the LPO, the MTT results do not revealed the capacity of this complex to reduce the MCF-7 line viability. According to literature, and as previously mentioned, ROS doesn't always have to contribute to decreasing the cell viability, they also can contribute to cell proliferation, signal transduction cascade and differentiation <sup>160</sup>.

Regarding to the MDA-231-MB cell line, the TBARS results showed that only complex (3) significantly increased the levels of LPO. Although it was possible to observe an increase for the LPO levels for complexes (4) and (5) these results were not significantly higher than the control. This observation can be well correlated with the MTT results since complexes (3), (4) and (5) were able to significantly decrease the cell viability of the MDA-231-MB cells but complex (3) was the only that was able to significantly decrease viability even for the lowest concentration. Combination of the MTT and TBARS results seems to evidence that LPO may not be the mainly mechanism of action of complexes (4) and (5) on the tumoral cells, phenomenon that was already seen with other complexes <sup>172,173</sup>.

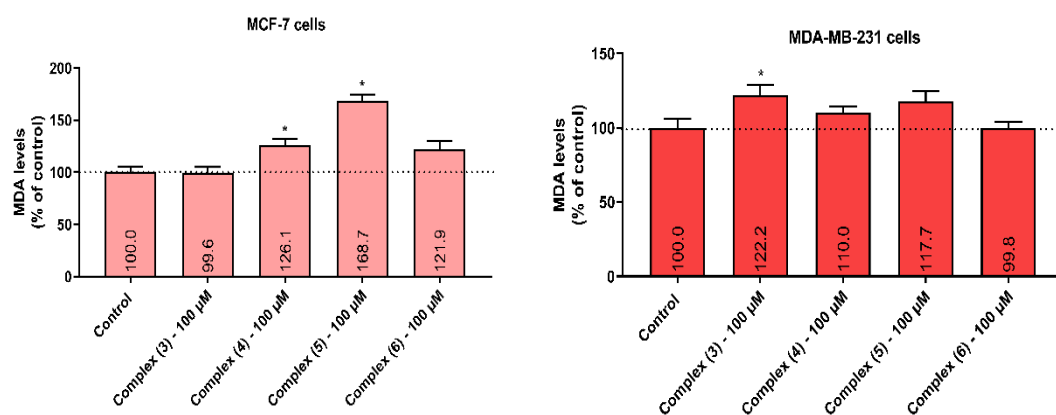


Figure 59: Lipid peroxidation levels of the cell lines after 24h treatment with the metal complexes. \* $p < 0,05$  vs control (t-test).





## **Chapter 4 – Conclusions and future perspectives**



## 4.1 Conclusions

In the present study, six novel metal complexes containing NSAIDs and N-donor ligands have been designed, synthesized, characterized and evaluated for *in vitro* anticancer activity. Investigation by several techniques (UV-vis, fluorescence and CD) revealed that intercalation seems to be the most probable interaction mechanism between all the complexes and CT-DNA. By the same techniques it can be observed that the interaction between the complexes and BSA, is probably by a static mechanism, in which they induce changes in the secondary structure of the protein with a decreased  $\alpha$ -helix content and interfere in the microenvironment of the tryptophan residues. With regard to the second group of complexes tested (3 to 6), the metal centre doesn't seem to determinate the type of interaction with DNA or BSA, since all of them present the same interaction properties.

Regarding to the *in vitro* biological assays, complex (1) and (2) were identified as anti-proliferative agents against both cancer cell lines, MCF-7 and MDA-MB-231 (a triple negative cell line). Complex (1) have the ability to disrupt the redox homeostasis (TBARS assay) of these cell lines which results on a decrease the cell viability (MTT assay). Complex (2) only increase the LPO on MDA-MB-231, which appears to contribute to the decrease on cell viability, however this not seem to be the mechanism on the MCF-7, in which complex (2) decrease the cell viability but did not cause significative changes on the MDA levels (lipid peroxidation).

The comparative studies between complex (3), (4), (5) and (6), led us to conclude that the nature of the metal centre is a key feature on the biological properties of the metal complex that need to be more investigated. Complex (5) and (6), that only are different on their metal centre, present great differences regarding their response on the MTT assays. The Co(II) complexes exhibit cytotoxic activity to the two tumoral cell lines, while the Ni(II) complex don't seem to have any effect of MCF-7 cell line. In the same way, complex (3) and (4) also present interesting differences, the Co(II) complex exhibit selectivity to the tumoral cells, once this complex didn't show cytotoxic activity for the non-tumoral cell line (MCF-12), while the Ni(II) complex presented higher cytotoxicity, in comparison with the tumoral cells, to the non-tumoral line (MCF-12A). Interesting differences were also found on the TBARS assay, complex (5) seems to decrease the cell vitality of the MCF-7 cells by causing significant lipid peroxidation, the

same conclusion can be made about complex (3) on the MDA-MB-231 cell line. Other complexes that cause a decrease on cell viability and did not increase the MDA levels seem to have other active mechanisms that are not related with lipid peroxidation.

On the basis of the obtained results it can be evidenced that the metal complexes resulting from the combination of NSAIDs and N-donor ligands, may be strong candidates for further evaluation as chemotherapeutic agents.

#### **4.2 Further perspectives**

In order to understand better the mode of action these complexes further studies can be carry out. Analysis the viscosity of the DNA upon the interaction with the metal complexes is another method that helps to clarify the binding mode of the complexes with DNA. Perform the BSA fluorescence quenching studies with different temperature is another way to elucidate if the interaction mechanism is static or dynamic.

Once the nature of the metal centre seems to make a major difference on the toxicity of cancer cells other features need to be examined, like measure the influence of the metal centre on the cell cycle of cancer cells using flow cytometry. Using the same method, it will be interesting to study the differences between complexes (3) to (6) on the type of death that they can inflict on cancer cells (apoptosis/necrosis), using the annexin V/PI method. It will be also interesting to see specific intracellular targets of these complexes and evaluate if different metal centres can determinate different targets, this study can be made by laser scanning confocal microscopy.

## Work Divulagation

### Poster presentation

#### **“Novel anticancer metallodrugs”**

Luís Monteiro; Adriana Gomes; C. Silva; F. Martel; R. Mendes; F. Paz; B.J.M. Leite Ferreira; T.M. Santos

- **4<sup>th</sup> Meeting of Medicinal Biotechnology** (17<sup>th</sup> May 2019, Porto, Portugal)
- **Jornadas CICECO 2019** (11 – 12<sup>nd</sup> June 2019, Aveiro, Portugal)
- **XXVI Encontro Nacional da SPQ** (24 – 26<sup>th</sup> July 2019, Porto, Portugal)

### Oral presentation

#### **“Development of new anticancer metallodrugs”**

Luís Monteiro; Adriana Gomes; C. Silva; F. Martel; R. Mendes; F. Paz; B.J.M. Leite Ferreira; T.M. Santos

- **XXV Encontro Galego-Português de Química** (20 – 22<sup>nd</sup> November 2019, Santiago de Compostela, Spain)



## References

1. Kannan N, Shanmuga Sundar S, Balaji S, Amuthan A, Anil Kumar N V., Balasubramanian N. Physiochemical characterization and cytotoxicity evaluation of mercury-based formulation for the development of anticancer therapeutics. *PLoS One*. 2018;13(6):1-13.
2. Muhammad N, Guo Z. Metal-based anticancer chemotherapeutic agents. *Curr Opin Chem Biol*. 2014;19:144-153.
3. Ndagi U, Mhlango N, Soliman ME. Metal complexes in cancer therapy – an update from drug design perspective. *Drug Des Devel Ther*. 2017;11:599-616.
4. Bhargava A, Vaishampayan UN. Satraplatin: leading the new generation of oral platinum agents. *Expert Opin Investig Drugs*. 2009;18(11):1787-1797.
5. Shi Y, Liu SA, Kerwood DJ, Goodisman J, Dabrowiak JC. Pt(IV) complexes as prodrugs for cisplatin. *J Inorg Biochem*. 2012;107(41):6-14.
6. Oun R, Moussa YE, Wheate NJ. The side effects of platinum-based chemotherapy drugs: A review for chemists. *Dalt Trans*. 2018;47(19):6645-6653.
7. Yano S, Ohi H, Ashizaki M, et al. Syntheses, characterization, and antitumor activities of platinum(II) and palladium(II) complexes with sugar-conjugated triazole ligands. *Chem Biodivers*. 2012;9:1903-1915.
8. Cucciolito ME, D'Amora A, De Feo G, et al. Five-Coordinate Platinum(II) Compounds Containing Sugar Ligands: Synthesis, Characterization, Cytotoxic Activity, and Interaction with Biological Macromolecules. *Inorg Chem*. 2018;57:3133-3143.
9. Weser U, Richter C, Wendel A, Younes M. Reactivity of antiinflammatory and superoxide dismutase active Cu(II)-salicylates. *Bioinorg Chem*. 1978;8:201-213.
10. Asirvatham S, Dhokchawle B V, Tauro SJ. Quantitative structure activity relationships studies of non-steroidal anti-inflammatory drugs : A review. *Arab J Chem*. 2016.
11. Chohan ZH, Iqbal MS, Iqbal HS, Scozzafava A, Supuran CT. Transition metal acetylsalicylates and their anti-inflammatory activity. *J Enzyme Inhib Med Chem*. 2002;17(2):87-91.
12. Ornelas A, Zacharias-Millward N, Menter DG, et al. Beyond COX-1: the effects of aspirin on platelet biology and potential mechanisms of chemoprevention. *Cancer Metastasis Rev*. 2017;36:289-303.
13. Hilário MOE, Terreri MT, Len CA. Nonsteroidal anti-inflammatory drugs: cyclooxygenase 2 inhibitors. *J Pediatr (Rio J)*. 2006;82:206-212.
14. Au JL-S, Yeung BZ, Wientjes MG, Lu Z, Wientjes MG. Delivery of cancer therapeutics to extracellular and intracellular targets: Determinants, barriers, challenges and opportunities. *Adv Drug Deliv Rev*. 2016;97:280-301.
15. Thamilarasan V, Sengottuvelan N, Stalin N, Srinivasan P, Chakkaravarthi G.

- Synthesis, interactions, molecular structure, biological properties and molecular docking studies on Mn, Co, Zn complexes containing acetylacetone and pyridine ligands with DNA duplex. *J Photochem Photobiol B Biol.* 2016;160:110-120.
16. Alberti E, Zampakou M, Donghi D. Covalent and non-covalent binding of metal complexes to RNA. *J Inorg Biochem.* 2016;163:278-291.
  17. Hostetter AA, Osborn MF, DeRose VJ. Characterization of RNA-Pt adducts formed from cisplatin treatment of *Saccharomyces cerevisiae*. *ACS Chem Biol.* 2012;7:218-225.
  18. Suh JM, Kim G, Kang J, Lim MH. Strategies Employing Transition Metal Complexes to Modulate Amyloid- $\beta$  Aggregation. *Inorg Chem.* 2019;58(1):8-17.
  19. Krstić NS, Nikolić RS, Stanković MN, Nikolić NG, Đorđević DM. Coordination Compounds of M ( II ) Biometal Ions with Acid- Type Anti-inflammatory Drugs as Ligands – A Review. *Trop J Pharm Res.* 2015;14(2):337-349.
  20. Caglar S, Aydemir IE, Adigüzel E, Caglar B, Demir S, Buyukgungor O. Four copper(II) diclofenac complexes with pyridine derivatives: Synthesis, crystal structures, spectroscopic properties, thermal analysis and catechol oxidase activities. *Inorganica Chim Acta.* 2013;408:131-138.
  21. Smolková R, Zeleňák V, Smolko L, et al. Novel zinc complexes of a non-steroidal anti-inflammatory drug, niflumic acid: Structural characterization, human-DNA and albumin binding properties. *Eur J Med Chem.* 2018;153:131-139.
  22. Abu-dahab R, Khalil E, Khdaib A, El-sabawi D, Hamdan I. Antiproliferative Activity of Selected Non-Steroidal Anti-Inflammatory Agents : Role of Iron Complexes. *J Pharm.* 2014;7(49).
  23. Tsiliou S, Kefala LA, Hatzidimitriou AG, et al. Cobalt(II) complexes with non-steroidal anti-inflammatory drugs and  $\alpha$  -diimines. *J Inorg Biochem.* 2015.
  24. Zampakou M, Rizeq N, Tangoulis V, et al. Manganese(II) complexes with the non-steroidal anti-inflammatory drug tolafenamic acid: Structure and biological perspectives. *Inorg Chem.* 2014;53:2040-2052.
  25. Kyropoulou M, Raptopoulou CP, Psycharis V, Psomas G. Ni(II) complexes with non-steroidal anti-inflammatory drug diclofenac: Structure and interaction with DNA and albumins. *Polyhedron.* 2013.
  26. Lawrance G a. *Introduction to Coordination Chemistry.*; 2010.
  27. Osredkar J, Sustar M. Copper and Zinc, Biological Role and Significance of Copper/Zinc Imbalance. *J Clin Toxicol.* 2011;3(1).
  28. Letelier ME, Sánchez-Jofré S, Peredo-Silva L, Cortés-Troncoso J, Aracena-Parks P. Mechanisms underlying iron and copper ions toxicity in biological systems: Pro-oxidant activity and protein-binding effects. *Chem Biol Interact.* 2010;118:220-227.
  29. Weder JE, Dillon CT, Hambley TW, et al. Copper complexes of non-steroidal anti-inflammatory drugs: An opportunity yet to be realized. *Coord Chem Rev.*



2002;232(1-2):95-126.

30. Sarkar S, Mondal A, Ribas J, Drew MGB, Pramanik K, Rajak KK. Mono, di and polynuclear Cu(II)-azido complexes incorporating N,N,N reduced schiff base: Syntheses, structure and magnetic behavior. *Inorganica Chim Acta*. 2005;358:641-649.
31. Tarushi A, Perontsis S, Hatzidimitriou AG, Papadopoulos AN, Kessissoglou DP, Psomas G. Copper(II) complexes with the non-steroidal anti-inflammatory drug tolfenamic acid: Structure and biological features. *J Inorg Biochem*. 2015;149:68-79.
32. Perontsis S, Hatzidimitriou AG, Begou OA, Papadopoulos AN, Psomas G. haracterization and biological properties of copper(II)-ketoprofen complexes. *J Inorg Biochem*. 2016;162:22-30.
33. Boodram JN, Mcgregor IJ, Bruno PM, Cressey PB, Hemann MT, Suntharalingam K. Breast Cancer Stem Cell Potent Copper(II)-Non-Steroidal Anti-Inflammatory Drug Complexes. *Angew Chemie - Int Ed*. 2016;55:2845-2850.
34. Conner EM, Reglinski J, Smith WE, Zeitlin IJ. Schiff base complexes of copper and zinc as potential anti-colitic compounds. *BioMetals*. 2017;30(3).
35. Lian W-J, Wang X-T, Xie C-Z, et al. Mixed-ligand copper(ii) Schiff base complexes: the role of the co-ligand in DNA binding, DNA cleavage, protein binding and cytotoxicity. *Dalt Trans*. 2016;45:9073-9087.
36. Jia L, Xu J, Zhao X, et al. Synthesis, characterization, and antitumor activity of three ternary dinuclear copper (II) complexes with a reduced Schiff base ligand and diimine coligands in vitro and in vivo. *J Inorg Biochem*. 2016;159:107-119.
37. Zhou X-Q, Li Y, Zhang D-Y, et al. Copper complexes based on chiral Schiff-base ligands: DNA/BSA binding ability, DNA cleavage activity, cytotoxicity and mechanism of apoptosis. *Eur J Med Chem*. 2016;114:244-256.
38. Ribeiro N, Roy S, Butenko N, et al. New Cu(II) complexes with pyrazolyl derived Schiff base ligands: Synthesis and biological evaluation. *J Inorg Biochem*. 2017;174:63-75.
39. Lu C, Eskandari A, Cressey PB, Suntharalingam K. Cancer Stem Cell and Bulk Cancer Cell Active Copper(II) Complexes with Vanillin Schiff Base Derivatives and Naproxen. *Chem - A Eur J*. 2017;23(47):11366-11374.
40. Leite SMG, Lima LMP, Gama S, et al. Copper(II) Complexes of Phenanthroline and Histidine Containing Ligands: Synthesis, Characterization and Evaluation of their DNA Cleavage and Cytotoxic Activity. *Inorg Chem*. 2016;55(22):11801-11814.
41. Iglesias S, Alvarez N, Torre MH, et al. Synthesis, structural characterization and cytotoxic activity of ternary copper(II)-dipeptide-phenanthroline complexes. A step towards the development of new copper compounds for the treatment of cancer. *J Inorg Biochem*. 2014;139:117-123.

42. Paixão DA, Marzano IM, Jaimes EHL, et al. Novel copper(II) complexes with hydrazides and heterocyclic bases: Synthesis, structure and biological studies. *J Inorg Biochem.* 2017;172:138-146.
43. Prosser KE, Chang SW, Saraci F, Le PH, Walsby CJ. Anticancer copper pyridine benzimidazole complexes: ROS generation, biomolecule interactions, and cytotoxicity. *J Inorg Biochem.* 2017;167:89-99.
44. Czerwińska K, Machura B, Kula S, et al. Copper(II) complexes of functionalized 2,2':6',2''-terpyridines and 2,6-di(thiazol-2-yl)pyridine: structure, spectroscopy, cytotoxicity and catalytic activity. *Dalt Trans.* 2017;44:3686-3700.
45. Salimi M, Abdi K, Kandelous HM, et al. Antiproliferative effects of copper(II)–polypyridyl complexes in breast cancer cells through inducing apoptosis. *BioMetals.* 2015;28:267-278.
46. Stafford VS, Suntharalingam K, Shivalingam A, White AJP, Mann DJ, Vilar R. Syntheses of polypyridyl metal complexes and studies of their interaction with quadruplex DNA. *Dalton Trans.* 2015;44(8).
47. Filho JCC, Sarria ALF, Becceneri AB, et al. Copper (II) and 2,2'-Bipyridine Complexation Improves Chemopreventive Effects of Naringenin against Breast Tumor Cells. *PLoS One.* 2014;9(9).
48. Jopp M, Becker J, Becker S, et al. Anticancer activity of a series of copper(II) complexes with tripodal ligands. *Eur J Med Chem.* 2017;132:274-281.
49. Bonaventura P, Benedetti G, Albarede F, Miossec P. Zinc and its role in immunity and inflammation. *Autoimmun Rev.* 2015;14(4):277-285.
50. Khomskii DI. *Transition Metal Compounds.*; 2014.
51. Krężel A, Maret W. The biological inorganic chemistry of zinc ions. *Arch Biochem Biophys.* 2016;611:3-19.
52. Maret W. New perspectives of zinc coordination environments in proteins. *J Inorg Biochem.* 2012;111. <http://dx.doi.org/10.1016/j.jinorgbio.2011.11.018>.
53. Dudev T, Lim C. Tetrahedral vs octahedral zinc complexes with ligands of biological interest: A DFT/CDM study. *J Am Chem Soc.* 2000;122:11146-11153.
54. Andreini C, Banci L, Bertini I, Rosato A. Counting the zinc-proteins encoded in the human genome. *J Proteome Res.* 2005;5:196-201.
55. Deng W, Zhang Q, Wang Y. Polynuclear complexes of main group and transition metals with polyaminopolycarboxylate and polyoxometalate. *Dalt Trans.* 2012;41(33):9971-9978.
56. Valentová J, Varényi S, Herich P, et al. Synthesis, structures and biological activity of copper(II) and zinc(II) Schiff base complexes derived from aminocyclohexane-1-carboxylic acid. New type of geometrical isomerism in polynuclear complexes. *Inorganica Chim Acta.* 2018;480:16-26.
57. Bai F, Ni Y, Jiang Y, et al. Synthesis, crystal structure and luminescence

- properties of “paddle wheel” and “butterfly” shaped polynuclear complexes. *J Mol Struct.* 2017;1131:190-195.
58. Jarosz M, Szkaradek N, Marona H, Nowak G, Młyniec K, Librowski T. Evaluation of anti-inflammatory and ulcerogenic potential of zinc–ibuprofen and zinc–naproxen complexes in rats. *Inflammopharmacology.* 2017;25:653-663.
  59. Smolková R, Zeleňák V, Smolko L, Sabolová D, Kuchár J, Gyepes R. Novel Zn(II) complexes with non-steroidal anti-inflammatory ligand, flufenamic acid: Characterization, topoisomerase I inhibition activity, DNA and HSA binding studies. *J Inorg Biochem.* 2017;177:143-158.
  60. Dixon SJ, Stockwell BR. The role of iron and reactive oxygen species in cell death. *Nat Chem Biol.* 2014;10(1):9-17.
  61. Kell DB. Iron behaving badly: Inappropriate iron chelation as a major contributor to the aetiology of vascular and other progressive inflammatory and degenerative diseases. *BMC Med Genomics.* 2009;2(2).
  62. Börzel H, Comba P, Hagen KS, et al. Iron coordination chemistry with tetra-, penta- and hexadentate bispidine-type ligands. *Inorganica Chim Acta.* 2002;337:407-419.
  63. Anupama B, Sunita M, Shiva Leela D, Ushaiah B, Gyana Kumari C. Synthesis, spectral characterization, DNA binding studies and antimicrobial activity of Co(II), Ni(II), Zn(II), Fe(III) and VO(IV) complexes with 4-aminoantipyrine schiff base of ortho-vanillin. *J Fluoresc.* 2014;24(4):1067–1076.
  64. Soliman MH, Mohamed GG. Cr(III), Mn(II), Fe(III), Co(II), Ni(II), Cu(II) and Zn(II) new complexes of 5-aminosalicylic acid: Spectroscopic, thermal characterization and biological activity studies. *Spectrochim Acta - Part A Mol Biomol Spectrosc.* 2013;107:8-15.
  65. Czarnek K, Terpilowska S, Siwicki AK. Selected aspects of the action of cobalt ions in the human body. *Cent Eur J Immunol.* 2015;40(2):236-242.
  66. Crichton R. R. *Biological Inorganic Chemistry - A New Introduction to Molecular Structure and Function.* Vol 34. 2nd ed. Elsevier; 2012.
  67. Miodragović DU, Bogdanović GA, Miodragović ZM, et al. Interesting coordination abilities of antiulcer drug famotidine and antimicrobial activity of drug and its cobalt(III) complex. *J Inorg Biochem.* 2006;100(9):1568-1574.
  68. leela DS, Ushaiah B, Anupama G, Sunitha M, Kumari CG. Synthesis, Characterization, Antimicrobial, DNA Binding and Cleavage Studies of Mixed Ligand Cu(II), Co(II) Complexes. *J Fluoresc.* 2015;25(1):185–197.
  69. Mendu P, Kumari CG, Ragi R. Synthesis, characterization, DNA binding, DNA cleavage and antimicrobial studies of schiff base ligand and its metal complexes. *J Fluoresc.* 2015;25(2):369-378.
  70. Peres T V., Schettinger MRC, Chen P, et al. Manganese-induced neurotoxicity: A review of its behavioral consequences and neuroprotective strategies. *BMC*

*Pharmacol Toxicol.* 2016;17(1):57.

71. Bouabid S, Tinakoua A, Lakhdar-Ghazal N, Benazzouz A. Manganese neurotoxicity: behavioral disorders associated with dysfunctions in the basal ganglia and neurochemical transmission. *J Neurochem.* 2016;136:677-691.
72. Feng J, Du X, Liu H, et al. Manganese-mefenamic acid complexes exhibit high lipooxygenase inhibitory activity. *Dalt Trans.* 2014;43(28):10930–10939.
73. Balzan S, Lubrano V. LOX-1 receptor: A potential link in atherosclerosis and cancer. *Life Sci.* 2018;198:79-86.
74. Satish Kumar AVT. A Review on Role of Nickel in the Biological System. *Int J Curr Microbiol Appl Sci.* 2016;5(3):719-727.
75. Zambelli B, Uversky VN, Ciurli S. Nickel impact on human health: An intrinsic disorder perspective. *Biochim Biophys Acta - Proteins Proteomics.* 2016;1864(12):1714–1731.
76. D.G. Barceloux. Nickel. *Clin Toxicol.* 1999;37(2):238-258.
77. Perontsis S, Hatzidimitriou AG, Papadopoulos AN, Psomas G. Nickel-diflunisal complexes: Synthesis, characterization, in vitro antioxidant activity and interaction with DNA and albumins. *J Inorg Biochem.* 2016;162:9-21.
78. Totta X, Papadopoulou AA, Hatzidimitriou AG, Papadopoulos A, Psomas G. Synthesis, structure and biological activity of nickel(II) complexes with mefenamato and nitrogen-donor ligands. *J Inorg Biochem.* 2015;145:79-93.
79. Leung CH, Lin S, Zhong HJ, Ma DL. Metal complexes as potential modulators of inflammatory and autoimmune responses. *Chem Sci.* 2015;6:871-884.
80. Petrucci RH, Herring FG, Madura JD, Bissonnette C. Bonding in Complex Ions: Crystal Field Theory. In: *General Chemistry - Principles and Modern Applications.* 10th ed. ; 2011.
81. Brandt WW, Dwyer FP, Gyrfas EC. Chelate complexes of 1,10-phenanthroline and related compounds. *Chem Rev.* 1954;54(6):959-1017.
82. Pal S. Pyridine: A Useful Ligand in Transition Metal Complexes. In: *Pyridine.* ; 2018:57-59.
83. Soderberg T. *Organic Chemistry with a Biological Emphasis.* Vol 1.; 2010.
84. Banti CN, Hadjidakou SK. Non-Steroidal Anti-Inflammatory Drugs (NSAIDs) in Metal Complexes and Their Effect at the Cellular Level. *Eur J Inorg Chem.* 2016;2016(19):3048-3071.
85. Gouda AA, Kotb El-Sayed MI, Amin AS, El Sheikh R. Spectrophotometric and spectrofluorometric methods for the determination of non-steroidal anti-inflammatory drugs: A review. *Arab J Chem.* 2013;6(2):145-163.
86. Chiniforoshan H, Tabrizi L, Hadizade M, Sabzalian MR, Chermahini AN, Rezapour M. Anti-inflammatory drugs interacting with Zn (II) metal ion based on thiocyanate and azide ligands: Synthesis, spectroscopic studies, DFT calculations

- and antibacterial assays. *Spectrochim Acta - Part A Mol Biomol Spectrosc.* 2014;128:183-190.
87. Dimiza F, Papadopoulos AN, Tangoulis V, et al. Biological evaluation of cobalt(II) complexes with non-steroidal anti-inflammatory drug naproxen. *J Inorg Biochem.* 2012;107(1):54-64.
  88. Dimiza F, Papadopoulos AN, Tangoulis V, et al. Biological evaluation of non-steroidal anti-inflammatory drugs-cobalt(II) complexes. *Dalt Trans.* 2010;39(19):4517–4528.
  89. Tarushi A, Karafidou Z, Kljun J, et al. Antioxidant capacity and DNA-interaction studies of zinc complexes with a non-steroidal anti-inflammatory drug, mefenamic acid. *J Inorg Biochem.* 2013;128:85-96.
  90. Trincherio A, Bonora S, Tinti A, Fini G. Spectroscopic Behavior of Copper Complexes of Nonsteroidal Anti-Inflammatory Drugs. *Biopolymers.* 2004;74(1-2):120-124.
  91. Bruijninx PC, Sadler PJ. New trends for metal complexes with anticancer activity. *Curr Opin Chem Biol.* 2008;12(2):197-206.
  92. Pages BJ, Ang DL, Wright EP, Aldrich-Wright JR. Metal complex interactions with DNA. *Dalt Trans.* 2015;44(8):3505–3526.
  93. Oguey C, Foloppe N, Hartmann B. Understanding the sequence-dependence of DNA groove dimensions: Implications for DNA interactions. *PLoS One.* 2010;5(12):e15931.
  94. Czaplá-Masztafiak J, Nogueira JJ, Lipiec E, et al. Direct Determination of Metal Complexes' Interaction with DNA by Atomic Telemetry and Multiscale Molecular Dynamics. *J Phys Chem Lett.* 2017;8(4):805-811.
  95. Sletten E, Hadjiladis N. *Metal Complex-Dna Interactions.* Blackwell Publishing Ltd; 2009.
  96. Turel I, Kljun J. Interactions of Metal Ions with DNA, Its Constituents and Derivatives, which may be Relevant for Anticancer Research. *Curr Top Med Chem.* 2011;11(21):2661-2687.
  97. Farrell N. *Transition Metal Complexes as Drugs and Chemotherapeutic Agents.* Vol 11.; 1989.
  98. Li S, Cooper VR, Thonhauser T, Lundqvist BI, Langreth DC. Stacking interactions and DNA intercalation. *J Phys Chem B.* 2009;113(32):11166-11172.
  99. He S-M, Sun S, Zheng J-R, Zhang J. Molecular spectrum of lanthanide complexes with 2,3-dichlorobenzoic acid and 2,2-bipyridine. *Spectrochim Acta - Part A Mol Biomol Spectrosc.* 2014;123:221-215.
  100. Heydari M, Moghadam ME, Tarlani AA, Farhangian H. DNA as a Target for Anticancer Phen-Imidazole Pd(II) Complexes. *Appl Biochem Biotechnol.* 2017;182(1):110–127.

101. Zhong YW, Vila N, Henderson JC, Flores-Torres S, Abruña HD. Dinuclear transition-metal terpyridine complexes with a dithienylcyclopentene bridge directed toward molecular electronic applications. *Inorg Chem.* 2007;46:10470-12572.
102. Erxleben A. Investigation of Non-covalent Interactions of Metal Complexes with DNA in Cell-free Systems. *Chim Int J Chem.* 2017;71(3):102-111.
103. C. Komor A, K. Barton J. The Path for Metal Complexes to a DNA Target. 2013;49(35):3617–3630.
104. Lau JKC, Ensing B. Hydrolysis of cisplatin - A first-principles metadynamics study. *Phys Chem Chem Phys.* 2010;12(35):10348-10355.
105. Reedijk J. Why does cisplatin reach guanine-N7 with competing S-donor ligands available in the cell? *Chem Rev.* 1999;99(9):2499-2510.
106. Neves AP, Vargas. Platinum(II) Complexes in Cancer Therapy. *Rev Virtual Quim.* 2011;3(3):196-209.
107. Mjos KD, Orvig C. Metallodrugs in medicinal inorganic chemistry. *Chem Rev.* 2014;114(8):4540-4563.
108. Williams MC, Almaqwashi AA, Yilmaz ÖH, et al. DNA Intercalation Facilitates Efficient DNA-Targeted Covalent Binding of Phenanthriplatin. *J Am Chem Soc.* 2019;141(4):1537-1545.
109. Manning GS. The molecular theory of polyelectrolyte solutions with applications to the electrostatic properties of polynucleotides. *Q Rev Biophys.* 1978;11(2):179-246.
110. Yousuf M, Youn IS, Yun J, et al. Violation of DNA neighbor exclusion principle in RNA recognition. *Chem Sci.* 2016;7(6):3581-3588.
111. Blackburn GM, Gait JM, Loakes D, Williams MD. *Nucleic Acids in Chemistry and Biology.* 3rd ed. RSC Publishing; 206AD.
112. Liu HK, Sadler PJ. Metal Complexes as DNA Intercalators. *Acc Chem Res.* 2011;44(5):349-359.
113. Smith JA, Keene FR, Li F, Collins JG. Noncovalent DNA Binding of Metal Complexes. In: *Comprehensive Inorganic Chemistry II.* Vol 3. 2nd ed. ; 2013:709-750.
114. Xu Y, Ishizuka T, Yang J, et al. Oligonucleotide models of telomeric DNA and RNA form a hybrid G-quadruplex structure as a potential component of telomeres. *J Biol Chem.* 2012;287(50):41796-41796.
115. Dixon IM, Lopez F, Tejera AM, et al. A G-quadruplex ligand with 10000-fold selectivity over duplex DNA. *J Am Chem Soc.* 2007;129(6):1502-1503.
116. Sullivan MP, Holtkamp HU, Hartinger CG. Antitumor Metallodrugs that Target Proteins. In: *Metal Ions in Life Sciences.* Vol 18. ; 2018:351-386.
117. Meggers E. Targeting proteins with metal complexes. *Chem Commun.*

2009;(9):1001-1010.

118. Cicenás J, Zalyte E, Bairoch A, Gaudet P. Kinases and cancer. *Cancers (Basel)*. 2018;10(3):1-7.
119. Feng L, Geisselbrecht Y, Blanck S, et al. Structurally sophisticated octahedral metal complexes as highly selective protein kinase inhibitors. *J Am Chem Soc*. 2011;133(15):5976-5986.
120. Kunick C, Ott I. Metal complexes as protein kinase inhibitors. *Angew Chemie - Int Ed*. 2010;49(31):5226-5227.
121. Larsen MT, Kuhlmann M, Hvam ML, Howard KA. Albumin-based drug delivery: harnessing nature to cure disease. *Mol Cell Ther*. 2016;4(3).
122. Topală T, Bodoki A, Oprean L, Oprean R. Bovine serum albumin interactions with metal complexes. *Med Pharm Reports*. 2014;87(4):215-219.
123. Zheng YR, Suntharalingam K, Johnstone TC, et al. Pt(IV) prodrugs designed to bind non-covalently to human serum albumin for drug delivery. *J Am Chem Soc*. 2014;136(24):8790-8798.
124. Huang BX, Kim HY, Dass C. Probing three-dimensional structure of bovine serum albumin by chemical cross-linking and mass spectrometry. *J Am Soc Mass Spectrom*. 2004;15(8):1237-1247.
125. Izumrudov VA, Zhiryakova M V., Goulko AA. Ethidium bromide as a promising probe for studying DNA interaction with cationic amphiphiles and stability of the resulting complexes. *Langmuir*. 2002;18(26):10348-10356 Ethidium.
126. Singh N, Pagariya D, Jain S, Naik S, Kishore N. Interaction of copper (II) complexes by bovine serum albumin: spectroscopic and calorimetric insights. *J Biomol Struct Dyn*. 2018;36(9).
127. Luedtke NW, Hwang JS, Nava E, Gut D, Kol M, Tor Y. The DNA and RNA specificity of eilatin Ru(II) complexes as compared to eilatin and ethidium bromide. *Nucleic Acids Res*. 2003;31(19):5732-5740.
128. Tiwari AD, Mishra AK, Mishra SB, Mamba BB, Maji B, Bhattacharya S. Synthesis and DNA binding studies of Ni(II), Co(II), Cu(II) and Zn(II) metal complexes of N 1,N 5-bis[pyridine-2-methylene]- thiocarbohydrazone Schiff-base ligand. *Spectrochim Acta - Part A Mol Biomol Spectrosc*. 2011;79(5):1050-1056.
129. Kumar Naik KH, Ashok B, Naik N, Mulla JAS, Prakasha A. DNA binding, anti-inflammatory and analgesic evaluation of metal complexes of N/S/O donor ligands; Synthesis, spectral characterization. *Spectrochim Acta - Part A Mol Biomol Spectrosc*. 2015;141:88-93.
130. Hussein BHM. Spectroscopic studies of 7, 8-dihydroxy-4-methylcoumarin and its interaction with bovine serum albumin. *J Lumin*. 2011;131(5):900-908.
131. Żurawska-Płaksej E, Rorbach-Dolata A, Wiglusz K, Piwowar A. The effect of glycation on bovine serum albumin conformation and ligand binding properties with regard to gliclazide. *Spectrochim Acta - Part A Mol Biomol Spectrosc*.

2018;189:625-633.

132. Ni Y, Zhu R, Kokot S. Competitive binding of small molecules with biopolymers: A fluorescence spectroscopy and chemometrics study of the interaction of aspirin and ibuprofen with BSA. *Analyst*. 2011;136:4794-4801.
133. Dash SP, Panda AK, Pasayat S, et al. Evaluation of the cell cytotoxicity and DNA/BSA binding and cleavage activity of some dioxidovanadium(V) complexes containing aroylhydrazones. *J Inorg Biochem*. 2015;144:1-12.
134. Martin S, Nzilibili M, Kurniadi M, Ekodiyanto H, Hardjanto P, Yudianto A. Concentration and Purity DNA Spectrophotometer : Sodium Monofluorophosphate forensic impended effect. *Egypt J Forensic Sci*. 2018;8(34).
135. Sindrewicz P, Li X, Yates EA, Turnbull JE, Lian LY, Yu LG. Intrinsic tryptophan fluorescence spectroscopy reliably determines galectin-ligand interactions. *Sci Rep*. 2019;9:11851.
136. An X, Zhao J, Cui F, Qu G. The investigation of interaction between Thioguanine and human serum albumin by fluorescence and modeling. *Arab J Chem*. 2017;10:1781-1787.
137. Chao WC, Shen JY, Yang CH, et al. The in situ tryptophan analogue probes the conformational dynamics in asparaginase isozymes. *Biophys J*. 2016;110(8):1732-1743.
138. Deepa S, Mishra AK. Fluorescence spectroscopic study of serum albumin-bromadiolone interaction: Fluorimetric determination of bromadiolone. *J Pharm Biomed Anal*. 2005;38:556-563.
139. Toneatto J, Garcia PF, Argüello GA. Advances on the interaction of polypyridyl Cr(III) complexes with transporting proteins and its potential relevance in photodynamic therapy. *J Inorg Biochem*. 2011;105:1299-1305.
140. Xie MX, Xu XY, Wang YD. Interaction between hesperetin and human serum albumin revealed by spectroscopic methods. *Biochim Biophys Acta - Gen Subj*. 2005;1724:215-224.
141. Grosjean R, Delacroix S, Gouget G, et al. New copper(II) complexes of anti-inflammatory drug mefenamic acid: a concerted study including synthesis, physicochemical characterization and their biological evaluation. *Dalt Trans*. 2016;6(91):88546-88558.
142. Sanatkar TH, Hadadzadeh H, Jannesari Z, et al. Characterization, photocleavage, molecular modeling, and DNA- and BSA-binding studies of Cu(II) and Ni(II) complexes with the non-steroidal anti-inflammatory drug meloxicam. *Inorganica Chim Acta*. 2014;423:256-272.
143. Dimiza F, Perdih F, Tangoulis V, Turel I, Kessissoglou DP, Psomas G. Interaction of copper(II) with the non-steroidal anti-inflammatory drugs naproxen and diclofenac: Synthesis, structure, DNA- and albumin-binding. *J Inorg Biochem*. 2011;105(3):476-489.



144. Hu YJ, Ou-Yang Y, Zhang Y, Liu Y. Affinity and specificity of ciprofloxacin-bovine serum albumin interactions: Spectroscopic approach. *Protein J.* 2010;29:234-241.
145. Daviter T, Chmel N, Rodger A. Circular and Linear Dichroism Spectroscopy for the Study of Protein–Ligand Interactions. In: *Protein-Ligand Interactions: Methods and Applications*. Vol 1008. ; 2013:211-240.
146. Bakaeen B, Kabiri M, Iranfar H, Saberi MR, Chamani J. Binding effect of common ions to human serum albumin in the presence of norfloxacin: Investigation with spectroscopic and zeta potential approaches. *J Solution Chem.* 2012;41:1777-1801.
147. Singh N, Pagariya D, Jain S, Naik S, Kishore N. Interaction of copper(II) complexes by bovine serum albumin : spectroscopic and calorimetric insights. *J Biomol Struct Dyn.* 2018;36(9):2449-2462.
148. Wang N, Ye L, Yan F, Xu R. Spectroscopic studies on the interaction of azelnidipine with bovine serum albumin. *Int J Pharm.* 2008;351(1-2):55-60.
149. Shiri F, Rahimi-Nasrabadi M, Ahmadi F, Ehrlich H. Multispectroscopic and molecular modeling studies on the interaction of copper-bupropfenate complex with bovine serum albumin (BSA). *Spectrochim Acta - Part A Mol Biomol Spectrosc.* 2018;203:510-521.
150. Liu Y, Ji F, Liu R. The interaction of bovine serum albumin with doxorubicin-loaded superparamagnetic iron oxide nanoparticles: Spectroscopic and molecular modelling identification. *Nanotoxicology.* 2013;7(1):97-104.
151. Zhao X, Liu R, Chi Z, Teng Y, Qin P. New Insights into the Behavior of Bovine Serum Albumin Adsorbed onto Carbon Nanotubes : Comprehensive Spectroscopic Studies. *Am Chem Soc.* 2010;114:5625-5631.
152. Yesaiyan M, Subramanian A, Arulkumar R, et al. Synthesis, DNA and BSA binding, in vitro anti-proliferative and in vivo anti-angiogenic properties of some cobalt(III) Schiff base complexes. *New J Chem.* 2019;43:11391-11407.
153. Nafisi S, Saboury AA., Keramat N, Jean-Francois N, Tajmir-Riahi H-A. Stability and structural features of DNA intercalation with ethidium bromide , acridine orange and methylene blue. *J Mol Struct.* 2007;827(1-3):35-43.
154. Kosiha A, Parthiban C, Elango KP. Metal(II) complexes of bioactive aminonaphthoquinone-based ligand: synthesis, characterization and BSA binding, DNA binding/cleavage, and cytotoxicity studies. *J Coord Chem.* 2018;71(10):1560-1574.
155. Kaushal R, Thakur S, Nehra K. ct-DNA Binding and Antibacterial Activity of Octahedral Titanium (IV) Heteroleptic (Benzoylacetone and Hydroxamic Acids) Complexes. *Int J Med Chem.* 2016:11.
156. Temerk YM, Ibrahim MS, Kotb M. Voltammetric and spectroscopic studies on binding of antitumor Morin, Morin-Cu complex and Morin- $\beta$ -cyclodextrin with DNA. *Spectrochim Acta - Part A Mol Biomol Spectrosc.* 2009;71(5):1830-1836.

157. Chavez KJ, Garimella S V., Lipkowitz S. Triple Negative Breast Cancer Cell Lines: One Tool in the Search for Better Treatment of Triple Negative Breast Cancer. *Breast Dis.* 2010;32(1-2):35-48.
158. Comşa Ş, Cîmpean AM, Raica M. The Story of MCF-7 Breast Cancer Cell Line : 40 years of Experience in Research. *Anticancer Res.* 2015;35:3147-3154.
159. Hero T, Bühler H, Kouam PN, Priesch-grzeszowiak B, Lateit T, Adamietz IA. The Triple-negative Breast Cancer Cell Line MDA-MB 231 Is Specifically Inhibited by the Ionophore Salinomycin. *Anticancer Res.* 2019;39:2821-2827.
160. Hussain A, Alajmi MF, Rehman MT, et al. Copper(II) complexes as potential anticancer and Nonsteroidal anti-inflammatory agents: In vitro and in vivo studies. *Sci Rep.* 2019;9:1-17.
161. Mašković JM, Hatzidimitriou A, Damjanović A, et al. Synthesis, characterization and biological evaluation of Pd(II), Cu(II), Re(I) and <sup>99m</sup>Tc(I) thiazole-based complexes. *Medchemcomm.* 2018;9:831-842.
162. Lorente L, Martín MM, Abreu-González P, et al. Sustained high serum malondialdehyde levels are associated with severity and mortality in septic patients. *Crit Care.* 2013;17(6):1-11.
163. Ayala A, Muñoz MF, Argüelles S. Lipid peroxidation: Production, metabolism, and signaling mechanisms of malondialdehyde and 4-hydroxy-2-nonenal. *Oxid Med Cell Longev.* 2014;2014.
164. Of E, Levels S, Reduced OF, et al. Evaluation of serum levels of reduced glutathione, glutathione-s-transferase and nitric oxide in breast cancer patients undergoing adjuvant chemotherapy. *IJCRR.* 2013;05(13):51-57.
165. Grotto D, Maria LS, Valentini J, Paniz C, Schmitt G, Garcia C. Importance of the lipid peroxidation biomarkers and methodological aspects for malondialdehyde quantification. *Quim Nov.* 2009;32(1):169-174.
166. Yang H, Villani RM, Wang H, et al. The role of cellular reactive oxygen species in cancer chemotherapy. *J Exp Clin Cancer Res.* 2018;37(266).
167. Bansal A, Simon MC. Glutathione metabolism in cancer progression and treatment resistance. *J Cell Biol.* 2018;217(7):2291-2298.
168. Su LJ, Zhang JH, Gomez H, et al. Reactive Oxygen Species-Induced Lipid Peroxidation in Apoptosis, Autophagy, and Ferroptosis. *Oxid Med Cell Longev.* 2019. doi:10.1155/2019/5080843
169. Pedrosa P, Carvalho A, Baptista P V., Fernandes ARF. Inorganic Coordination Chemistry: Where We Stand in Cancer Treatment? In: *Basic Concepts Viewed from Frontier in Inorganic Coordination Chemistry.* ; 2018:37-65.
170. Totta X, Hatzidimitriou AG, Papadopoulos AN, Psomas G. Nickel(II)-naproxen mixed-ligand complexes: Synthesis, structure, antioxidant activity and interaction with albumins and calf-thymus DNA. *New J Chem.* 2017;41(11):4478-4492.

171. Sohrabi N. Binding and UV/Vis spectral investigation of interaction of Ni(II) piroxicam complex with calf thymus deoxyribonucleic acid (Ct-DNA): A thermodynamic approach. *J Pharm Sci Res.* 2015;7(8):533-537.
172. Pallis M, Bradshaw TD, Westwell AD, Grundy M, Stevens MFG, Russell N. Induction of apoptosis without redox catastrophe by thioredoxin-inhibitory compounds. *Biochem Pharmacol* 66. 2003;66:1695-1705.
173. Pia M, Folda A, Dani B, Menabò R, Scutari G, Bindoli A. Gold(I) complexes determine apoptosis with limited oxidative stress in Jurkat T cells. *Eur J Pharmacol.* 2008;582:26-34.
174. Chakkarapani SK, Park G, Kang SH. Base pair distance analysis in single DNA molecule by direct stochastic optical reconstruction microscopy. *Chinese Chem Lett.* 2015;26(12):1490-1495.
175. Lakshmipraba J, Arunachalam S, Solomon RV, et al. Surfactant-copper(II) Schiff base complexes: Synthesis, structural investigation, DNA interaction, docking studies, and cytotoxic activity. *J Biomol SFstructure Dyn.* 2015;33(4):877-891.
176. Anu MMD, Kumar SD, Subramanian S, Pillai SI. Synthesis , structural characterization , DNA binding activity studies of Cu(II), Ni(II ) and Zn(II) metal complexes containing thiazole moiety. *J Med Chem Pharm Chem Pharm Sci Comput Chem.* 2016;8(18):325-335.
177. Szumilak M, Merecz A, Strek M, Stanczak A, Inglot TW, Karwowski BT. DNA interaction studies of selected polyamine conjugates. *Int J Mol Sci.* 2016;17(9):1560.
178. Martin MB, Reiter R, Pham T, et al. Estrogen-like activity of metals in MCF-7 breast cancer cells. *Endocrinology.* 2003;144(6):2425-2436.
179. Darbre PD. Metalloestrogens: An emerging class of inorganic xenoestrogens with potential to add to the oestrogenic burden of the human breast. *J Appl Toxicol.* 2006;26(3):191-197.
180. Aquino NB, Seigny MB, Sabangan J, Louie MC. Role of Cadmium and Nickel in Estrogen Receptor Signaling and Breast Cancer: Metalloestrogens or Not? *J Env Sci Heal.* 2012;30(3):189–224.



## Annexes

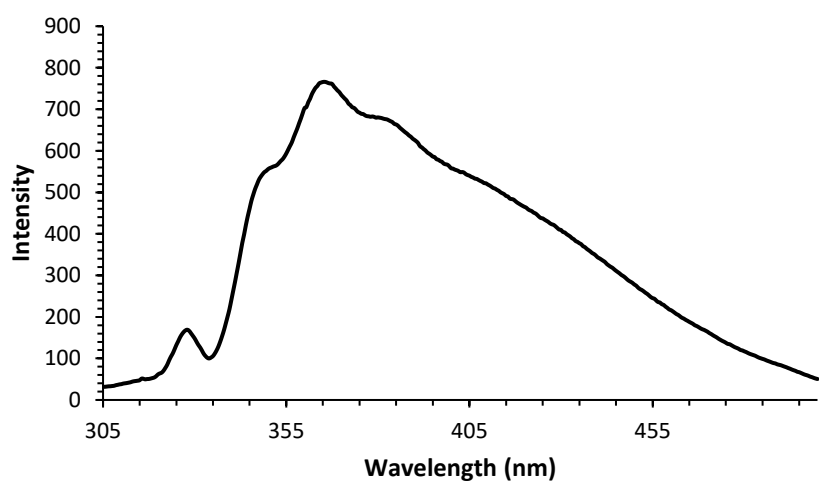
Annex I: Crystal data collection and structure refinement details of complex (1) and (2).

	Complex (1)	Complex (2)
<b>Formula</b>	C <sub>23</sub> H <sub>22</sub> ClCuN <sub>3</sub> O <sub>2</sub>	C <sub>58</sub> H <sub>58</sub> Cl <sub>4</sub> N <sub>8</sub> NiO <sub>12</sub>
<b>Formula weight</b>	471.42	1259.64
<b>Temperature / K</b>	150(2)	150(2)
<b>Crystal system</b>	Monoclinic	Orthorhombic
<b>Space group</b>	<i>P2<sub>1</sub></i>	<i>Pbcn</i>
<b><i>a</i> / Å</b>	7.0886 (5)	18.9673 (12)
<b><i>b</i> / Å</b>	8.8940 (6)	16.5441 (12)
<b><i>c</i> / Å</b>	34.759 (3)	36.632 (2)
<b><math>\alpha</math> / °</b>	90	90
<b><math>\beta</math> / °</b>	92.211 (5)	90
<b><math>\gamma</math> / °</b>	90	90
<b>Volume / Å<sup>3</sup></b>	2189.8 (3)	11495.1 (13)
<b><i>Z</i></b>	4	16
<b><math>\mu</math>(Mo K<math>\alpha</math>) / mm<sup>-1</sup></b>	1.14	0.59
<b>Crystal type</b>	Green Plate	Colourless Plate
<b>Crystal size / mm</b>	0.17×0.10×0.04	0.23×0.20×0.06
<b><math>\theta</math> range (°)</b>	2.34 – 25.57	2.33 – 29.18
<b>Index ranges</b>	-8 ≤ <i>h</i> ≤ 8 -10 ≤ <i>k</i> ≤ 10 -36 ≤ <i>l</i> ≤ 42	-25 ≤ <i>h</i> ≤ 25 -22 ≤ <i>k</i> ≤ 16 -50 ≤ <i>l</i> ≤ 50
<b>Collected Reflections</b>	21254	122187
<b>Independent Reflections</b>	7979 ( <i>R</i> <sub>int</sub> = 0.141)	15492 ( <i>R</i> <sub>int</sub> = 0.040)
<b>Completeness to <math>\theta</math> = 25.24</b>	99.9%	99.9%
<b>Final <i>R</i> indices [<i>I</i> &gt; 2<math>\sigma</math>(<i>I</i>)]</b>	<i>R</i> 1 = 0.2177 <i>wR</i> 2 = 0.5054	<i>R</i> 1 = 0.0372 <i>wR</i> 2 = 0.0817
<b>Final <i>R</i> indices (all data)</b>	<i>R</i> 1 = 0.2379 <i>wR</i> 2 = 0.5151	<i>R</i> 1 = 0.0477 <i>wR</i> 2 = 0.0859
<b>Largest diff. peak and hole / eÅ<sup>-3</sup></b>	3.66 and -2.16	0.38 and -0.33

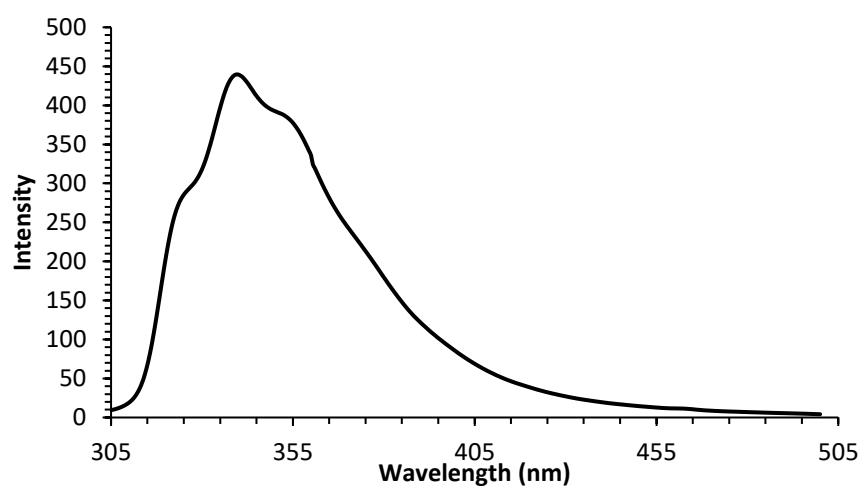
$$^a R1 = \sum \|F_o\| - \|F_c\| / \sum \|F_o\|$$

$$^b wR2 = \sqrt{\sum [w(F_o^2 - F_c^2)^2] / \sum [w(F_o^2)^2]}$$

$$^c w = 1 / [\sigma^2(F_o^2) + (mP)^2 + nP] \text{ where } P = (F_o^2 + 2F_c^2) / 3$$



Annex II: Fluorescence spectra of complex (2) at 0.8 μM.



Annex II: Fluorescence spectra of complex (4) at 1.0 μM